BTO 2016.011 | Maart 2016

BTO rapport

Inbouw van bodemnutriënten en zuurgraad in PROBE

KWR Watercycle Research Institute

BTO

Inbouw van bodemnutriënten en zuurgraad in PROBE

BTO 2016.011| Maart 2016

Opdrachtnummer
400554-047

Projectmanager
E. Dorland

Opdrachtgever
BTO - Thematisch onderzoek - Klimaatbestendige watersector

Auteurs
D.G. Cirkel, Y. Fujita, R.P. Bartholomeus & J.P.M. Witte

Verzonden aan
Themagroep Klimaatbestendige Watersector

Jaar van publicatie
2016

Meer informatie
J.P.M. Witte
T 06-15239215
E flip.witte@xs4all.nl

Keywords
Biodiversity, climate change, ecosystem model, nutrient availability, processes, soil pH, succession, vegetation

PO Box 1072
3430 BB Nieuwegein
The Netherlands

T +31 (0)30 60 69 511
F +31 (0)30 60 61 165
E info@kwrwater.nl
I www.kwrwater.nl

KWR Watercycle Research Institute

BTO *Managementsamenvatting*

Bodemnutriënten en zuurgraad procesmatig gemodelleerd voor PROBE-2

Auteurs
Dr. ir. Gijsbert Cirkel, dr. Yuki Fujita, dr. ir. Ruud Bartholomeus & prof. dr. ir. Jan-Philip Witte

De vegetatiesamenstelling in zoete natuurgebieden kan worden verklaard aan de hand van de vochttoestand, de voedselrijkdom en de zuurgraad van de bodem. Om betrouwbaar te beoordelen hoe de vegetatie zal reageren op klimaatverandering en adaptatiemaatregelen, dienen deze factoren procesmatig te worden gemodelleerd. In het vegetatiemodel PROBE is dat voor de vochttoestand goed gedaan, maar de simulatie van de andere twee factoren liet te wensen over, want die was grotendeels gebaseerd op beslisregels voortkomend uit deskundigenoordeel. In dit BTO onderzoek werd de fosfaatmineralisatie, als schatter voor de voedselrijkdom, door ons procesmatig gemodelleerd en opgenomen in PROBE-2. De procesmatige berekening van de zuurgraad lukte technisch, maar voor inbouw in PROBE-2 is een vervolgproject nodig.

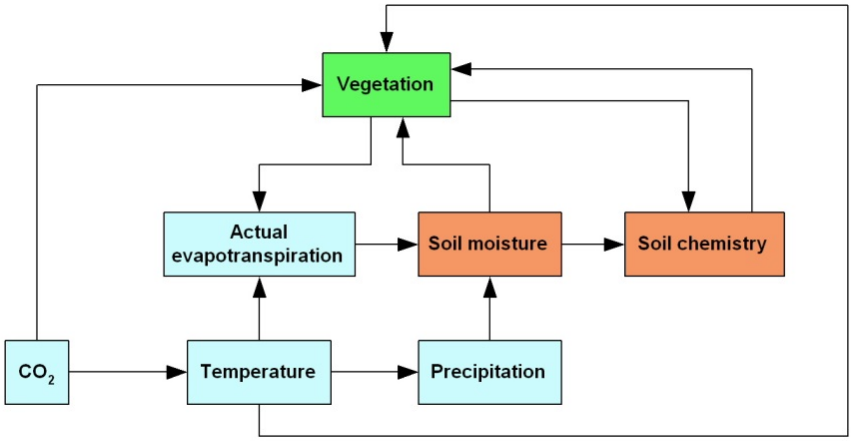

Procesdiagram van de invloed van klimaatverandering op bodem, water en vegetatie

Belang: robuuste vegetatievoorspellingen

Een procesmatige modellering van voedselrijkdom en pH is nodig om de haalbaarheid van natuur-doelen onder een toekomstig klimaat te kunnen beoordelen. Bovendien maakt een procesmatige modellering het mogelijk om gefundeerd van wettelijk vastgelegde natuurdoelen te kunnen afwijken en toekomstige hotspots van biodiversiteit in kaart te brengen.

Aanpak: meten en modelleren

Als maat voor de voedselrijkdom voor de bodem bleek de fosfaatmineralisatie het geschiktst te zijn. Om deze te berekenen, koppelden we een model voor de opbouw en afbraak van organische stof, CENTURY, aan een model voor bodemvocht, SWAP.

Dit onderzoek werd substantieel ondersteund met subsidie van het programma Kennis voor Klimaat aan het project CARE. Voor de zuurgraad van de bodem koppelden we het bodemchemische model ORCHESTRA aan SWAP. Resultaten van beide modelparen werden vergeleken met metingen.

Implementatie: alleen fosfaat in PROBE-2

De mineralisatie van fosfaat is opgenomen in PROBE-2, waardoor dit model nog meer geschikt is voor klimaatprojecties. Wegens enkele praktische bezwaren is dat nog niet gedaan voor de zuurgraad. De wijze waarop we de zuurgraad bodemchemisch hebben gemodelleerd is echter zeer innovatief en breder toepasbaar dan voor PROBE alleen.

Rapport

Dit onderzoek is beschreven in rapport *Inbouw van bodemnutriënten en zuurgraad in PROBE* (BTO 2016.011). Deelonderzoeken zijn beschreven in vier internationale wetenschappelijke publicaties:

1) Fujita, Y., P.M. Van Bodegom, H. Olde Venterink, H. Runhaar en J.P.M. Witte (2013) Towards a proper integration of hydrology in predicting soil nitrogen mineralization rates along natural moisture gradients. *Global Biogeochemical Cycles*, vol 58, pag 302-312.
2) Fujita, Y., P.M. Van Bodegom en J.P.M. Witte (2013) Relationships between nutrient-related plant traits and combinations of soil N and P Fertility. *PLoS ONE* 8(12), vol 8, no 12, pag e83735.
3) Fujita, Y., J.P.M. Witte en P.M. Van Bodegom (2014) Incorporating microbial ecology concepts into soil mineralization models to improve regional predictions of carbon and nitrogen fluxes. *Soil biology and biochemistry*, vol 28, no 3, pag 223-238.
4) Witte, J.-P.M., R.P. Bartholomeus, P.M. van Bodegom, D.G. Cirkel, R. van Ek, Y. Fujita, G.M. Janssen, T.J. Spek en H. Runhaar (2015) A probabilistic eco-hydrological model to predict the effects of climate change on natural vegetation at a regional scale. *Landscape Ecology*, vol 30, pag 835–854.

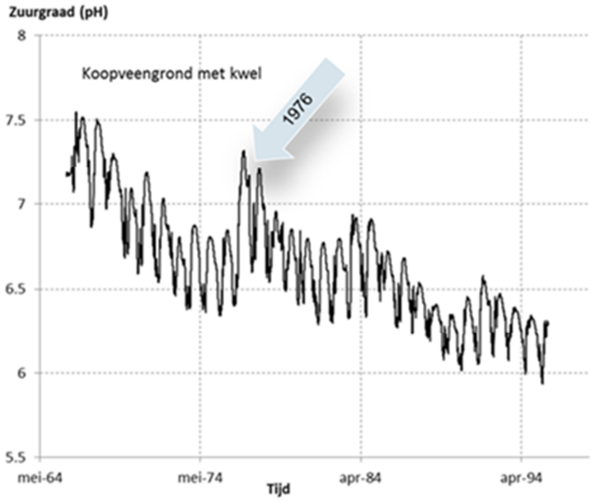

Het met SWAP-ORCHESTRA berekende pH-verloop over de periode 1965-1995 voor een koopveengrond onder invloed van kwel.

Meer informatie
J.P.M. Witte
T 06-15239215
E flip.witte@xs4all.nl

KWR
PO Box 1072
3430 BB Nieuwegein
The Netherlands

KWR Watercycle Research Institute

Inhoud

1 Aanleiding en doel

In PROBE 2.0 worden de voedselrijkdom en de zuurgraad van de bodem bepaald aan de hand van grotendeels op deskundigenoordeel gestelde beslisregels (uit de zogenaamde kansrijkdommodule van Waternood; De Haan e.a. (2010)). Deze aanpak is onvoldoende op processen gebaseerd en daardoor niet klimaatbestendig.

Het doel van dit onderzoek is daarom een goede, procesmatige modellering van bodemnutriënten en de bodemzuurgraad. Zulks is van belang voor het betrouwbaar vaststellen van natuurdoelen en het bepalen van de instandhoudingsmogelijkheden van habitattypen, zowel op de korte termijn, als op de (middel-)lange termijn onder het toekomstige klimaat. Dit geldt voor natuurdoelen op de terreinen van de waterbedrijven zelf, maar ook voor natuurgebieden binnen het beïnvloedingsgebied van de winningen. Bovendien is het ruimtelijk kunnen modelleren van de bodem pH van belang voor het kunnen schatten van de uitspoeling uit de bodem van diffuse chemische verontreinigingen en micro-organismen.

Van de modellen afgeleide reprofuncties dienen te worden ingebouwd in PROBE. Door PROBE uit te bouwen met op processen gebaseerd modules voor bodemnutriënten en zuurgraad, wordt het meer geschikt voor het beoordelen van de gevolgen van klimaatscenario's en adaptatiestrategieën op de vegetatie en de haalbaarheid van natuurdoelen.

In het projecthandvest zijn verschillende activiteiten en daaraan gerelateerde opbrengsten voorzien om dit doel te bereiken:

1. Bouw van PROBE-2.1, toepasbaar voor Pleistoceen Nederland, waarin de voedselrijkdom van de bodem op procesmatige wijze wordt berekend.
2. Bouw van PROBE-2.2, toepasbaar voor Pleistoceen Nederland, waarin de zuurgraad van de bodem op procesmatige wijze wordt berekend.
3. Bouw van PROBE-2.3, dat de ontwikkeling van bodemfysische en bodemchemische eigenschappen onder invloed van de opbouw- en afbraak van organische stof dynamisch simuleert.
4. Opstellen van een bestand met chemische gegevens over bodemprofielen waarmee Nederlandse bodems kunnen worden gekarakteriseerd.
5. Relaties tussen enerzijds de gesimuleerde voedselrijkdom van de bodem en anderzijds gemiddelde indicatiewaarden of planteigenschappen van de vegetatie opstellen. Deze relaties worden als reprofuncties ingebouwd in PROBE.
6. Toepassing en validatie op een proefgebied. De gesimuleerde mineralisatie van organische stof leidt tot een bepaalde nitraatflux, die wordt vertaald naar de nitraatconcentratie van het door de wortelzone percolerende regenwater. Deze berekende concentratie vergelijken met gemeten nitraatconcentraties in het bovenste grondwater;
7. Simulatieresultaten voor (zand)bodems van Nederland voor verschillende combinaties van geohydrologische gesteldheid, bodemchemie en chemische samenstelling van het grondwater, klimaatscenario en atmosferische depositie. De resultaten hebben betrekking op de beschikbare hoeveelheid N en P, bodemvocht, verdamping, en nitraatconcentratie in percolerend bodemvocht.

8. Een onderzoeksrapport en minimaal één artikel in een vakblad en één in een wetenschappelijk tijdschrift.

In het projecthandvest is ervan uitgegaan dat we cofinanciering konden vinden om het onderzoeksbudget te verdubbelen. Dat is niet gelukt, waardoor bovenstaande doelen niet allemaal zijn gerealiseerd. We komen hier in Hoofdstuk 3 op terug.

2 Methode en resultaten

2.1 Inleiding

Het onderzoek bestond uit twee gedeelten: het modelleren van de voedselrijkdom, resulterend in PROBE-2.1, en het modelleren van de zuurgraad, resulterend in PROBE-2.2. De ontwikkeling van een dynamisch model (versie 2.3) is bij gebrek aan cofinanciering niet doorgegaan.

2.2 Modellering P-beschikbaarheid

Uit onderzoek van Fujita e.a. (2013b) blijkt dat de beschikbaarheid van fosfaat (P) een goede voorspeller is van de voedselrijkdom van de bodem voor de vegetatie. Eerst hebben we geprobeerd de P-beschikbaar te simuleren met het model ANIMO (Groenendijk e.a., 2005), dat vooral wordt gebruikt in landbouwkundige en milieustudies. Dat leverde bij een validatie aan metingen in natuurgebieden echter niet zulke goede resultaten op (Figuur 1). Mogelijk wordt dit veroorzaakt door de gebruikte Langmuir-relatie. De vastlegging en vrijmaking van fosfaat in bodems is namelijk zeer complex. Zo is in natuurlijke bodems de adsorptie aan ijzer(hydr)oxiden behalve pH-afhankelijk tevens sterk afhankelijk van de concentratie natuurlijk opgelost organisch materiaal (NOM) en van polyvalente kationen, zoals Ca^{2+}. Calciumionen hebben een synergistisch effect op de adsorptie van P aan oxiden en NOM concurreert sterk met fosfaat voor de adsorptie aan oxiden (Weng e.a., 2011). Als alternatief zijn door ons verkennende speciatieberekeningen uitgevoerd met ORCHESTRA, waarbij we het synergistische effect van calcium hebben meegenomen, net als het neerslaan van calciumfosfaten. Volgens Weng e.a. (2011) is de invloed van NOM adsorptie echter cruciaal en zou dus ook in het ORCHESTRA-model moeten worden meegenomen. Gegevens hierover ontbreken echter geheel in onze datasets. Daarom is de modellering van anorganisch-P gestaakt. De resultaten (zonder invloed van NOM) die we voor enkele bodems verkregen zijn echter veelbelovend voor een vervolgproject (Figuur 2).

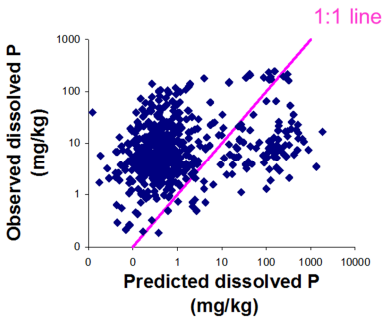

Figuur 1. Validatie van ANIMO aan gegevens van Ertsen (1998).

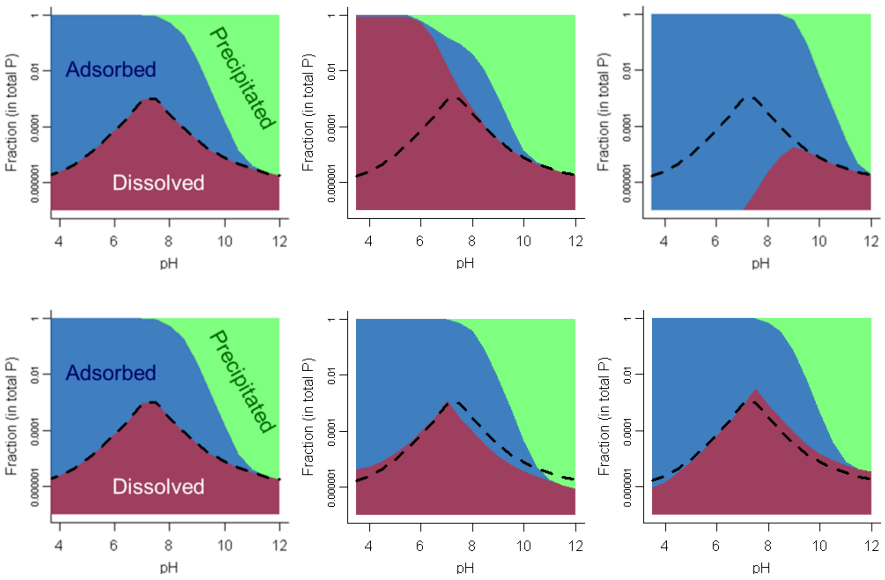

Figuur 2. Resultaten van de verkennende berekeningen met: boven, van links naar rechts: een gemiddeld (0.00215 kg/kg), laag (0.0001 kg/kg) en hoog (0.1 kg/kg) gehalte ijzer(hydr)oxiden; onder, van links naar rechts: een gemiddelde (0.00139 mol/l), lage (0.0005 mol/L en hoge (0.005 mol/L) calciumconcentratie. Gemodelleerde ranges gebaseerd op de ITORS database

We zijn daarna verder gegaan met de simulatie van de hoeveelheid beschikbaar P die vrij komt bij de afbraak van organische stof. Deze P-mineralisatie hebben we gesimuleerd met een eigen versie van het model CENTURY, dat de opbouw en afbraak van organische stof in de bodem beschrijft. De dynamiek, en daarmee de vastlegging en het vrijkomen van nutriënten, hangt sterk af van de bodemvochtcondities. In de oorspronkelijke versie van CENTURY worden deze op een vrij primitieve wijze voor hangwaterprofielen beschreven, dus zonder rekening te houden met de capillaire beïnvloeding door ondiepe grondwaterstanden (Parton e.a., 1993). Daarom hebben we CENTURY gekoppeld aan de uitkomsten van het model SWAP (Van Dam e.a., 2008), dat de vochtcondities in de bodem dynamisch beschrijft. Ook hebben we onderzocht hoe de afbraak van organische stof modelmatig het beste kan worden beschreven. Over deze koppeling en de afbraakmodellering hebben we verslag gedaan in twee wetenschappelijke publicaties (Fujita e.a., 2013a; Fujita e.a., 2014) (Bijlage III). Vervolgens hebben we de P-mineralisatie module van CENTURY ingebouwd en daarna onderzocht welke maat voor de voedselrijkdom van de bodem het beste correspondeert met de gemiddelde vegetatie-eigenschappen van vegetatieopnamen (zoals de indicatiewaarde voor voedselrijkdom, of de ‘specific leaf area index’). Ook hierover is wetenschappelijk gerapporteerd (Fujita e.a., 2013b) (Bijlage III).

In Bijlage I beschrijven we hoe we met SWAP-CENTURY reprofuncties voor PROBE hebben afgeleid. Bodemtypen zijn daartoe door ons geparametriseerd op basis van hun indeling in bodemfysische eenheden door Wösten e.a. (2001). Voor allerlei geohydrologische omstandigheden en slootpeilen hebben we het modellenpaar SWAP-CENTURY talloze keren laten rekenen om vervolgens met het programma GTST (Bartholomeus en Witte, 2013) voor PROBE reprofuncties af te leiden. Deze beschrijven P-mineralisatie en de daarmee samenhangende indicatiewaarde voor de voedselrijkdom (Figuur 3) als functie van enkele grondwaterstandskarakteristieken (GLG, GHG, GG), het bodemtype, het door de gebruiker geselecteerde klimaatscenario en zichtjaar, en de geografische ligging (zodat rekening wordt gehouden met klimatologische verschillen binnen Nederland). De reprofuncties zijn ingebouwd in versie twee van PROBE (Witte e.a., 2015) en vervolgens toegepast in twee

proefgebieden (Van der Knaap e.a., 2015; Witte e.a., 2015; Van der Knaap e.a., submitted). Bovendien is de nieuwe versie van PROBE-2 op nationale schaal vergeleken met andere vegetatiemodellen en gevalideerd aan gelokaliseerde vegetatieopnamen (Van Ek e.a., 2014). Uit de vergelijking werd de conclusie getrokken dat PROBE-2 de basis moet worden voor een door KWR en Alterra te ontwikkelen 'Waterwijzer Natuur' (http://waterwijzer.stowa.nl).

De modellering van de P-mineralisatie met SWAP-CENTURY en de inbouw in en toepassing van PROBE-2 is mede mogelijk gemaakt dankzij subsidie aan het Kennis voor Klimaat project CARE (Van den Brink e.a., 2012). Bovendien hebben we dankbaar gebruik kunnen maken van door derden verzamelde veldgegevens (zoals de referentiepunten van Staatsbosbeheer, Humbase van Alterra en ITORS van Universiteit Utrecht; Bijlage I). De wetenschappelijke publicaties die zijn verschenen naar aanleiding van het onderzoek zijn opgenomen in Bijlage III.

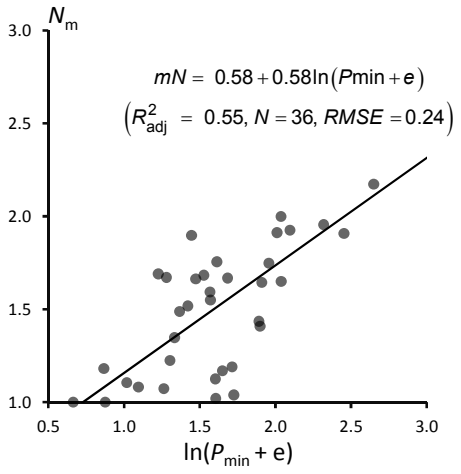

Figuur 3. Relatie tussen gesimuleerde mineralisatie P_{min} (e is het natuurlijke grondgetal) in de bodem (0-10 cm) en de waargenomen gemiddelde indicatiewaarde N_m (Witte e.a., 2015). Gegevens van Fujita e.a. (2013b).

2.3 Bodem-pH

Voor het modelleren van de pH is een binnen de ORCHESTRA omgeving ontwikkeld bodemchemisch model gekoppeld aan het hydrologische model SWAP (Cirkel et al., 2015). Hiermee is op basis van recente modelconcepten berekend hoe de pH in de bovenste 10 cm van de bodem zich ontwikkeld. In het bodemchemische model zijn de volgende processen opgenomen: sorptie en desorptie aan oxides, humus en klei; oplossen en neerslaan van gibsite en calciet; productie en diffusie van CO_2(g); silicaverwering; carbonaatevenwichten. Het transport van opgeloste stoffen en de gasdiffusie in de onverzadigde zone is berekend op basis van de in SWAP uitgerekende waterfluxen en vochtgehaltes. Naast de opzet van het model is een eerste aanzet gegeven voor een chemische karakterisering van bodemfysische eenheden en grondwater. Voor detailinformatie over de modelopzet en model resultaten wordt verwezen naar Bijlage II.

Bodemchemische informatie is slechts beperkt beschikbaar. Chemische gegevens over de vaste fase in combinatie met informatie over de chemie van de waterfase zijn nog schaarser. De chemische schematisering van de bodems is hierdoor grof en initieel niet altijd geheel intern consistent. Door het ontbreken van gecombineerde hydrochemische en bodemchemische informatie is besloten de profielen initieel in evenwicht te brengen met een vooraf bepaald grondwatertype. Gekozen is voor de grondwaterkwaliteit zoals onttrokken bij pompstation Vlierden (representatief voor gebufferd kwelwater). De initialisatie van de

bodemchemische modellen in SWAP-ORCHESTRA is echter tijdrovend. Uiteindelijk is voor vijf veel voorkomende en onderling verschillende eenheden succesvol een stabiele en representatieve beginconditie afgeleid. Het gaat hierbij om de volgende eenheden: koop- en madeveengronden (BoFy2), kalkrijke vaaggronden (BoFy7a), veldpodzolen (BoFy9), lichte kleigronden (BoFy16) en zware kleigronden (BoFy17).

De simulaties resulteren in een plausibele pH-range (Figuur 4) en laten zien dat de hydrologie doorwerkt op het verloop van de pH in de tijd (
Figuur 5). In het hier weergegeven geval van een (natte) koopveengrond met kwelinvloed treedt de hoogste pH steeds op in het najaar (meestal halverwege oktober). Door de geringe grondwateraanvulling tot de herfst is de grondwaterinvloed dan maximaal. Met de toenemende grondwater-aanvulling in de herfst en winter daalt de pH weer tot in het begin van de zomer weer een stijging wordt ingezet. In het voorbeeld is tevens de sterke invloed van een droog jaar (1976) zichtbaar waardoor de kwelinvloed in de wortelzone maximaal wordt en de pH sterk stijgt. Uit
Figuur 5 blijkt echter ook dat de gekozen beginconditie van grote invloed is op het verdere verloop van de pH. Het kan hierdoor een veel rekenjaren duren voordat stabilisatie optreedt.

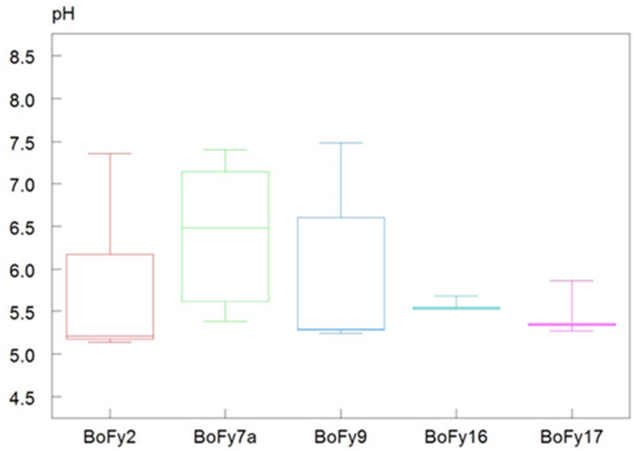

Figuur 4. Box-whisker plots van de resultaten (pH na 30 jr) van de vijf voor het huidige klimaat doorgerekende bodemfysische eenheden.

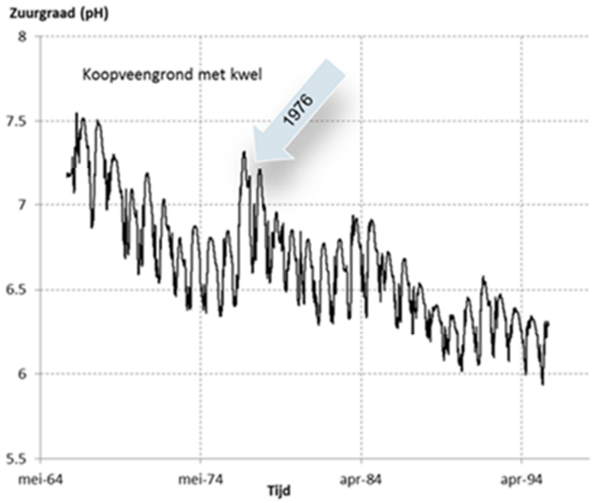

Figuur 5. Het met SWAP-ORCHESTRA berekende pH-verloop over de periode 1965-1995 voor een koopveengrond onder invloed van kwel.

Zoals vermeld heeft de initialisatie van de modellen veel tijd gekost, en kampten we bij toepassing dus met een groot gebrek aan gegevens om bodems goed te kunnen parameteriseren. Ook de rekentijden bleken hoog (ca. 12-24 uur) per run van 30 jaar. Om deze reden hebben we naast het aantal bodemfysische eenheden ook het aantal scenarios moeten beperken tot 15. Op basis van deze beperkte set hebben we reprofuncties kunnen afleiden waarbij de bodem pH per eenheid en kwelkwaliteit het beste kan worden beschreven als een functie van de oppervlakkige afstroming (surface runoff) in combinatie met de GLG (Figuur 6). Hoe hoger de term voor oppervlakkige afvoer, des te minder neerslagwater de bodem indringt en des te meer de bodem-pH wordt beïnvloed door de aanvoer van grondwater. De GLG is vervolgens een maat voor het daadwerkelijk bereiken van toestromend grondwater van de wortelzone. Hoe dieper de GLG, hoe kleiner de kans dat toestromend gebufferd grondwater de wortelzone kan bereiken.

Geconcludeerd wordt dat, ondanks dat het mogelijk is om met de huidige set berekeningen reprofuncties af te leiden voor bodem-pH, deze functies nog verre van volmaakt zijn. Zowel de statistische robuustheid als de range van uitkomsten maakt dat het in onze optiek nog te vroeg is om deze functies in te bouwen in PROBE-2. Daarnaast is PROBE-2 nog niet toegerust op oppervlakkige afstroming als verklarende variabele.

Met name door het verbeteren van de set met bodemchemische gegevens per bodemfysische eenheid en het uitbreiden van de range hydrologische scenario (meer punten voor een meer robuuste fit) kan de significantie van de relaties worden verbeterd. Bijzondere aandacht dient hierbij uit te gaan naar drogere of zelfs grondwateronafhankelijke profielen. Ook dient de kwelwaterkwaliteit in eventuele toekomstige berekeningen gevarieerd te worden. Daarnaast kan dan ook de bodemchemische kant van het model worden verbeterd door onder meer het meenemen van redoxreacties, die in zeer natte milieus van grote invloed zijn op de zuurgraad dynamiek. Voor gedetailleerde (technische) conclusies en aanbevelingen wordt verwezen naar Bijlage II).

De voor het onderzoek relevante publicaties die zijn verschenen zijn opgenomen in Bijlage III.

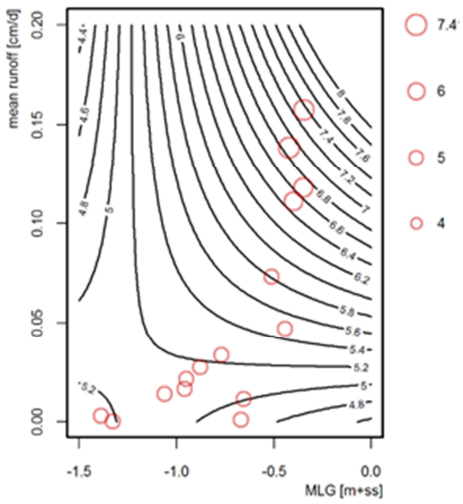

Figuur 6. Afgeleide reprofunctie voor pH (contourplot) voor het huidige klimaat op basis van GLG en runoff voor bodemfysische eenheid 2 (R^2_{adj} = 0.894).

3 Conclusies en aanbevelingen

Over de in Hoofdstuk 1 genoemde opbrengsten kan het volgende worden geconcludeerd:

a. 🟢 Bouw van PROBE-2.1 voor Pleistoceen Nederland, waarin de voedselrijkdom van de bodem op procesmatige wijze wordt berekend is grotendeels gerealiseerd.
Er kan echter nog wel het nodige worden verbeterd, want de berekening van zowel organisch als anorganisch gebonden fosfaat hebben we technisch voor elkaar gekregen, maar wegens gebrek aan gegevens hebben we alleen de P-mineralisatie gebruikt als schatter voor de voedselrijkdom. Via reprofuncties berekent PROBE-2 nu de P-mineralisatie overal in Nederland als functie van bodemtype, karakteristieke grondwaterstanden, klimaatscenario en zichtjaar.

b. 🟡 Onvoldoende gerealiseerd is de bouw van PROBE-2.2, toepasbaar voor Pleistoceen Nederland, waarin de zuurgraad van de bodem op procesmatige wijze wordt berekend.
De berekening van de bodem-pH hebben we wegens een gebrek aan gegevens en sterk oplopende rekentijden vooralsnog alleen voor een gedeelte van de bodemfysische eenheden en hydrologische scenario's kunnen uitvoeren. De simulaties resulteren in een realistische pH-range en weerspiegelen de invloed van hydrologie en het klimaat. De rekenmethode ligt echter klaar voor gebruik voor heel Nederland, en dat gebruikt reikt verder dan alleen ecologische toepassingen: ook voor bijvoorbeeld de uitspoeling uit de bodem van diffuse chemische verontreinigingen en micro-organismen kan de methode worden ingezet.

c. 🔴 Bouw van PROBE-3, dat de ontwikkeling van bodemfysische en bodemchemische eigenschappen dynamisch simuleert. Niet gerealiseerd wegens gebrek aan cofinanciering. Wordt nu opgepakt in BTO-project 400554-115 (PROBE-3).

d. 🟢 Opstellen van een bestand met chemische gegevens over bodemprofielen waarmee Nederlandse bodems kunnen worden gekarakteriseerd. Is gelukt (Bijlage I en Bijlage II), maar het aantal gegevens valt tegen.

e. 🟢 Reprofuncties voor de berekening van de voedselrijkdom van de bodem en de gemiddelde indicatiewaarde van de vegetatie zijn ingebouwd in PROBE-2.1.

f. 🟡 Toepassing en validatie op een proefgebied, berekende nitraatconcentratie percolatiewater vergelijken met metingen bovenste grondwater.
Gedeeltelijk meer dan gerealiseerd : PROBE-2.1 is toegepast in het stroomgebied van de Baakse beek (Witte e.a., 2015), het stroomgebied van de Tungelroyse beek (Van der Knaap e.a., 2015; Van der Knaap e.a., submitted), en gevalideerd op nationale schaal (Van Ek e.a., 2014). Aan de simulatie en validatie van de nitraatuitspoeling zijn we echter niet toegekomen; wordt nu opgepakt in BTO-project 400554-115 (PROBE-3).

g. 🟡 Simulatieresultaten voor (zand)bodems van Nederland.
Voor alle bodems zijn simulaties uitgevoerd, maar de gevolgen van atmosferische depositie hebben we niet kunnen meenemen wegens een gebrek aan bodemgegevens om de denitrificatie goed te kunnen berekenen.

h. ● De toegezegd wetenschappelijke publicatie is er gekomen, en meer dan dat (Bijlage III), alleen zijn we niet toegekomen aan het schrijven van een artikel voor een vakblad. We willen dat artikel alsnog schrijven bij de promotie van de gebruiksvriendelijke schil die in 2015 voor PROBE-2 is gebouwd. Dit artikel zal beging 2016 worden ingediend.

Op basis van ons onderzoek bevelen we het volgende aan:

1. In de loop der jaren is er, vooral door de WUR maar ook door KWR en universiteiten, in diverse projecten veel gemeten aan bodemchemische eigenschappen. Laat deze meetgegevens bij elkaar brengen in een database. Ze zijn onmisbaar voor het goed parametriseren van bodemtypen ten behoeve van bodemchemische simulaties.
2. Start een vervolgproject om alsnog de anorganisch gebonden P te betrekken bij de schatting van de voedselrijkdom van de bodem.
3. Start een vervolgproject om volledige reprofuncties voor de pH af te leiden voor PROBE.
4. Zoek in voorgaande projecten de samenwerking met Alterra en enkele universiteiten.
5. Zoek voor deze projecten financiering bij overheden (provincies, waterschappen).

We zijn bezig met pogingen deze aanbevelingen om te zetten in concrete acties.

Referenties

Bartholomeus, R.P. en J.P.M. Witte (2013) Ecohydrological Stress - Groundwater To Stress Transfer. Theory and manual version 1.0. KWR Watercycle Research Institute.

Bartholomeus, R.P., J.P.M. Witte, P.M. van Bodegom, J.C. van Dam en R. Aerts (2008) Critical soil conditions for oxygen stress to plant roots: Substituting the Feddes-function by a process-based model; in: *Journal of Hydrology*, vol 360, no 1-4, pag 147-165.

Breeuwsma, A.J.H.M. (1990) Mineralogische samenstelling van de Nederlandse zand- en kleigronden; in: *Bodemkunde van Nederland*, ed. W. P. D. B. Locher, H. Malmberg, Den Bosch.

Breeuwsma, A.J.H.M., J.H.M. Wösten, J.J. Vleeshouwer, A.M. Van Slobbe en J. Bouma (1986) Derivation of land qualities to assess environmental problems from soil surveys; in: *Soil Science Society of America Journal*, vol 50, no 1, pag 186-190.

Cirkel, D.G., S.E.A.T.M. Van der Zee en J.C.L. Meeussen (2015) Front spreading with nonlinear sorption for oscillating flow; in: *Water Resources Research*, vol 51, no 4, pag 2986-2993.

De Haan, M., H. Runhaar en G. Cirkel (2010) Waternood Kansrijkdommodule; Pilotstudie in Noord-Nederland en toepassing voor vervaardiging waterkansenkaarten voor natuur. KWR 55.

Dzombak, D.A. en F.M. Morel (1990) Surface complexation modeling: hydrous ferric oxide.

Ertsen, A.C.D. (1998) Ecohydrological response modelling; predicting plant species response to changes in site conditions, Knag/Faculteit Ruimtelijke Wetenschappen, Universiteit Utrecht, Utrecht.

Fujita, Y., P.M. Van Bodegom, H. Olde Venterink, H. Runhaar en J.P.M. Witte (2013a) Towards a proper integration of hydrology in predicting soil nitrogen mineralization rates along natural moisture gradients; in: *Global Biogeochemical Cycles*, vol 58, pag 302-312.

Fujita, Y., P.M. Van Bodegom en J.P.M. Witte (2013b) Relationships between nutrient-related plant traits and combinations of soil N and P Fertility; in: *PLoS ONE 8(12)*, vol 8, no 12, pag e83735.

Fujita, Y., J.P.M. Witte en P.M. Van Bodegom (2014) Incorporating microbial ecology concepts into soil mineralization models to improve regional predictions of carbon and nitrogen fluxes; in: *Soil biology and biochemistry*, vol 28, no 3, pag 223-238.

Groenendijk, P., L.V. Renaud en J. Roelsma (2005) Prediction of Nitrogen and Phosphorus leaching to groundwater and surface waters; Process descriptions of the Animo4.0 model. Alterra 114.

McBride, M.B. (1994) Environmental chemistry of soils; Oxford university press.

Meeussen, J.C.L. (2003) ORCHESTRA: An Object-Oriented Framework for Implementing Chemical Equilibrium Models; in: *Environmental Science & Technology*, vol 37, no 6, pag 1175-1182.

Milne, C.J., D.G. Kinniburgh, W.H. Van Riemsdijk en E. Tipping (2003) Generic NICA–Donnan Model Parameters for Metal-Ion Binding by Humic Substances; in: *Environmental Science & Technology*, vol 37, no 5, pag 958-971.

Mol-Dijkstra, J.P., J. Kros, G.J. Reinds, H.J.J. Wieggers en M. Posch (2006) Model description and Users guide SMART2 version 3.4. Alterra 100.

Parton, W.J., J.M.O. Scurlock, D. Ojima, T.G. Gilmanov, R.J. Scholes, D.S. Schimel, T. Kirchner, J.C. Menaut, T. Seastedt, E. Garcia Moya, A. Kamnalrut en J.I. Kinyamario (1993) Observations and modeling of biomass and soil organic matter dynamics for the grassland biome worldwide; in: *Global Biogeochemical Cycles*, vol 7, pag 785-809.

Penning de Vries, F.W.T. en H.H. Van Laar (1982) Simulation of Plant Growth and Crop Production; Pudoc, Wageningen.

Scheffer, F., P. Schachtschabel en H.P. Blume (2002) Lehrbuch der Bodenkunde; Spektrum.

Van Dam, J.C., P. Groenendijk, R.F.A. Hendriks en J.G. Kroes (2008) Advances of modeling water flow in variably saturated soils with SWAP; in: *Vadose Zone J.*, vol 7, no 2, pag 640-653.

Van den Brink, A., M.M. Bakker, C.C. Vos en J.P.M. Witte (2012) Climate Adaptation for Rural arEas (CARE); Midterm review report; Knowledge for Climate Theme 3. National Research Programme Knowledge for Climate 51.

Van der Knaap, Y., M.M. Bakker, S.J. Alam, J.P.M. Witte, R. Van Ek, M.F.P. Bierkens en P.M. Van Bodegom (submitted) Land use changes determine vegetation patterning more than climate change or climate adaptation measures; in: *Land Use Policy*, vol, pag.

Van der Knaap, Y.A.M., M. De Graaf, R. van Ek, J.-P.M. Witte, R. Aerts, M.F.P. Bierkens en P.M. Van Bodegom (2015) Potential impacts of groundwater conservation measures on catchment-wide vegetation patterns in a future climate; in: *Landscape Ecology*, vol 30, no 5, pag 855-869.

Van der Salm, C. en W. De Vries (2001) A review of the calculation procedure for critical acid loads for terrestrial ecosystems; in: *Science of the total environment*, vol 271, no 1, pag 11-25.

Van Ek, R., J.P.M. Witte, J.P. Mol-Dijkstra, W. De Vries, G.W.W. Wamelink, J. Hunink, W. Van der Linden, J. Runhaar, L. Bonten, R. Bartholomeus, H.M. Mulder en Y. Fujita (2014) Ontwikkeling van een gemeenschappelijke effect module voor terrestrische natuur. STOWA 150.

Weng, L., F.A. Vega en W.H. Van Riemsdijk (2011) Competitive and synergistic effects in pH dependent phosphate adsorption in soils: LCD modeling; in: *Environmental science & technology*, vol 45, no 19, pag 8420-8428.

Witte, J.-P.M., R.P. Bartholomeus, P.M. van Bodegom, D.G. Cirkel, R. van Ek, Y. Fujita, G.M. Janssen, T.J. Spek en H. Runhaar (2015) A probabilistic eco-hydrological model to predict the effects of climate change on natural vegetation at a regional scale; in: *Landscape Ecology*, vol 30, pag 835–854.

Witte, J.P.M., R. Pastoors, D.J. Van der Hoek, R.P. Bartholomeus, A. Van Loon en P.M. Van Bodegom (2011) Is het Nationaal Hydrologische Instrumentarium gereed voor het voorspellen van natuureffecten?; in: *Stromingen*, vol 17, no 2, pag 15-26.

Wösten, J.H.M., F. De Vries, J. Denneboom en A.F. Van Holst (1988) Generalisatie en bodemfysische vertaling van de bodemkaart van nederland, 1: 250 000, ten behoeve van de PAWN-studie. Stichting voor Bodemkartering.

Wösten, J.H.M., G.J. Veerman, W.J.M. de Groot en J. Stolte (2001) Waterretentie- en doorlatendheidskarakteristieken van boven- en ondergronden in Nederland: de Staringreeks. Vernieuwde uitgave 2001 [Water retention and permeability characteristics of top and sub soils in the Netherlands: the Staring series. Renewed edition 2001]; Alterra, Research Instituut voor de Groene Ruimte, Wageningen.

Bijlage I Estimation of soil parameters for CENTURY

Aim

Estimate soil parameters necessary for CENTURY model (i.e. soil total C, NC ratio, PC ratio) from soil type ('bodemcode').

Soil data

- Fujita et al., 2013 (N=36)
- Olde Venterink et al., 2002 (N=54)
- Ordonez et al., 2010 (N=55)
- ITORS (N=126)
- Soil map (N=8)
- SBB referentiepunten (N=74)
- Mankor & Kemmers, 1987 (N=4)
- Herwaarden, 1990 (N=9)
- HumBase (N=257)

Procedures of estimation

For each soil sample, the soil type was retrieved from 1:50,000 soil maps. The soil type was translated into a Soil Physical Unit (23 categories). The 'bouwsteen' of the top layer of the SPU was taken as the category of the soil sample. When necessary, the 'bouwsteen' was adjusted to better reflect the local condition based on expert knowledge.

Soil total C, NC ratio, and PC ratio was averaged within each bouwsteen (Table I.1, Figure I.1).

Usage

For any given sopil type, soil total C, NC ratio, and PC ratio is approximated via their top-layer 'bouwsteen' (See examples in Table I.2).

Table I.1. *Summary of soil properties for each bouwsteen (Av, N, SE = average, number and standard error) .*

Bouw-steen	Soil C(%)			Soil NC			Soil PC		
	Av	N	SE	Av	N	SE	Av	N	SE
O1	4.32	125	0.57	0.058	110	0.002	0.009	125	0.001
O15	6.86	23	0.80	0.107	23	0.012	0.012	23	0.002
B1	4.34	54	0.72	0.050	54	0.003	0.008	53	0.001
B2	3.85	68	0.31	0.061	67	0.003	0.012	67	0.001
B3	7.61	71	0.98	0.056	48	0.003	0.009	71	0.001
B8	10.21	40	1.45	0.082	33	0.006	0.014	40	0.002
B10	5.61	16	0.66	0.085	16	0.006	0.015	14	0.004
B11	21.29	13	4.12	0.077	13	0.006	0.009	13	0.002
B12	13.96	14	3.04	0.082	14	0.010	0.010	14	0.003
B16	19.80	97	1.14	0.063	83	0.002	0.009	97	0.001
B18	29.00	94	1.30	0.072	82	0.006	0.009	94	0.001

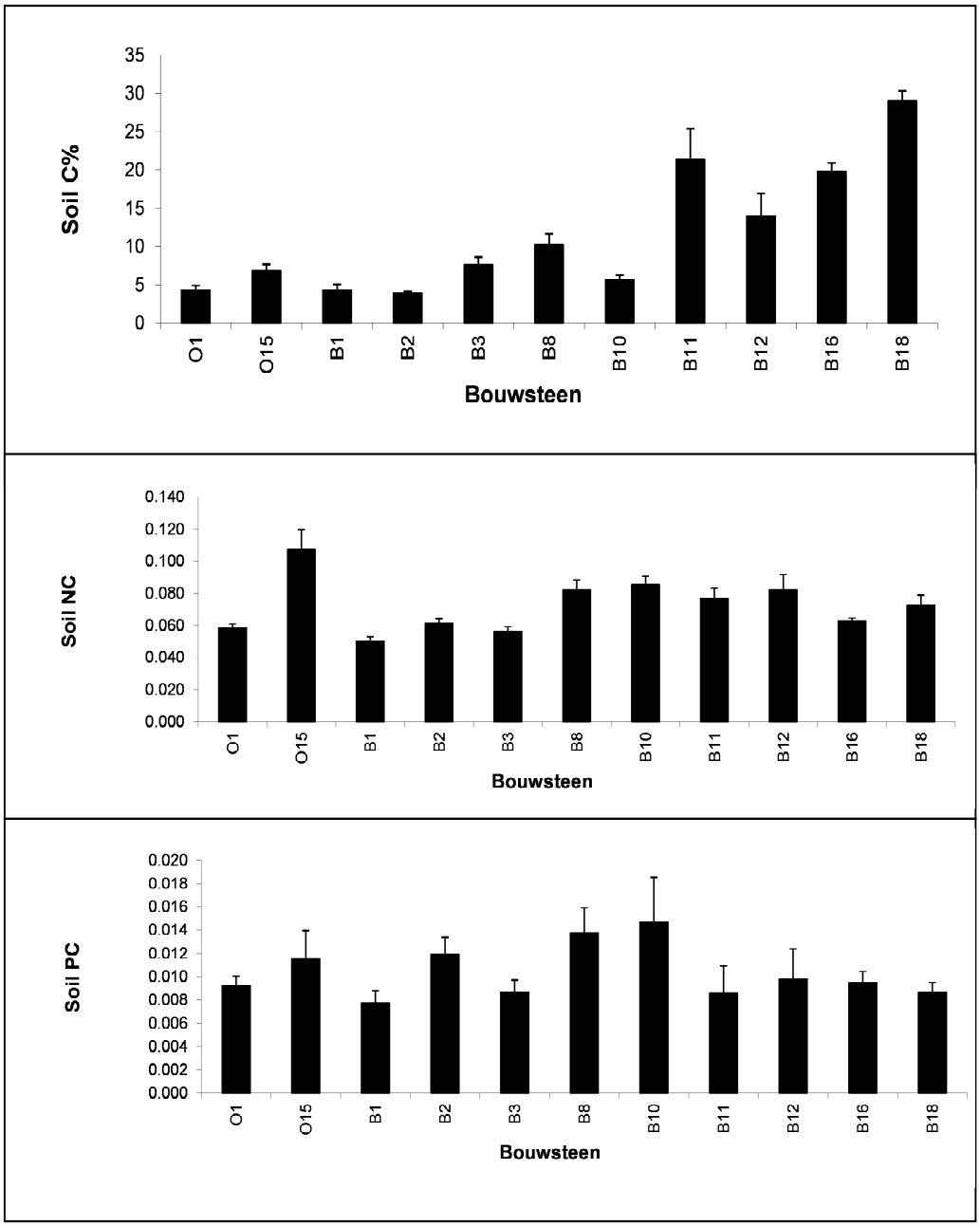

Figure I.1. *Average (plus standard error) of soil total C (%), NC ratio, and PC ratio for each bouwsteen.*

Table I.2. *Examples of translation from bodemcode to soil properties*

Bodemcode	SPU
ABv	**5**
ABvF	**5**
ABvg	**5**
ABv-II*/ABv-IV	**5**
ABv-II/ABv-III	**5**
ABv-II/ABv-III*	**5**
ABv-II/ABv-III/ABv-V/ABv-VI	**5**
ABv-II/ABv-V	**5**
ABv-IV/ABv-V/ABv-VI	**5**
ABvt	**5**
ABv-V/ABv-VI	**5**
ABvx	**5**
ABz	**13**
ABz-II/ABz-III	**13**
ABzt	**13**
AD-I/AD-II/AD-VI	**7**
AD-I/AD-III/AD-VI/AD-VII	**7**
AD-I/AD-VI/AD-VII	**7**
AD-II/AD-III/AD-VI/AD-VII	**7**
AD-II/AD-III/AD-VII	**7**
AEk9	**16**
AEk9-V/AEk9-VI	**16**
AEm5	**15**
AEm5-III*/AEm5-V*	**15**
AEm8	**16**
AEm8-III*/AEm8-V*	**16**
AEm8-III*/AEm8-VI	**16**

SPU	bouwsteen top-layer	SoilC (%)	SoilNC	SoilPC
1	B18	29.00	0.072	0.009
2	B16	19.80	0.063	0.009
3	B11	21.29	0.077	0.009
4	B11	21.29	0.077	0.009
5	B2	3.85	0.061	0.012
6	B18	29.00	0.072	0.009
7	O1	4.32	0.058	0.009
8	B1	4.34	0.050	0.008
9	B2	3.85	0.061	0.012
10	B2	3.85	0.061	0.012
11	B3	7.61	0.056	0.009
12	B2	3.85	0.061	0.012
13	B3	7.61	0.056	0.009
14	B1	4.34	0.050	0.008
15	B8	10.21	0.082	0.014
16	B10	5.61	0.085	0.015
17	B12	13.96	0.082	0.010
18	B12	13.96	0.082	0.010
19	B8	10.21	0.082	0.014
20	B8	10.21	0.082	0.014
21	O15	6.86	0.107	0.012
22	-	-	-	-
23	-	-	-	-

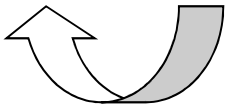

Bijlage II Dynamische modellering bodemzuurgraad

Aanleiding en achtergrond

Om te kunnen komen tot op processen gebaseerde reprofuncties voor zuurgraad is het hydrologische model SWAP (Van Dam e.a., 2008) door Cirkel e.a. (2015) gekoppeld aan het objectgeoriënteerde raamwerk voor chemische speciatie en stoftransport Orchestra (Meeussen, 2003). Deze koppeling (SWAP-ORCHESTRA V1.0) is noodzakelijk omdat de zuurgraad in de bodem zowel door chemische processen als door de af en aanvoer van stoffen wordt bepaald. In de koppeling levert het model SWAP de fluxen en worden het stoftransport en de chemische reacties in het in de Orchestra omgeving gebouwde model uitgerekend.

Fluxen

Waterfluxen die in het model worden meegenomen zijn:

- Neerslag
- Bodemverdamping
- Wortelopname (t.b.v. transpiratie)
- Run-off
- Drainage
- Kwel/wegzijging

Voor de berekening van gasfluxen door de bodem (vooralsnog alleen CO_2) wordt uitgegaan van gasdiffusie waarbij rekening wordt gehouden met de mate van waterverzadiging van de bodem.

In Figuur II.1 is een schematisch overzicht weergegeven van de in de modelstructuur meegenomen fluxen. Alle water-, gas- en stoffluxen worden tijdsafhankelijk doorgerekend. Op basis van de waterverzadiging en berekende CO_2 spanning wordt na elke tijdstap de verzadiging van het profiel uitgerekend. Ook worden tijdsafhankelijk chemische reacties en sorptieprocessen doorgerekend.

De schematisering in het ORCHESTRA model is gelijk gehouden aan die in SWAP. In deze studie is gekozen voor een systeem met in totaal 65 modellaagjes. De lengte van de verticale bodemkolom bedraagt 5 meter. In de bovenste 10 cm hebben de modellaagjes een dikte van 1 cm, van 10 tot 60 cm m-mv bedraagt de dikte 5 cm en van 60-500 cm –m.v. is deze 10 cm. De wortelzone heeft een dikte van 40 cm. In deze studie is uitgegaan van grondwaterafhankelijke condities omdat veranderingen in het waterbeheer en in het klimaat juist de waterstromen, en daarmee de zuurgraad, van natte gebieden zullen beïnvloeden, Bovendien onderscheidt de gekozen modelopzet zich juist voor deze condities ten opzichte van bestaande modellen.

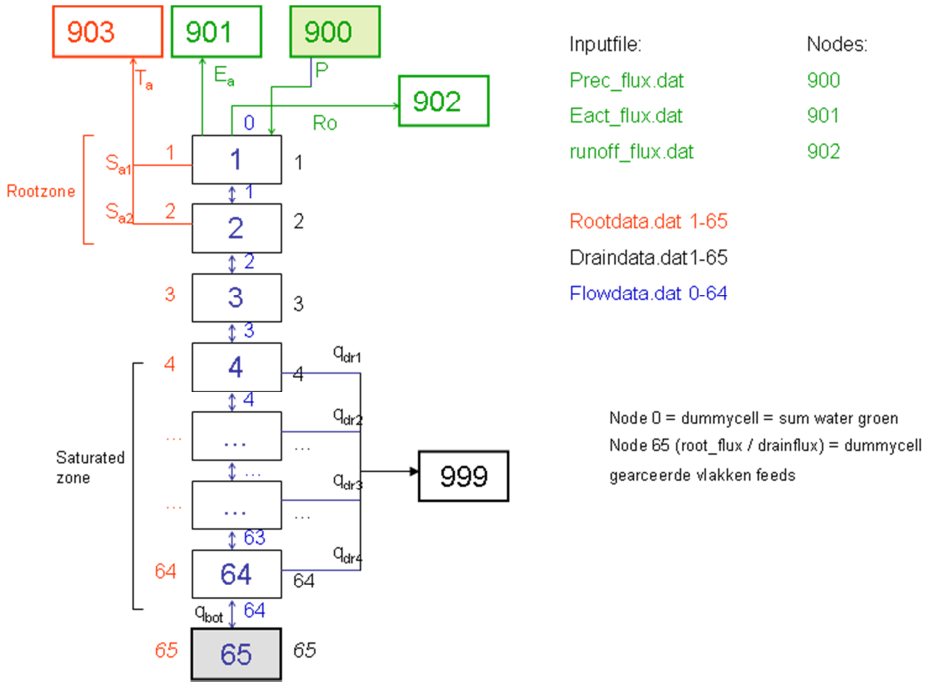

Figuur II.1. *Schematische weergave van de in Orchestra gebouwde modelstructuur (met arbitrair gekozen aantal cellen). De volgende fluxen worden meegenomen (900) Neerslag gecorrigeerd voor interceptieverdamping, (901) Bodemverdamping, (902) Run-off, (903) Transpiratie (wortelopname), (999) Drainage.*

Chemische processen

In deze versie worden de volgende chemische processen meegenomen:

- Sorptie/desorptie aan organisch materiaal (NICA-Donnan model voor Humic acid en Fulvic acid parameters gepubliceerd in Milne e.a. (2003)
- Sorptie/desorptie aan klei (Donnan model met parameters voor illitic clay minerals (McBride, 1994)
- Sorptie/desorptie aan oxides (Diffuse layer model voor hydrous ferric oxide met parameters zoals gepubliceerd in Dzombak en Morel (1990)
- Oplossen/neerslaan van Gibbsite
- Oplossen/neerslaan van Calciet
- pH afhankelijke Silica-verwering
- Carbonaatevenwichten
- Productie van CO_2 (wortelrespiratie) als functie van de gewasgroei (functie van de wateropname door wortels)
- Gasdiffusie van CO_2 afhankelijk van het vochtgehalte van de bodem

Voor de evenwichtsberekeningen wordt gebruik gemaakt van de Minteqv4 database. In het Orchestra model is voor chemische reacties gebruik gemaakt van standaardparameterwaarden. pH-afhankelijke chemische verwering en het vrijkomen van Ca^{2+} is vooralsnog in sterk versimpelde vorm meegenomen met een gemiddelde parameterwaarde voor verwering in de wortelzone onder graslanden naar Van der Salm en De Vries (2001). In het model is hierbij uitgegaan van 327 molc/ha/jaar over een wortelzone van 30 cm; in een vervolg kan, vooral als ook grondwateronafhankelijke profielen worden doorgerekend, een meer gedetailleerde opzet worden ingebouwd. Omgerekend naar in Orchestra gangbare eenheden geeft dit 1.15 10^{-12} molc/m^2/s/cm. Hierbij wordt er van uitgegaan dat het bij basische kationen alleen Ca^{2+} betreft en wordt geen verder onderscheid naar andere kationen gemaakt. De pH-afhankelijkheid van de verwering is meegenomen

door de verweringssnelheid te vermenigvuldigen met de volgende factor: $10^{0.5(pH_{ref}-pH_{act})}$, met pH_{ref} = referentie pH = 3.5 en pH_{act} = de actuele pH (Van der Salm en De Vries, 2001; Mol-Dijkstra e.a., 2006).

De productie van CO_2 is meegenomen door de wateropname door wortels (transpiratie, T, kg $H_2O/m^2/d$) te relateren aan de gewasproductie van de plant (yield, Y, kg droge stof/ha) volgens: $Y = 20T$; hierbij uitgaande van grasland met weinig of geen bemesting (Feddes, 1985). Vervolgens is de relatie tussen de opbrengst en onderhoudsrespiratie ($X_{m,r}$, kg CH_2O/kg droge stof/d) gelegd volgens $X_{m,r} = 0.015Y$ (Penning de Vries en Van Laar, 1982). Uit $CH_2O + O_2 \Rightarrow H_2O + CO_2 + energy$ volgt vervolgens de hoeveelheid vrijkomende CO_2.

Uiteraard is bovenstaande een versimpeling omdat ook de temperatuur een belangrijke factor is bij de onderhoudsrespiratie van planten. Bovenstaande zal hiermee een overschatting geven van de respiratie door planten. Echter, ook micro-organismen in de bodem respireren en produceren CO_2, wat in deze aanpak niet is meegenomen. Als het temperatuursverloop in de bodem bekend is kan de plantrespiratie nauwkeuriger worden berekend volgens: $X_m = X_{m,r} \cdot 2^{(T-T_r)/10}$ met T_r = 25 °C (Penning de Vries en Van Laar, 1982; Bartholomeus e.a., 2008). Een eerste verkenning met de simpele aanpak gaf een realistische range voor de CO_2-productie in de bodem gedurende het groeiseizoen.

Hydrochemie van grond- en regenwater

Voor de parameterisatie van de modellen zijn vijf grondwaterkwaliteitstypen gedefinieerd en twee neerslagtypen. Voor de grondwaterkwaliteitstypen is gebruik gemaakt van door representatieve drinkwaterpompstations opgepompt grondwater. Voor de definitie van de regenwaterkwaliteit is gebruik gemaakt van historische data van het LMR en recente metingen. Twee types zijn gedefinieerd: één type representatief voor samenstelling van infiltrerend regenwater in het begin van de jaren 80, met lage pH en hoge gehaltes stikstof en zwavel, en een tweede type representatief voor het huidige regenwater, met fors hogere pH en lage(re) zwavel en stikstofconcentraties (Tabel II.1).

Tabel II.1 Invoertypes waterchemie (grondwater en regenwater) (concentraties in mol/l)

Name	WatChemID	pH	Cl-.diss	HCO3-.diss	NO3-.diss	SO4-2.diss	PO4-3.diss	Ca+2.diss	Mg+2.diss	Na+.diss	K+.diss	Mn+2.diss	NH4+.diss	CO2[g].logact
NEERSLAGhuidig	1	5.27	8.24E-05	0.00E+00	4.52E-05	3.35E-05	1.75E-07	6.82E-06	8.50E-06	7.26E-05	4.42E-06	0.00E+00	8.22E-05	-3.50E+00
MANDERVEEN	2	5.59	9.07E-04	1.97E-04	4.44E-04	6.15E-04	2.33E-06	7.21E-04	2.72E-04	7.00E-04	9.41E-05	1.53E-06	1.33E-06	-1.40E+00
VORDEN	3	7.11	1.20E-03	5.82E-03	5.00E-07	8.11E-04	3.16E-07	3.44E-03	4.52E-04	7.87E-04	5.32E-05	3.82E-07	1.65E-05	-1.47E+00
VLIERDEN	4	7.1	2.28E-04	5.20E-03	5.00E-07	3.96E-05	1.09E-05	1.83E-03	4.38E-04	8.05E-04	1.05E-04	3.22E-06	8.60E-05	-1.51E+00
WOUDENBERG	5	7.8	3.18E-04	2.46E-03	5.00E-07	1.15E-05	5.20E-06	9.01E-04	2.65E-04	3.78E-04	8.59E-05	8.19E-07	1.85E-05	-2.53E+00
EPE	6	6.35	4.22E-04	3.61E-04	5.27E-05	1.89E-04	1.75E-06	2.72E-04	1.05E-04	4.26E-04	3.81E-05	3.82E-07	2.77E-07	-1.87E+00
NEERSLAGDeelen1979	7	3.95	3.70E-05	0.00E+00	9.00E-05	8.95E-05	0.00E+00	1.60E-05	5.00E-06	3.00E-05	3.00E-06	0.00E+00	1.19E-04	-3.50E+00

Bodemchemische karakterisering van de bodemfysische eenheden

Daarnaast is op basis van literatuurcijfers een eerste bodemchemische karakterisering gemaakt van bodemlagen per bodemfysische eenheid. Binnen de bodemfysische eenheden kunnen echter verschillende bodemchemische eigenschappen voorkomen. Om deze reden zijn per bodemfysische eenheid op basis van Wösten e.a. (1988) de dominante bodemtypes opgezocht en bodemchemisch gekarakteriseerd (Tabel II.2); vervolgens zijn parameterwaarden gekozen die zoveel mogelijk recht doen aan de dominante bodemtypen. Het gaat hierbij om waarden voor het gehalte klei en organische stof, de hoeveelheid ijzer(hydr)oxiden, de hoeveelheid Gibbsite en de hoeveelheid calcium (Tabel II.3). De hoeveelheid calcium in de bodem is geschat door allereerst het kalkpercentage van het dominante bodemtype per bodemfysische eenheid om te rekenen naar mol Ca^{2+} per kg vaste fase. Het geadsorbeerde deel is berekend door allereerst de CEC te schatten op basis van het

lutum- (*L*) en het organische-stofgehalte (*OM*) van het dominante bodemtype volgens de vergelijking van Breeuwsma e.a. (1986), waarbij de CEC van het organische deel pH-afhankelijk is gemaakt volgens Scheffer e.a. (2002). Vervolgens is de calciumbezetting van het adsorptiecomplex geschat afhankelijk van de kalkrijkdom van de bodem. Hierbij is uitgegaan van 90% bezetting met calcium in kalkrijke bodems, 70% bezetting in kalkarme bodems en 60% bezetting in kalkloze bodems. De CEC vermenigvuldigd met de calciumbezetting geeft vervolgens een schatting van de geadsorbeerde hoeveelheid calcium. De geadsorbeerde hoeveelheid calcium en de in kalk aanwezige hoeveelheid calcium zijn vervolgens opgeteld. De hoeveelheden ijzer(hydr)oxiden (HFO) en de hoeveelheid aluminiumoxiden (Gibbsite) zijn geschat op basis van de massafractie en lutum en getallen van Breeuwsma (1990) voor de bijbehorende mineralogische samenstelling per bodemfysische eenheid. Het reactieve oppervlak van de ijzer- en aluminiumoxiden is constant gehouden. Dit kan echter ook dynamisch afhankelijk worden gemaakt van oplossen of juist neerslaan van deze oxiden.

Tabel II.2. *Dominante bodemtypes per bodemfysische eenheid naar Wösten et al. (1988)*

Bodemfysische	Dominante bodemtypes			
eenheid	1	2	3	4
1	hVb	hVc	ohVc	
2	aVz	hVz		
3	pVb	kVb		
4	kVz			
5	iWz	iWp		
5	iWz	iWp		
6	Wo			
7	Zd20	Zd21		
8	Hd21			
9	Hn21			
10	Hn21g			
10	Hn21g			
11	Hn23x			
12	zEZ21			
13	pZg23			
14	gHd30			
15	Mn25A			
16	Mn35A	Rd90A	Rd90C	
17	Rn44C	gMn83C	kMn48C	Rn47C
18	Rv01C	Mv41C		
19	Mn22A			
20	Rn52A			
21	BLd6			

Tabel II.3. *Bodemchemische karakterisering bodemlagen per bodemfysische eenheid (in de tabel wordt uitgegaan van instroom van grondwater van het 'Vlierden' type (4)*

soilID	ISOILLAY1	porosity	density	CLAY_kgkg	SHA_kgkg	HFO_kgkg	Gibbsite.kg	Ca+2.kg	WatChemID
1	1	0.77	0.6	0.2363	0.475	0.0191	0.1264	0.331	4
1	2	0.86	0.35	0.0045	0.7	0.0065	0.0229	0.332	4
2	1	0.8	0.6	0.0184	0.54	0.0103	0.0394	0.261	4
2	2	0.86	0.35	0.0045	0.7	0.0065	0.0229	0.276	4
2	3	0.38	1.55	0.0294	0.02	0.0216	0.0802	0.006	4
3	1	0.59	1.3	0.3868	0.09	0.0325	0.1311	0.094	4
3	2	0.86	0.35	0.0045	0.7	0.0065	0.0229	0.332	4
4	1	0.59	1.3	0.3868	0.09	0.0325	0.1311	0.094	4
4	2	0.86	0.35	0.0045	0.7	0.0065	0.0229	0.276	4
4	3	0.38	1.55	0.0294	0.02	0.0216	0.0802	0.006	4
5	1	0.42	1.4	0.0284	0.055	0.0208	0.0774	0.031	4
5	2	0.89	0.4	0.0048	0.68	0.0069	0.0244	0.276	4
5	3	0.38	1.55	0.0294	0.02	0.0216	0.0802	0.006	4
6	1	0.77	0.6	0.2363	0.475	0.0191	0.1264	0.331	4
6	2	0.56	1.25	0.4088	0.015	0.0348	0.1402	0.155	4
7	1	0.36	1.6	0.0148	0.015	0.0212	0.075	0.089	4
7	2	0.36	1.6	0.0148	0.015	0.0212	0.075	0.309	4
8	1	0.43	1.55	0.0146	0.025	0.021	0.0743	0.031	4
8	2	0.36	1.6	0.0148	0.015	0.0212	0.075	0.006	4
9	1	0.42	1.4	0.0284	0.055	0.0208	0.0774	0.031	4
9	2	0.38	1.55	0.0294	0.02	0.0216	0.0802	0.006	4
10	1	0.42	1.4	0.0284	0.055	0.0208	0.0774	0.031	4
10	2	0.38	1.55	0.0294	0.02	0.0216	0.0802	0.006	4
10	3	0.32	1.6	0.0099	0.01	0.0211	0.0735	0.006	4
11	1	0.46	1.3	0.046	0.08	0.0209	0.0823	0.031	4
11	2	0.38	1.55	0.0294	0.02	0.0216	0.0802	0.006	4
11	3	0.33	1.35	0.0528	0.04	0.022	0.0877	0.006	4
12	1	0.42	1.4	0.0284	0.055	0.0208	0.0774	0.031	4
12	2	0.38	1.55	0.0294	0.02	0.0216	0.0802	0.006	4
13	1	0.46	1.3	0.046	0.08	0.0209	0.0823	0.031	4
13	2	0.34	1.6	0.0495	0.01	0.0225	0.0885	0.006	4
13	3	0.38	1.55	0.0294	0.02	0.0216	0.0802	0.006	4
14	1	0.43	1.55	0.0146	0.025	0.021	0.0743	0.031	4
14	2	0.32	1.6	0.0099	0.01	0.0211	0.0735	0.006	4
15	1	0.43	1.4	0.1372	0.02	0.0253	0.0928	0.779	4
15	2	0.46	1.5	0.1436	0.01	0.0257	0.0946	0.742	4
16	1	0.43	1.35	0.2943	0.035	0.0304	0.119	0.813	4
16	2	0.48	1.4	0.197	0.015	0.0275	0.1035	0.857	4
17	1	0.54	1.1	0.6144	0.04	0.0414	0.174	0.177	4
17	2	0.57	1.2	0.6255	0.015	0.0423	0.1777	0.148	4
18	1	0.54	1.1	0.6144	0.04	0.0414	0.174	0.177	4
18	2	0.57	1.2	0.6255	0.015	0.0423	0.1777	0.148	4
18	3	0.86	0.35	0.0045	0.7	0.0065	0.0229	0.332	4
19	1	0.43	1.4	0.1372	0.02	0.0253	0.0928	0.629	4
19	2	0.48	1.4	0.197	0.015	0.0275	0.1035	0.757	4
19	3	0.38	1.55	0.0294	0.02	0.0216	0.0802	0.709	4
20	1	0.43	1.4	0.1372	0.02	0.0253	0.0928	0.3	4
20	2	0.48	1.4	0.197	0.015	0.0275	0.1035	0.557	4
20	3	0.32	1.6	0.0099	0.01	0.0211	0.0735	0.509	4
21	1	0.41	1.35	0.147	0.02	0.0256	0.1247	0.006	4
21	2	0.41	1.35	0.147	0.02	0.0256	0.1247	0.006	4

Modelsimulaties

De eerste stap van de modelsimulaties is het in evenwicht brengen van de grondwatersamenstelling met de geschematiseerde bodemchemische condities. Na deze initialisatie wordt vervolgens verder gerekend met in de bodemkolom instromend neerslagwater en grondwater. Per tijdstap worden de fluxen, saturatie en de uitkomsten van een groot aantal bodem- en hydrochemische berekeningen als uitvoer weggeschreven.
Uit de eerste modelsimulaties blijkt dat de simulaties resulteren in een plausibele pH range en dat de hydrologie duidelijk doorwerkt op het verloop van de pH in de bodem (Figuur II.2). In het hier weergegeven geval van een (natte) koopveengrond met kwelinvloed treedt de hoogste pH steeds op in het najaar (meestal halverwege oktober). Door de geringe grondwateraanvulling tot de herfst is de grondwaterinvloed dan maximaal. Met de toenemende grondwateraanvulling in de herfst en winter daalt de pH weer tot het begin van de zomer, waarna weer een stijging wordt ingezet. In het voorbeeld is tevens de sterke invloed van een droog jaar (1976) zichtbaar waardoor de kwelinvloed in de wortelzone maximaal wordt en de pH sterk stijgt.

Uit de figuur wordt echter ook duidelijk dat de gekozen beginconditie van grote invloed is op het verdere verloop van de pH. Het kan een groot aantal rekenjaren duren voordat stabilisatie optreedt.

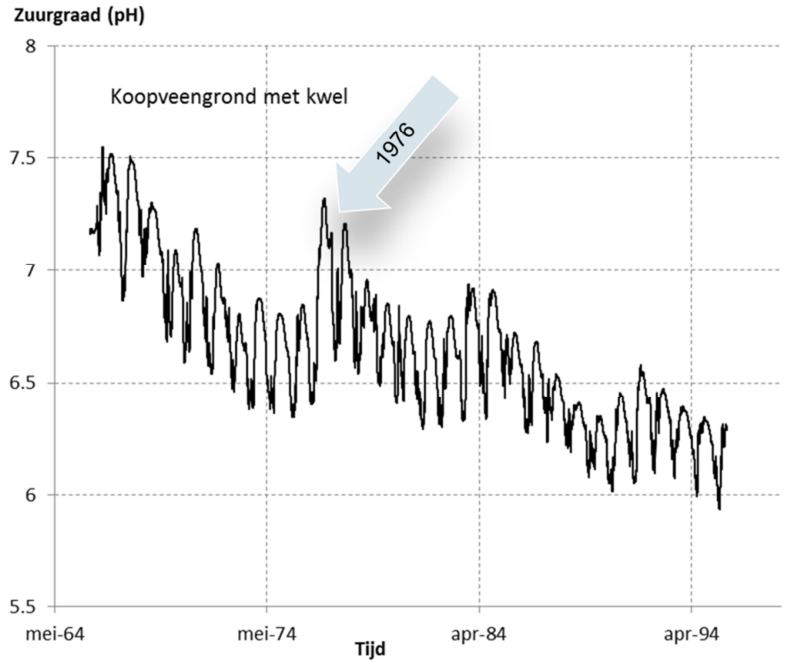

Figuur II.2. Verloop van de pH over een rekenperiode van 30 jaar voor bodemfysische eenheid 2 en een initiële pH van 7.1.

Modelresultaten

Een in de vorige paragraaf besproken modelsimulatie vraagt ca. 12 -24 uur rekentijd. Online doorrekenen per modelgridcel van een bepaald gebied is daardoor extreem rekenintensief. Er zijn immers vele honderden tot duizenden unieke combinaties van parameters mogelijk, en oneindig veel hydrologische randvoorwaarden. Om deze reden is getracht om reprofuncties op basis van een beperkt aantal representatieve modelruns af te leiden. Vooralsnog zijn 5 representatieve bodemfysische eenheden geselecteerd (Tabel II.4). De 5 bodemfysische eenheden omvatten gezamenlijk 38 % van het landoppervlak van Nederland. Voor de stuifzandgronden is een kalkrijke eenheid doorgerekend, de overige eenheden zijn

kalkarm of kalkloos. De keuze voor een kalkrijke variant is gelegen in het feit dat deze het grootste areaal vormt van deze eenheid in de kustduinen. In een vervolgstudie zou getracht moeten worden de overige bodemfysische eenheden in te vullen.

Per bodemfysische eenheid zijn vervolgens 15 verschillende combinaties van diepe stijghoogte, slootafstand en drainageweerstand doorgerekend (Tabel II.5). De diepe stijghoogte is gesimuleerd als een sinusoïde met een amplitude van 25 cm en een periode van 365 d. De weerstand van de scheidende laag is gesteld op 100 d. Deze scenario's resulteerden in een GLG-bereik van ca. -1.5 m –m.v. tot 0.4 m –m.v. en een GHG bereik rond maaiveld en een kwelflux van -0.7 – 2.6 mm/d. Het gaat hierbij dus om grondwaterafhankelijke omstandigheden met kwel of beperkte wegzijging.

De doorgerekende scenario's voor het 'huidige' klimaat resulteren in realistische pH's in de wortelzone (gemiddelde over de bovenste 10 cm van de bodem) (Figuur II.4). Opvallend is de stabiel hogere pH van de kalkhoudende stuifzandbodem en het zeer nauwe pH bereik van de (kalkarme) kleibodems. Bij deze laatste twee bodems wordt de pH in grote mate bepaald door de bodemchemische eigenschappen en niet zozeer door de hydrologische scenario's.

Echt lage pH waarden (rond pH 4) zijn in de modelscenario's niet bereikt; de pH zakt tot minimaal 5.13 bij de Koopveen en Madeveengronden en tot minimaal 5.24 bij de Veldpodzolgronden. De oorzaak hiervoor is gelegen in de bewust gekozen grondwaterafhankelijke condities van de scenario's. Aanvoer van basen via capillaire nalevering heeft een dempend effect op de verzuring van de bodems; daarnaast zijn de effecten van (historische) atmosferische depositie vooralsnog beperkt meegenomen in de scenario's. Ook de gekozen beginconditie en de samenstelling van het opwellende grondwater is van invloed op de na 30 jaar bereikte verzuring. In de scenario's is vooralsnog als startconditie uitgegaan van 100% grondwaterinvloed, hierbij uitgaande van een 'Vlierden' (Tabel II.1) grondwatersamenstelling.

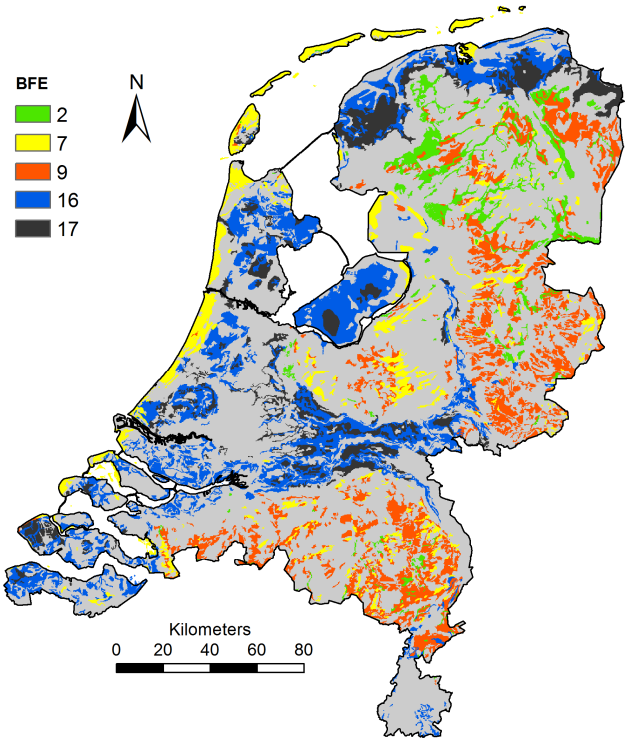

Figuur II.3. Verspreiding geselecteerde bodemfysische eenheden (BFE).

Tabel II.4. *Beschrijving doorgerekende bodemfysische eenheden (BFE) (van eenheid 7 is vooralsnog alleen de kalkrijke variant doorgerekend).*

BFE	Omschrijving		Dominante eenheden op bodemkaart 1:50.000
	Bodemkaart	Beschrijving	
2	Koopveengronden en madeveengronden	Broekveen op zand met veraarde bovengrond	aVz, hVz
7a	Stuifzandgronden	(Kalkrijk), leemarm fijn zand	Zd20, Zd21
9	(Veld)podzolgronden in zwak lemig fijn zand	Zwak lemig fijn zand, humeuze toplaag	Hn21
16	Homogene lichte kleigronden	Kalkloze humeuze lichte klei op zavel	Mn35A, Rd90A, Rd90C
17	Zware klei	Humeuze zeer zware klei	Rn44C, gMn83C, kMn48C, Rn47C

Tabel II.5. *De 15 doorgerekende hydrologische scenario's.*

Gemiddelde stijghoogte aquifer (m +m.v.)	Slootafstand (m)	Drainage-weerstand (d)
-62.2	207	310
-58.0	46	70
-41.2	245	368
-34.2	197	295
-33.8	241	361
-10.5	40	59
-29.0	236	354
-11.0	84	127
-21.3	198	297
1.1	161	242
14.4	91	137
17.4	140	210
10.2	231	347
29.0	111	166
22.7	170	255

Na het doorrekenen van de scenario's met 'huidige' meteorologische condities, zijn de scenario's vervolgens doorgerekend met meteorologische condities volgens het KNMI W+ klimaatscenario. Onder het W+ scenario en de gekozen modelcondities blijven de bodem-pH's gemiddeld hoger en worden bij verschillende hydrologische condities hoge pH-waarden bereikt (Figuur II.4 en Figuur II.5). Opvallend verschil met de huidige situatie is de gemiddeld hoog blijvende pH in de kalkrijke duingrond. Bij het droge W+ scenario lijkt beduidend langzamere ontkalking op te treden dan in de huidige situatie. Bij de andere bodems speelt vooral het in het W+ scenario vaker verdwijnen van de neerslaglens en tot maaiveld geraken van basenrijk grondwater een belangrijke rol bij de buffering van de bodem. Geconcludeerd kan worden dat de door ons gekozen modelopzet duidelijk gevoelig is voor de invloed van het klimaat en hiermee samenhangende hydrologische veranderingen,

dit in tegenstelling tot andere modelkoppelingen (Figuur II.6). De duidelijke koppeling met de hydrologie maakt de SWAP-ORCHESTRA opzet een klimaat-robuuste methode om relaties af te leiden tussen bodemchemie, hydrologie en hydrochemie in grondwaterafhankelijke systemen.

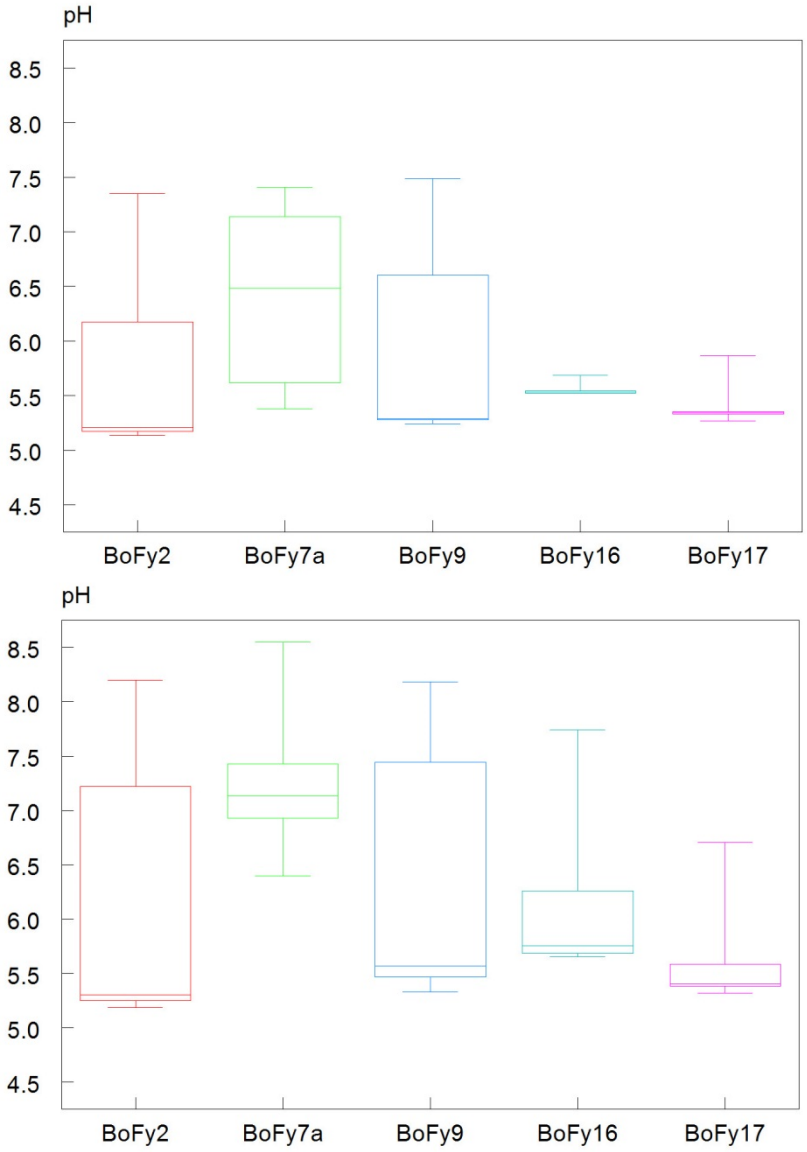

Figuur II.4. Box-Whisker plots van de resultaten van de 5 doorgerekende bodemfysische eenheden uitgaande van: boven, het huidige klimaat, onder het W+ scenario in 2050 (zie Tabel II.4 voor een beschrijving van de bodems).

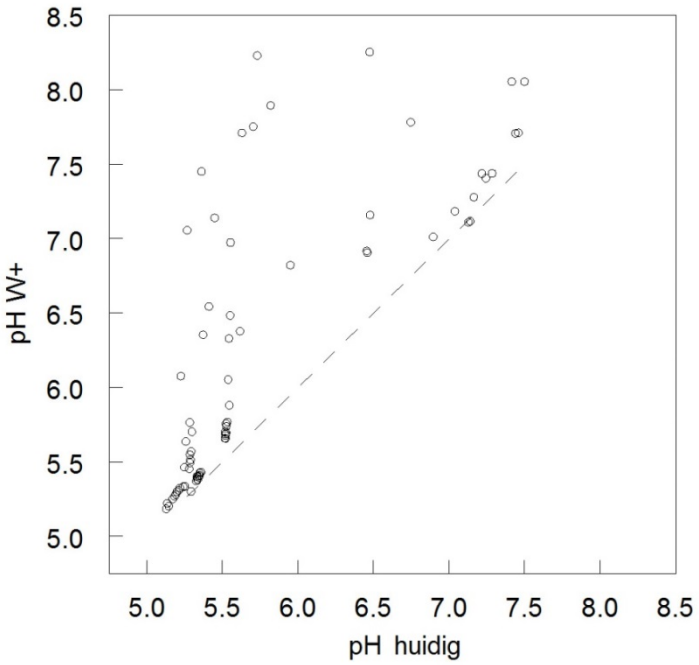

Figuur II.5. *Vergelijking tussen de met de SWAP-ORCHESTRA berekende bodem pH voor huidige meteorologische condities en het W+ scenario. Er treden volgens deze modelberekeningen duidelijke veranderingen op die vooral samenhangen met de mate van uitloging en neerslaglensdynamiek.*

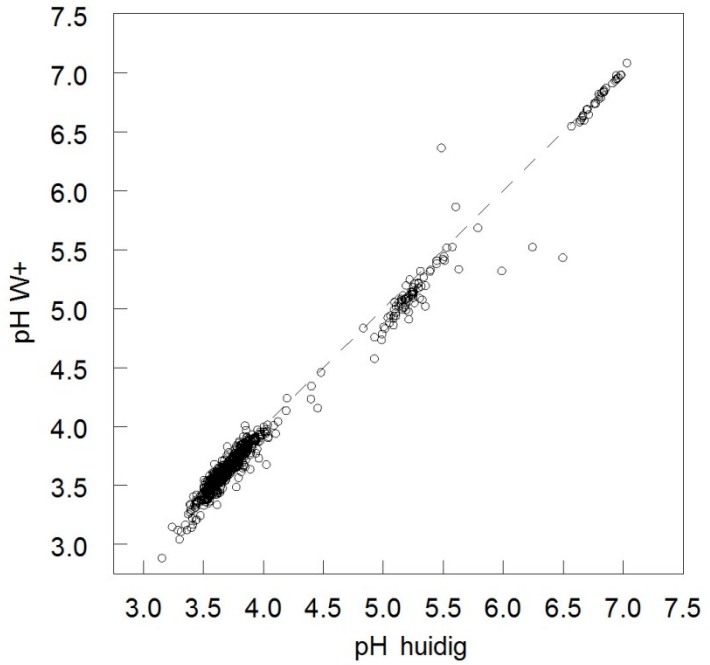

Figuur II.6*. Vergelijking tussen de met NHI-SMART-SUMO berekende bodem pH voor huidige meteorologische condities en het W+ scenario. Er treden volgens deze modelberekeningen nauwelijks veranderingen op (berekeningswijze beschreven in Witte e.a. (2011)).*

Verkenning mogelijkheden reprofuncties

Onderzocht is in hoeverre reprofuncties kunnen worden afgeleid uit de modeluitkomsten. Er is er voor gekozen om de berekende pH te relateren aan de GLG, de kwelflux en de run-off flux (respectievelijk MLG, mean flux en mean runoff in Figuur II.7). De kwelflux en de run-off flux zijn sterk bepalend voor de dynamiek van de neerslaglens en de GLG bepaalt mede de

positie van de lens in het profiel. Andere verklarende variabelen bleken ofwel van geen invloed of sterk gecorreleerd met genoemde variabelen. Daarnaast is als criterium de databeschikbaarheid van de verklarende variabelen in regionale modelstudies gehanteerd. In verband met de lange rekentijd zijn slechts 15 hydrologische randvoorwaarden doorgerekend. De simulaties werden automatische aangeroepen met het eerder voor PROBE ontwikkelde programma GTST (Bartholomeus en Witte, 2013). In Figuur II.7 is als voorbeeld de relatie tussen zuurgraad en de verschillende verklarende variabelen geplot voor bodemfysische eenheid 2 (Koopveengronden).

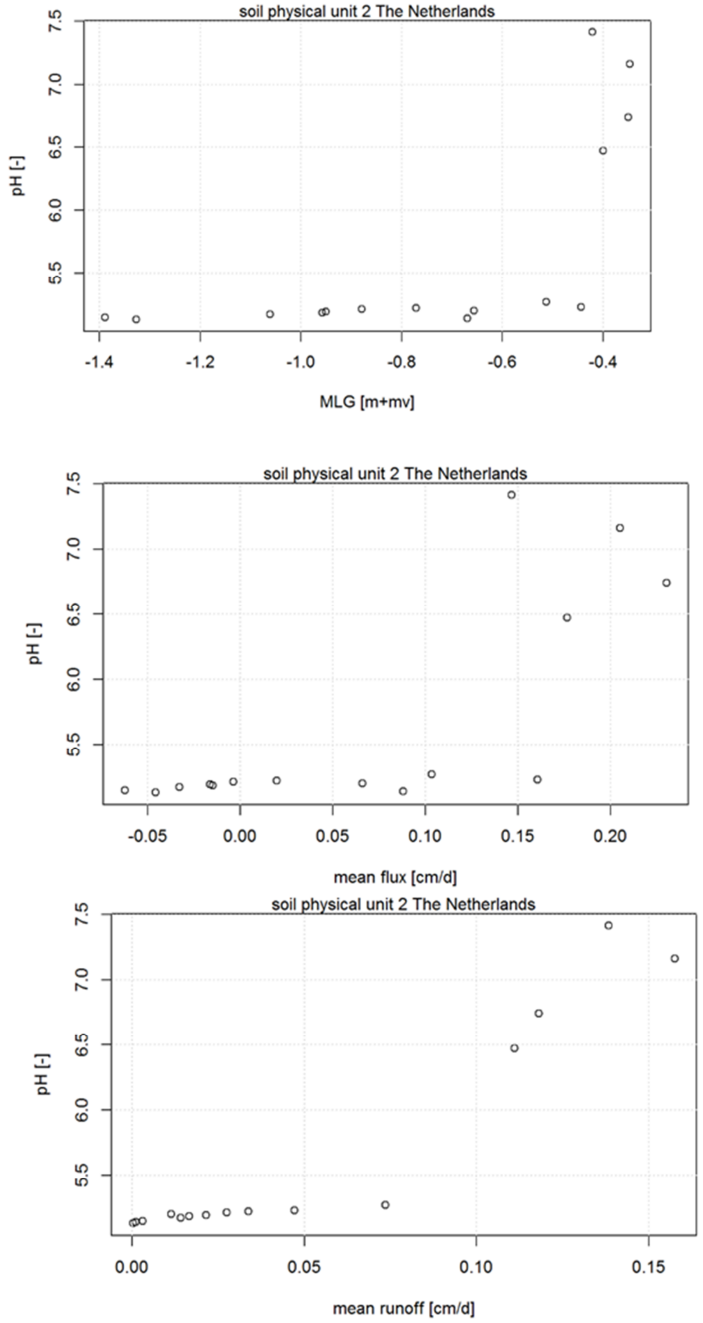

Figuur II.7. *Voorbeeld van relaties tussen de verklarende variabelen GLG, kwelflux en run-off flux en de bodem pH in de bovenste 10 cm van de bodem (BoFy 2)*

Uiteindelijk bleken reprofuncties met een combinatie van runoff en GLG als verklarende variabelen de beste fit te geven op de met de SWAP-ORCHESTRA koppeling gesimuleerde data (Figuur II.8 en Figuur II.9). De verklaarde variantie is voor de zand-, veen- en lichte-kleibodem goed met waarden voor R^2_{adj} variërend tussen 0.67 en 0.89. De fit op de simulaties met de zware kleibodem (bodemfysische eenheid 17) is echter onbevredigend met een R^2_{adj} van 0.36. Daarnaast is de verdeling van de berekende pH-waarden over de functie discutabel voor zowel bodemfysische eenheid 16 als 17. De slechte fit komt doordat de pH in deze kleibodems tamelijk ongevoelig is voor hydrologische condities en meer wordt bepaald door de bodemchemische condities. Binnen de nu gehanteerde (representatieve) range van hydrologische scenario's is dan ook niet veel variatie in de berekende bodem-pH te verwachten.

Geconcludeerd wordt dat het met de in deze studie ontwikkelde methodiek mogelijk is reprofuncties af te leiden voor de bodem-pH, maar dat de nu gegenereerde functies nog verre van volmaakt zijn. Zowel de statistische robuustheid, als het feit dat we niet alle bodemfysische eenheden hebben kunnen doorrekenen, maakt dat het nog te vroeg is om deze functies in te bouwen in PROBE. Inbouw is momenteel ook niet aan de orde omdat PROBE dan moet worden aangepast aan andere hydrologische invoer (run-off).

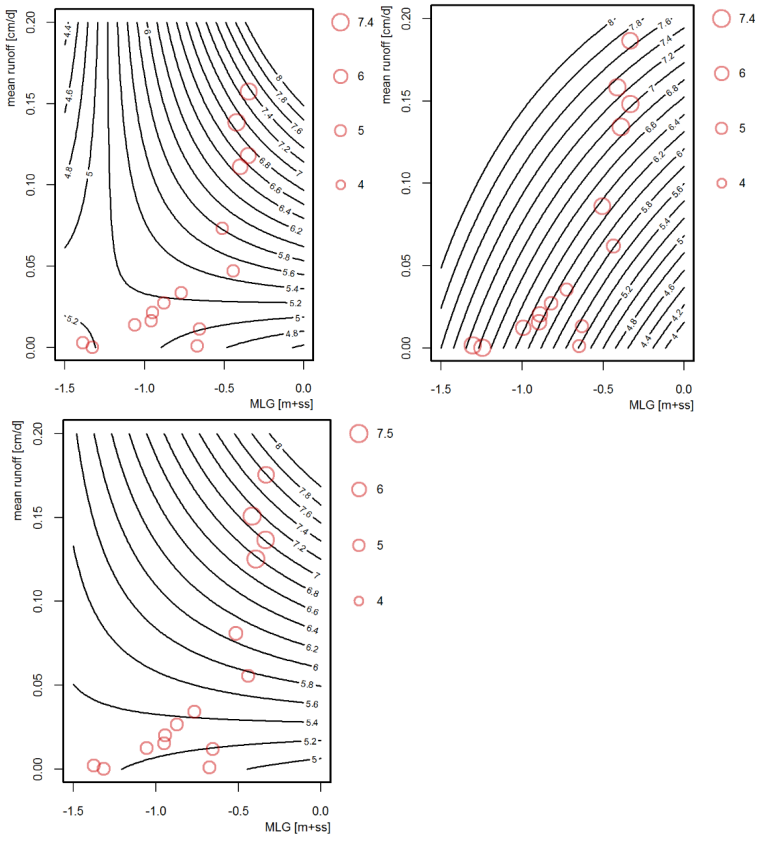

Figuur II.8. *Afgeleide reprofuncties voor pH (contourplots) voor het huidige klimaat op basis van GLG en runoff voor (van links naar rechts) bodemfysische eenheid 2 (R2adj = 0.894), bodemfysische eenheid 7 (R2adj= 0.666) en bodemfysische eenheid 9 (R2adj= 0.832). De rode punten zijn de simulaties met SWAP-ORCHESTRA waarop de reprofuncties zijn gefit.*

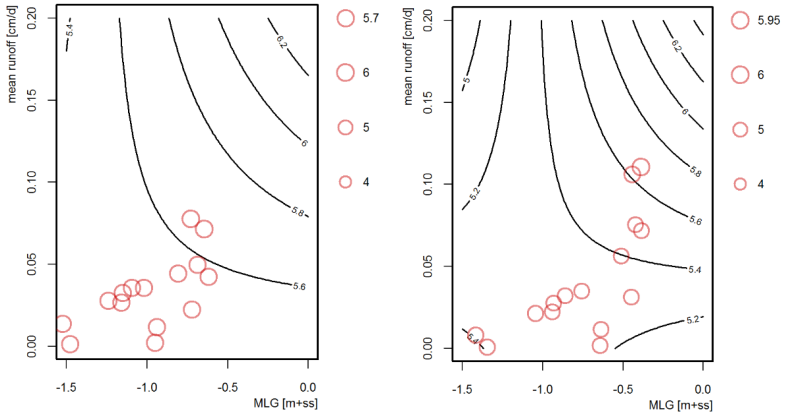

Figuur II.9. *Afgeleide reprofuncties voor pH (contourplots) voor het huidige klimaat op basis van GLG en runoff voor (van links naar rechts) bodemfysische eenheid 16 (R2adj = 0.681) en bodemfysische eenheid 17 (R2adj= 0.362). De rode punten zijn de simulaties met SWAP-ORCHESTRA waarop de reprofuncties zijn gefit.*

Met name door het verbeteren van de set met bodemchemische gegevens per bodemfysische eenheid en het uitbreiden van de range hydrologische scenario's (meer punten voor een meer robuuste fit) kan de significantie van de relaties worden verbeterd. Bijzondere aandacht dient hierbij uit te gaan naar drogere of zelfs grondwateronafhankelijke profielen. Ook dient de kwelwaterkwaliteit in eventuele toekomstige berekeningen gevarieerd te worden. Daarnaast kan dan ook de bodemchemische kant van het model worden verbeterd door onder meer het meenemen van redoxreacties, die in zeer natte milieus van grote invloed zijn op de zuurgraaddynamiek, en rekening te houden met de opbouw en afbraak van organische stof. Het laatst houdt in dat SWAP-ORCHESTRA wordt uitgebreid met een koppeling aan CENTURY.

Conclusies

- **Dynamische modellering pH in grondwaterafhankelijke profielen geslaagd**
  In deze studie zijn we, na het oplossen van enkele lastige en tijdrovende numerieke problemen, erin geslaagd het bodemfysische model SWAP te koppelen aan een binnen de ORCHESTRA omgeving ontwikkeld bodemchemisch model. Met deze koppeling is het mogelijk de pH dynamisch te modelleren.

- **Duidelijke invloed van meteorologische condities**
  Uit de modelresultaten blijkt dat de invloed van klimaatverandering via de hydrologie doorwerkt op de pH in de bovenste 10 cm van de bodem. Deze invloed wordt vooral bepaald door verdampingsgedreven capillaire nalevering en de omvang van de run-off. Hierdoor kan tijdelijk de neerslaglens verdwijnen en het adsorptiecomplex worden opgeladen. Daarnaast zijn de meteorologische condities via de bodemvochtdynamiek van invloed op de diffusie van CO_2(g) in de bodem en daarmee via de carbonaatchemie van invloed op de pH. De modelopzet maakt het mogelijk om rekening te houden met deze gevoeligheden, wat vooral van belang is bij klimaatprojecties.

- **Realistische pH ranges worden gesimuleerd**
  De voor de vijf bodemfysische eenheden berekende pH-ranges zijn realistisch voor grondwater-beïnvloede systemen met deze bodems.

- **Run-off in combinatie de GLG sterk bepalend voor pH dynamiek**
  Uit de analyse van de resultaten komt naar voren dat de mate waarin run-off wordt gegenereerd sterk bepalend is voor de dynamiek van de neerslaglenzen en daarmee voor de oplading van het adsorptiecomplex en uiteindelijk voor de pH in de wortelzone.

- **Inzicht in effecten klimaatverandering**
  In tegenstelling tot eerdere studies (Figuur II.6) blijkt de modelopzet gevoelig voor meteorologische condities. Juist in grondwaterafhankelijke systemen is daardoor nadrukkelijk invloed van klimaatverandering te verwachten.

Discussie en aanbevelingen

- **Beperkte set hydrologische scenario's**
  In deze studie hebben we ons specifiek gericht op grondwaterafhankelijke systemen met basenrijk grondwater. De doorgerekende range van grondwaterstanden en grondwaterkwaliteiten is hierdoor beperkt. Aanbeveling 1: breidt de modelering verder uit naar grondwateronafhankelijke bodems en wegzijgingsscenario's en varieer met de kwaliteit van het kwelwater.

- **Beperkt aantal bodemtypen**
  De vijf bodemfysische eenheden waarvoor we voorlopige reprofuncties hebben afgeleid komen veel voor in Nederland en zijn representatief voor een grotere range aan bodems. In onze optiek was een nadere onderverdeling op basis van de beschikbare bodemchemische gegevens vooralsnog onvoldoende verdedigbaar. Aanbeveling 2: ontwikkel een vrij beschikbaar nationaal bestand van bodemchemische gegevens, liefst in samenwerking met Alterra.

- **Simpel scenario voor regenwatersamenstelling**
  Vooralsnog is uitgegaan van een constante regenwatersamenstelling. Grote veranderingen in atmosferische depositie zijn hierdoor niet in de berekeningen meegenomen. De modelopzet maakt het echter mogelijk om atmosferische depositiescenario's door te rekenen.

- **Sterke invloed van hydrochemische beginconditie**
  De hydrochemische beginconditie blijkt een forse invloed te hebben op het verloop van de pH gedurende de simulatieperiode. Het kiezen van een realistische en stabiele beginconditie blijkt echter maatwerk. Generieke invoerparameters voor de bodemeigenschappen moeten namelijk aansluiten bij de gekozen hydrochemische condities. Vooralsnog is er voor gekozen om het bodemchemische profiel in evenwicht te brengen met grondwater van het 'Vlierden' type. Idealiter wordt echter gebruik gemaakt van representatieve (zowel qua bodem als hydrochemisch) goed omschreven en bemeten proeflocaties per door te rekenen eenheid. Zie Aanbeveling 2.

- **Beperking aantal bodemchemische processen**
  Besloten in om vooralsnog geen redoxprocessen mee te nemen in de modellering. Zeker in natte kwelgebieden kunnen redoxprocessen echter van grote invloed zijn op de pH (Cirkel et al. 2014a,b). Aanbeveling 3: **bouw** deze functionaliteit in. Daarnaast is verwering vooralsnog erg simpel meegenomen, voor grondwateronafhankelijke profielen is deze verwering echter een belangrijke factor, verbetering van deze functionaliteit is gewenst (Aanbeveling 4). Tenslotte wordt aanbevolen (Aanbeveling 5) om voor de omzetting en opbouw van organische stof en de nutriënten huishouding in de bodem een koppeling te maken met het model CENTURY.

- **Optimalisatie verhouding rekentijden en kwaliteit modeluitkomsten**
  De huidige modelopzet resulteert in plausibele resultaten maar vergt erg veel rekentijd, zelfs op een hiervoor speciaal toegeruste rekenserver (16 core). Om bovenstaande verbeteringen door te kunnen voeren dient de rekentijd omlaag gebracht te worden. Dit kan door te kiezen voor een grovere bodemschematisering en/of grotere tijdstappen en door te rekenen op een netwerk van computers. Aanbeveling 6: Onderzoek de gevoeligheid van de modeluitkomsten voor deze aanpassingen.

Bijlage III Mede door project gegenereerde publicaties

1) Fujita, Y., P.M. Van Bodegom, H. Olde Venterink, H. Runhaar en J.P.M. Witte (2013a) Towards a proper integration of hydrology in predicting soil nitrogen mineralization rates along natural moisture gradients. *Global Biogeochemical Cycles*, vol 58, pag 302-312.
2) Fujita, Y., P.M. Van Bodegom en J.P.M. Witte (2013b) Relationships between nutrient-related plant traits and combinations of soil N and P Fertility. *PLoS ONE* 8(12), vol 8, no 12, pag e83735.
3) Fujita, Y., J.P.M. Witte en P.M. Van Bodegom (2014) Incorporating microbial ecology concepts into soil mineralization models to improve regional predictions of carbon and nitrogen fluxes. *Soil biology and biochemistry*, vol 28, no 3, pag 223-238.
4) Witte, J.-P.M., R.P. Bartholomeus, P.M. van Bodegom, D.G. Cirkel, R. van Ek, Y. Fujita, G.M. Janssen, T.J. Spek en H. Runhaar (2015) A probabilistic eco-hydrological model to predict the effects of climate change on natural vegetation at a regional scale. *Landscape Ecology*, vol 30, pag 835–854.

AGU PUBLICATIONS

Global Biogeochemical Cycles

RESEARCH ARTICLE
10.1002/2013GB004595

Key Points:
- We modeled soil C and N flux with various microbial parameters and structures
- Mineralization rates were validated with lab incubation data from diverse soils
- Inclusion of microbial biomass and C:N stoichiometry improves global models

Supporting Information:
- Readme
- AppendixA_fs01fs02.docx
- AppendixB_fs03.docx
- AppendixC_fs04.docx
- AppendixD_fs05.docx
- AppendixE_fs06.docx
- AppendixF_fs07.docx
- AppendixG_fs08.docx
- ts01.xlsx

Correspondence to:
Y. Fujita,
Yuki.Fujita@kwrwater.nl

Citation:
Fujita, Y., J.-P. M. Witte, and P. M. van Bodegom (2014), Incorporating microbial ecology concepts into global soil mineralization models to improve predictions of carbon and nitrogen fluxes, *Global Biogeochem. Cycles*, *28*, doi:10.1002/2013GB004595.

Received 26 FEB 2013
Accepted 15 FEB 2014
Accepted article online 17 FEB 2014

Incorporating microbial ecology concepts into global soil mineralization models to improve predictions of carbon and nitrogen fluxes

Yuki Fujita[1], Jan-Philip M. Witte[1,2], and Peter M. van Bodegom[2]

[1]Team Ecohydrology, KWR Watercycle Research Institute, Nieuwegein, Netherlands, [2]Department of Ecological Science, subdepartment of Systems Ecology, Vrije Universiteit, Amsterdam, Netherlands

Abstract Global models of soil carbon (C) and nitrogen (N) fluxes become increasingly needed to describe climate change impacts, yet they typically have limited ability to reflect microbial activities that may affect global-scale soil dynamics. Benefiting from recent advances in microbial knowledge, we evaluated critical assumptions on microbial processes to be applied in global models. We conducted a sensitivity analysis of soil respiration rates (*Cmin*) and N mineralization rates (*Nmin*) for different model structures and parameters regarding microbial processes and validated them with laboratory incubation data of diverse soils. Predicted *Cmin* was sensitive to microbial biomass, and the model fit to observed *Cmin* improved when using site-specific microbial biomass. *Cmin* was less affected by the approach of microbial substrate consumption (i.e., linear, multiplicative, or Michaelis-Menten kinetics). The sensitivity of *Cmin* to increasing soil N fertility was idiosyncratic and depended on the assumed mechanism of microbial C:N stoichiometry effects: a C overflow mechanism upon N limitation (with decreased microbial growth efficiency) led to the best model fit. Altogether, inclusion of microbial processes reduced prediction errors by 26% (for *Cmin*) and 7% (for *Nmin*) in our validation data set. Our study identified two important aspects to incorporate into global models: site-specific microbial biomass and microbial C:N stoichiometry effects. The former requires better understandings of spatial patterns of microbial biomass and its drivers, while the latter urges for further conceptual progress on C-N interactions. With such advancements, we envision improved predictions of global C and N fluxes for a current and projected climate.

1. Introduction

Current concerns about climate change urge for robust estimates of greenhouse gas emissions on national to global scales [*IPCC*, 2007]. At the same time, regional and national policymakers keep seeking for better tools to assess N loading to ecosystems. The increasing number of global soil organic matter (SOM) models (i.e., models developed for global-scale application [in the sense of *Manzoni and Porporato*, 2009]) in the last decades mirrors this general interest for predictions of soil carbon (C) and nitrogen (N) fluxes on large spatial scales. These SOM models typically have simple mathematical formulations [*Manzoni and Porporato*, 2009], whereas validation of such models is generally limited due to the inherent difficulty of collecting data on a large spatial scale.

In parallel, recent advances in knowledge about soil microbial processes have led to major improvements in small-scale SOM models (i.e., models describing small-scale processes, e.g., microbiology, rhizosphere, and aggregate models [in the sense of *Manzoni and Porporato*, 2009]). From a mechanistic point of view, SOM decomposition is increasingly seen as an enzyme-catalyzed process by microbes rather than an entirely substrate-controlled process [*Fang et al.*, 2005; *Schimel and Weintraub*, 2003; *Sinsabaugh et al.*, 2008]. Accordingly, an increasing number of small-scale SOM models include microbes as a state variable, through which physiological characteristics of microbes can be readily incorporated. The explicit treatment of microbial biomass not only improved the ability of models to capture C dynamics in fluctuating environments (e.g., through varying soil moisture [*Lawrence et al.*, 2009] and upon varying substrate supply [*Blagodatsky and Richter*, 1998]) but also provided a tool to theoretically investigate how functionally different microbes affect decomposition of C [*Allison et al.*, 2010; *Allison*, 2012].

Including microbe-mediated processes also facilitates a better understanding of the link between C and N flows. The traditional way of seeing decomposition as a completely C-limited process evolves toward an

integrated treatment of C-N interactions via microbial stoichiometry [*Schimel and Weintraub*, 2003]. An increasing, but still limited, number of small-scale SOM models adopt mechanisms of soil N controlling C flows [*Manzoni and Porporato*, 2009], and a series of analytical studies revealed that C-N interactions strongly determine the dynamics in soil C [*Manzoni and Porporato*, 2007; *Porporato et al*., 2003]. Empirical studies also support the importance of C-N interactions for predicting litter decomposition rates [*Manzoni et al*., 2008; *Parton et al*., 2007]. A possible mechanism responsible for the microbe-mediated effect of N on C is altered microbial growth efficiency (MGE) (i.e., the fraction of microbial C uptake that is incorporated into new microbial biomass). For example, MGE tends to decrease with decreasing availability of litter substrate N [*Manzoni et al*., 2008]. In addition, a theoretical analysis showed that MGE predominantly determines the threshold of the substrate C:N ratio where soil switches from an N sink to an N source [*Manzoni et al*., 2010]. High sensitivity of MGE to other environmental factors such as temperature and moisture [*Frey et al*., 2013; *Manzoni et al*., 2012] further indicates that microbial control on C-N interactions could be dynamic and complex.

This knowledge on microbe-mediated processes is, however, seldom incorporated into SOM models applied to large spatial scales [*Ostle et al*., 2009; *Wieder et al*., 2013]. Simple, substrate-controlled linear functions are typically used in global SOM models [e.g., *Todd-Brown et al*., 2013]. Such functions are argued to be sufficient to describe decomposition processes in long-term SOM models [*Manzoni and Porporato*, 2007], since fluctuations of microbial biomass, which can be captured only when microbe-substrate relations are explicitly included, will be masked by other predominating variability (e.g., climate) in the long term. Because spatial and temporal scales of most SOM models are correlated, global models are usually built for long-term simulations and therefore employ linear decomposition functions. We may question, however, if the omission of microbial properties in global models is truly justified. On the one hand, one may argue that among-site variations in biotic and abiotic factors are so large that differences in microbial properties may be ignored. On the other hand, there is enough evidence that predominantly biomass and physiological characteristics of microbes drive the biogeochemical cycles of C and N [*Falkowski et al*., 2008]. The fact that, for instance, microbial biomass differs by almost an order of magnitude among biomes [*Fierer et al*., 2009] may thus have important implications for global C and N fluxes. Moreover, even slightly different assumptions on C:N stoichiometry effects result in contrasting predictions of soil C efflux [*Manzoni and Porporato*, 2009], implying that analytical and empirical investigation of the C-N coupling in global SOM models merits serious consideration. This underlies the increasing number of calls for integrating microbial activity into SOM models to predict responses to global change [e.g., *Bardgett et al*., 2008; *McGuire and Treseder*, 2010; *Todd-Brown et al*., 2011; *Wieder et al*., 2013]. However, empirical data on a broad range of conditions to parameterize and validate such models are critically lacking [*Treseder et al*., 2012], which hampers a judgment of how much and where current models need to be improved [*Todd-Brown et al*., 2011].

Therefore, this study aims at evaluating the need to incorporate knowledge from microbial ecology into SOM models for predicting soil C and N fluxes across different soil conditions. For simplification, throughout this paper, we consider short-term fluxes from soils at steady-state conditions, without their long-term dynamical changes. To meet our research aim, we examined (using a simple process-based SOM model modified from CENTURY) whether incorporating small-scale microbial processes and microbial parameters improves across-site predictions of soil respiration and N mineralization rates. First, we tested the sensitivity of soil respiration and N mineralization rates to model parameter values of microbes (microbial biomass, microbial growth efficiency, microbial C:N ratio) under different model structures (i.e., three approaches of microbial substrate consumption kinetics and four presumed mechanisms of microbial C:N stoichiometry effects on C fluxes). Second, we validated the model outputs with empirical data obtained from laboratory incubation experiments of various soils. This allowed us to investigate whether inclusion of site-specific microbial data improves the model prediction across sites and which model structures seem generally most appropriate. Finally, we infer from our findings how global models can be improved by incorporating knowledge of microbial ecology, in terms of its variation in parameters and of its approaches, to allow more robust predictions of soil effluxes upon global change.

2. Methods

2.1. Model Approaches

We base our modeling framework on CENTURY [*Parton et al*., 1987], a commonly applied SOM decomposition model on large spatial (i.e., across-ecosystems) scale. Predicted carbon pools and fluxes of CENTURY have

been well validated with empirical data sets across ecosystems [e.g., *Kelly et al*., 2000; *Schimel*, 1994]. Moreover, CENTURY is simple enough to evaluate the components that we were interested in, while concepts similar to those in CENTURY are applied in most if not all global models.

CENTURY consists of three carbon pools with contrasting decomposition rates (i.e., active, slow, and passive pools). The active pool implicitly represents living microbes and microbial products, with microbes accounting for approximately one half to one third of carbon mass in the active pool [*Parton et al*., 1993]. Here we modified CENTURY to explicitly represent microbes, by splitting the active pool into a microbial pool and an easily decomposable substrate pool. For simplicity, we merged the slow and passive pools of CENTURY into one recalcitrant substrate pool. Parameter values were adjusted so that C flows remained realistic and equal to those in default CENTURY settings (see Appendix A for a full description about the model modifications). Table 1 summarizes all abbreviations of variables and parameters used in our model.

In most SOM models, the decomposition rate of the substrate is described in relation to microbes and substrate, as it is a process of microbes consuming the substrate. The way that substrate consumption is modeled, however, differs among current SOM models [*Manzoni and Porporato*, 2009]. The most commonly used approach (as in CENTURY) is a linear function, in which the decomposition rate is expressed as simple first-order kinetics with substrate (Figure 1a). This approach postulates that decomposition is a donor-controlled process, implicitly assuming that microbes respond so rapidly to changes in substrate availability that their biomass never limits the decomposition rates. The decomposition rate of this linear model, $DEC_{i,\mathrm{LIN}}$ (g C kg^{-1} soil day^{-1}), equals:

$$DEC_{i,\mathrm{LIN}} = k_{i,\mathrm{LIN}} \cdot C_i \tag{1}$$

where i is the substrate pool (i = S1 [easily decomposable substrate] or i = S2 [recalcitrant substrate]), C_i is the carbon concentration of substrate i (g C kg^{-1} soil), and $k_{i,\mathrm{LIN}}$ is the decomposition coefficient of C_i (day^{-1}). Here, $k_{i,\mathrm{LIN}}$ is described according to CENTURY, and it is modified by soil temperature, moisture, and texture (Appendix A).

Another approach of decomposition takes limitations by microbes into consideration (Figure 1b), and decomposition is assumed to increase linearly with concentrations of both microbes and substrates [e.g., *Porporato et al*., 2003]. The decomposition rate of this multiplicative model, $DEC_{i,\mathrm{MUL}}$ (g C kg^{-1} soil day^{-1}), equals:

$$DEC_{i,\mathrm{MUL}} = k_{i,\mathrm{MUL}} \cdot C_i \cdot C_\mathrm{B} \tag{2}$$

where $k_{i,\mathrm{MUL}}$ is the decomposition coefficient of C_i (day^{-1}) and C_B is the microbial biomass (g C kg^{-1} soil). We estimated the value of $k_{i,\mathrm{MUL}}$ such that equation (1) equals equation (2) when C_B is the median value of a global study ($C_{\mathrm{B\_gl}}$ = 0.87 g C kg^{-1} soil [*Cleveland and Liptzin*, 2007]): $k_{i,\mathrm{MUL}} = k_{i,\mathrm{LIN}} / C_{\mathrm{B\_gl}}$.

Alternatively, decomposition can be formulated as an enzyme-catalyzed reaction (Figure 1c). Decomposition depends on the enzymes produced by microbes as well as on substrate concentration [e.g., *Allison et al*., 2010; *Manzoni and Porporato*, 2007; *Schimel and Weintraub*, 2003]. Assuming that enzyme production is proportional to microbial biomass, the decomposition rate, $DEC_{i,\mathrm{MM}}$ (g C kg^{-1} soil day^{-1}), can be formulated with a simple Michaelis-Menten kinetics:

$$DEC_{i,\mathrm{MM}} = k_{i,\mathrm{MM}} \cdot \frac{C_i}{km_i + C_i} \cdot C_\mathrm{B} \tag{3}$$

where $k_{i,\mathrm{MM}}$ is the decomposition coefficient of C_i (day^{-1}) and km_i is the half saturation constant of C_i (g C kg^{-1} soil). We took the km_i values from *Allison et al*. [2010] assuming a soil temperature of 20°C and a bulk density of 1 g/cm^3: km_{S1} = 0.3 and km_{S2} = 600 g C kg^{-1} soil. We estimated the value of $k_{i,\mathrm{MM}}$ such that equation (1) equals equation (3) at global median values of microbial biomass and soil total C ($C_{\mathrm{TOT\_gl}}$ = 46 g C kg^{-1} soil [*Cleveland and Liptzin*, 2007]) with additional assumptions of $C_\mathrm{B} = 0.5 \cdot C_{\mathrm{S1}}$ and $C_{\mathrm{S2}} \approx C_{\mathrm{TOT}}$: $k_{\mathrm{S1,MM}} = k_{\mathrm{S1,LIN}} \cdot (km_{\mathrm{S1}} + 2 \cdot C_{\mathrm{B\_gl}}) / C_{\mathrm{B\_gl}}$, and $k_{\mathrm{S2,MM}} = k_{\mathrm{S2,LIN}} \cdot (km_{\mathrm{S2}} + C_{\mathrm{TOT\_gl}}) / C_{\mathrm{B\_gl}}$.

Soil respiration rates can be calculated for each type of microbial substrate consumption kinetics as:

$$potCmin_c = \sum_{i=\mathrm{S1}}^{\mathrm{S2}} (1 - e_i) \cdot DEC_{i,c} \tag{4}$$

Table 1. Model Variables and Parameters

Symbol	Unit	Description
Variables (continuous)		
C_B	g C kg^{-1} soil	Microbial biomass
C_{B_gl}	g C kg^{-1} soil	Median value of C_B in a global study
C_i	g C kg^{-1} soil	Carbon concentration in substrate *i*
C_{TOT}	g C kg^{-1} soil	Soil total C
C_{TOT_gl}	g C kg^{-1} soil	Median values of C_{TOT} in a global study
$Cmin_{m,c}$	g C kg^{-1} soil day^{-1}	Actual soil respiration rates, with substrate consumption kinetics *c* and with C:N stoichiometry effect *m*
$DEC_{i,c}$	g C kg^{-1} soil day^{-1}	Decomposition rate of substrate *i* with substrate consumption kinetics *c*
e_i	Fraction between 0 and 1	Microbial growth efficiency when assimilating substrate *i*
$e_{i,m}$	Fraction between 0 and 1	Microbial growth efficiency when assimilating substrate *i*, with C:N stoichiometry effect *m*
imm_max	g N kg^{-1} soil day^{-1}	Maximum N immobilization rate
$k_{i,c}$	day^{-1}	Decomposition coefficient of C_i with substrate consumption kinetics *c*
km_i	g C kg^{-1} soil	Half saturation constant of C_i
$I_{m,c}$	Fraction between 0 and 1	Inhibition factor on decomposition, with substrate consumption kinetics *c* and with C:N stoichiometry effect *m*
N_i	g N kg^{-1} soil	Nitrogen concentration in substrate *i*
NC_B	–	N:C ratio of microbes
NC_i	–	N:C ratio of substrate *i*
$Nmin_{m,c}$	g N kg^{-1} soil day^{-1}	Actual N mineralization rates, with substrate consumption kinetics *c* and with C:N stoichiometry effect *m*
$O_{m,c}$	g C kg^{-1} soil day^{-1}	Overflow of C at low N, with substrate consumption kinetics *c* and with C:N stoichiometry effect *m*
$potCmin_c$	g C kg^{-1} soil day^{-1}	Potential soil respiration rates with substrate consumption kinetics *c* (when N is not limiting decomposition processes)
$potNmin_c$	g N kg^{-1} soil day^{-1}	Potential N mineralization rate with substrate consumption kinetics *c*
Variables (category)		
c		Substrate consumption kinetics (*c* = LIN, MM, or MUL)
i		Substrate pool (*i* = S1 or S2)
m		Microbial C:N stoichiometry effect (*m* = none, INHin, INHorg, COin, or COorg)
Category labels		
LIN		Linear consumption kinetics
MUL		Multiplicative consumption kinetics
MM		Michaelis-Menten consumption kinetics
S1		Easily decomposable substrate
S2		Recalcitrant substrate
none		No C:N stoichiometry effect
INHin		Inhibition effects of N limitation on decomposition triggered by inorganic N
INHorg		Inhibition effect of N limitation on decomposition triggered by organic N
COin		C overflow upon N limitation triggered by inorganic N
COorg		C overflow upon N limitation triggered by organic N

where $potCmin_c$ (g C kg^{-1} soil day^{-1}) is the soil respiration rate calculated with microbial substrate consumption kinetics *c* (*c* = LIN, MUL, or MM) and e_i (fraction between 0 and 1) is the growth efficiency of microbes when assimilating substrate *i*. Note that $potCmin_c$ is the potential decomposition rate when C, but not N, is limiting decomposition processes. The actual soil respiration rates can deviate from the potential decomposition rates when N is limiting (see the following section).

N mineralization is coupled strongly to the decomposition of C, as both N and C are bound to organic compounds. When soil N is not limiting, the rate of N mineralization (i.e., potential N mineralization rate $potNmin_c$, g N kg^{-1} soil day^{-1}) depends solely on the amount of C decomposed and the C:N ratios of microbes

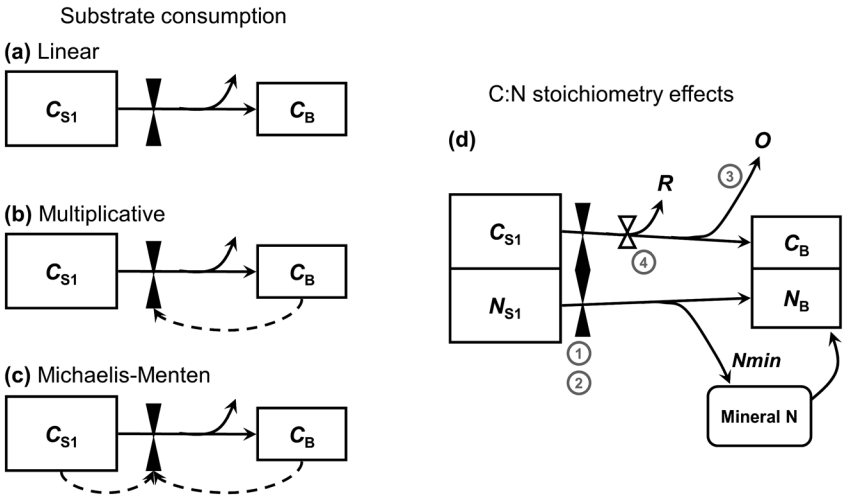

Figure 1. Model structure of C and N in microbes (C_B and N_B) and in easily decomposable substrate pool (C_{S1} and N_{S1}). The interactions between microbes and recalcitrant substrate pool (C_{S2} and N_{S2}) are not shown but identical to C_B-C_{S1} and N_B-N_{S1} interactions. Solid lines represent flows of C and N, whereas dashed lines represent influence on flow rates. (a–c) Three approaches of substrate consumption by microbes: linear (LIN), multiplicative (MUL), and Michaelis-Menten (MM). (d) Four mechanisms of microbial C:N stoichiometry effects on C flows: 1. inhibition effect triggered by inorganic N (INHin); 2. inhibition effect triggered by organic N (INHorg); 3. C overflow triggered by inorganic N (COin); and 4. C overflow triggered by organic N (COorg). INHin and INHorg influence decomposition rates, COin affects C overflow which is not related to microbial growth (*O*), and COorg influences microbial growth efficiency. *R* represents growth-related respiration, and *Nmin* represents N mineralization.

and substrate. When assuming that all available organic N is assimilated by microbes prior to mineralization to ammonium, $potNmin_c$ can be formulated as the difference between N released from the decomposed organic compounds and N assimilated into microbial biomass as [*Manzoni and Porporato*, 2009]:

$$potNmin_c = \sum_{i=S1}^{S2} \left(DEC_{i,c} \cdot NC_i - DEC_{i,c} \cdot e_i \cdot NC_B \right) \tag{5}$$

where NC_i is the N:C ratio of substrate i and NC_B is the N:C ratio of microbes. This is the same approach as in the original version of CENTURY (although later versions allow varying N:C ratio of receiving pools depending on soil mineral N concentrations [*Metherell et al*., 1993; *Parton et al*., 1993]: see *Manzoni and Porporato* [2009] for the possible consequences of relaxing the constant N:C ratio on decomposition). Negative values of $potNmin_c$ mean net N immobilization, instead of N mineralization.

In N-poor conditions, microbial activities can be limited by N rather than C, because microbes are stoichiometrically constrained. The hypothetical mechanisms behind the microbial C:N stoichiometry effects on C and N fluxes (denoted as m, explained in detail later) are diverse across SOM models. Independent of the approach, however, actual soil respiration rates, $Cmin_{m,c}$ (g C kg^{-1} soil day^{-1}), and actual N mineralization rates, $Nmin_{m,c}$ (g N kg^{-1} soil day^{-1}), can be expressed as:

$$Cmin_{m,c} = \sum_{i=S1}^{S2} \left(1 - e_{i,m}\right) \cdot I_{m,c} \cdot DEC_{i,c} + O_{m,c} \tag{6}$$

$$Nmin_{m,c} = \sum_{i=S1}^{S2} \left(I_{m,c} \cdot DEC_{i,c} \cdot NC_i - I_{m,c} \cdot DEC_{i,c} \cdot e_{i,m} \cdot NC_B \right) \tag{7}$$

where $e_{i,m}$ is the microbial growth efficiency when assimilating substrate i, $I_{m,c}$ is an inhibition factor on decomposition (ranging from 0 for full to 1 for no inhibition), and $O_{m,c}$ is an overflow of C at low N (g C kg^{-1} soil day^{-1}) (these variables are explained in detail below) for the microbial substrate consumption kinetics c. When N is not limiting (m = none), the parameter values are set as: $e_{i,\mathrm{none}} = 0.45$ (as in CENTURY); $I_{\mathrm{none},c} = 1$ (no reduction in decomposition); and $O_{\mathrm{none},c} = 0$ (no C overflow). This leads to $Cmin_{\mathrm{none},c} = potCmin_c$ and $Nmin_{\mathrm{none},c} = potNmin_c$. Below, we identify four contrasting types of C:N stoichiometry effects on soil respiration and N mineralization (m = INHin, INHorg, COin, or COorg; see Table 2 and Figure 1d for an overview).

Table 2. Different Assumptions of C:N Stoichiometry Effects (m) Employed in the Model[a]

	m =				
	INHin	INHorg	COin	COorg	None
$I_{m,c}$	Equation ((8))	Equation ((9))	1	1	1
$e_{i,m}$	0.45	0.45	0.45	Equation ((11))	0.45
$O_{m,c}$	0	0	Equation ((10))	0	0

[a]See equations (6) and (7) for how soil respiration and N mineralization rates are affected by $I_{m,c}$, $e_{i,m}$, and $O_{m,c}$. Note that $I_{m,c}$, $e_{i,m}$, and $O_{m,c}$ depend on substrate i (i = S1 or S2) and/or the choice of microbial substrate consumption kinetics c (c = LIN, MM, or MUL).

Most commonly (including later versions of CENTURY), the decomposition rate at N-limited conditions is reduced to the point that inorganic N in soil can provide enough N for the microbial needs (the "INHin" mechanism, affecting the decomposition process (1) in Figure 1d). The inhibition factor $I_{\mathrm{INHin},c}$ can be formulated as [*Manzoni and Porporato*, 2007; *Porporato et al*., 2003]:

$$I_{\mathrm{INHin},c} = \begin{cases} 1 & potNmin_c \geq imm\_max \\ \dfrac{imm\_max}{potNmin_c} & potNmin_c < imm\_max \end{cases} \tag{8}$$

where imm_max is the maximum N immobilization rate (g N kg^{-1} soil day^{-1}), which is by definition a negative value. imm_max can be a function of soil inorganic N or of microbial biomass. Here, we arbitrarily chose a value of -0.0002 g N kg^{-1} soil day^{-1}.

Alternatively, it is proposed that the inhibition effect of N limitation is directly triggered by organic N (the "INHorg" mechanism, affecting the decomposition process (2) in Figure 1d), rather than inorganic N. Here, organic N inhibits decomposition as soon as N demand of microbes according to C decomposition (i.e., $DEC_{i,c} \cdot e_{i,m} \cdot NC_{\mathrm{B}}$) is larger than N assimilated from organic N (i.e., $DEC_{i,c} \cdot NC_i$). The inhibition factor $I_{\mathrm{INHorg},c}$ is formulated as [*Manzoni and Porporato*, 2009]:

$$I_{\mathrm{INHorg},c} = \begin{cases} 1 & potNmi_{nc} \geq 0 \\ \dfrac{\sum_{i=\mathrm{S1}}^{\mathrm{S2}} DEC_{i,c} \cdot NC_{\mathrm{i}}}{\sum_{i=\mathrm{S1}}^{\mathrm{S2}} DEC_{i,c} \cdot e_{i,\mathrm{INHorg}} \cdot NC_{\mathrm{B}}} & potNmin_c < 0 \end{cases} \tag{9}$$

Another possible mechanism of C:N stoichiometry effects is that, when N is limited, excess C is released as waste through an overflow metabolism (the "COin" mechanism, affecting the respiration not related to microbial growth (3) in Figure 1d) [*Schimel and Weintraub*, 2003], instead of inhibiting decomposition. The overflow of C, $O_{\mathrm{COin},c}$ (g C kg^{-1} soil day^{-1}), can be formulated as the difference between assimilated C and C fixed in microbial biomass using total incoming N (i.e., mineralized N from organic sources and immobilized N from inorganic sources):

$$O_{\mathrm{COin},c} = \begin{cases} 0 & potNmin_c \geq imm\_max \\ \sum_{i=\mathrm{S1}}^{\mathrm{S2}} DEC_{i,c}\left(e_{i,\mathrm{COin}} - \dfrac{NC_i}{NC_{\mathrm{B}}}\right) - \dfrac{imm\_max}{NC_{\mathrm{B}}} & potNmin_c < imm\_max \end{cases} \tag{10}$$

Note that this model does not have any impact on N mineralization rates but only on C mineralization.

C overflow may also occur in response to organic N limitation (the "COorg" mechanism, affecting the C overflow process (4) in Figure 1d). In that case, it is assumed that microbes decrease their growth efficiency to use C when the organic substrate is N poor. Thus, unlike with the COin mechanism which has a threshold value of N availability to trigger extra C outflow, C outflow increases gradually as the substrate becomes N poor. Based on a global analysis of litter decomposition, an empirical relationship was derived as [*Manzoni et al*., 2008]:

$$e_{i,\mathrm{COorg}} = 0.43 \cdot \left(\frac{NC_i}{NC_{\mathrm{B}}}\right)^{0.6} \tag{11}$$

Note that equation (11) describes only one possible mechanism through which MGE is influenced. Other factors include temperature, moisture, and substrate quality [*Manzoni et al*., 2012]. Provided that NC_i partly reflects substrate quality, equation (11) can be more broadly interpreted as an integrative description of

substrate quality effects on MGE. Most existing models (including CENTURY) use constant MGE values [*Manzoni et al.*, 2012], whereas the sensitivity of MGE to C and N fluxes has rarely been tested [but see *Allison et al.*, 2010; *Frey et al.*, 2013]. Therefore, this study also intends to examine the effect of adaptive MGE (to substrate N richness) on model behavior.

2.2. Model Sensitivity Analysis

We tested the sensitivity of modeled *Cmin* and *Nmin* to different model settings. The sensitivity was tested within the typical ranges of the parameter values in a surface soil layer as derived from global studies [*Cleveland and Liptzin*, 2007; *Manzoni et al.*, 2008; *Six et al.*, 2006] in terms of relative rates per unit soil C ($Cmin/C_{TOT}$ and $Nmin/C_{TOT}$), rather than *Cmin* and *Nmin*, in order to standardize the model outputs. When not specified, we assumed: $e_{i,m} = 0.45$ (value in CENTURY); $C_B/C_{TOT} = 0.023$ and $C_{TOT} = 46$ (global median values); $C_{S1} = 2 \cdot C_B$; $C_{S2} = C_{TOT}\text{-}C_{S1}\text{-}C_B$; $NC_{S1} = NC_{S2}$ = (soil total N):(soil total C); 50% sand content; 5% clay content; soil temperature 20°C; and no reduction effect by soil moisture.

First, for each type of microbial substrate consumption kinetics (LIN/MM/MUL), relative respiration ($Cmin/C_{TOT}$) was compared to the global ranges of soil total C (C_{TOT}), microbial fraction (C_B/C_{TOT}), and microbial growth efficiency ($e_{i,m}$). Here, no C:N stoichiometry effects were assumed. Second, for each type of C:N stoichiometry effect (INHin/INHorg/COin/COorg/none), relative respiration ($Cmin/C_{TOT}$) and relative N mineralization ($Nmin/C_{TOT}$) were compared to the global range of substrate N:C ratio (NC_i), with three levels of microbial N:C ratio (NC_B). Here, the LIN model was used.

2.3. Model Validation Data Set

We collected top soils from 36 sites in the Netherlands, covering a wide range of nutrient, acidity, and moisture conditions [*Fujita et al.*, 2013], in order to determine soil physical and chemical variables, microbial biomass and stoichiometry, and C and N fluxes in soil incubation experiments. In addition, we retrieved published data with a similar set of soil information from temperate and boreal ecosystems (Table 3). This led to 154 sites for *Cmin* and 45 sites for *Nmin*.

Microbial C was estimated with either the chloroform fumigation-extraction method or the substrate-induced respiration method. See Appendix B for justification to treat the estimates of both methods as being equivalent. *Cmin* was measured for incubation periods of 2 h to 1 day, with a few exceptions of 10 days (five sites). Soil moisture condition was in most cases adjusted to be "optimal" (i.e., respiration not hampered by either oxygen or water stress), and temperature was adjusted to 20–25°C. See Table 3 for methodological details of each study. *Nmin* was measured at the same conditions as *Cmin* but for longer periods (6 weeks to 1 month). For one data set in which soil moisture was adjusted to the highest level (db1 in Table 3, WFPS 80%), measured N mineralization rates were corrected for N loss by adding denitrification rates predicted with DAYCENT model equations [*Del Grosso et al.*, 2002] (for details, see *Fujita et al.* [2013]). For the majority of the sites, the predicted denitrification rates were small. For 13 out of the 36 sites, however, the modeled denitrification rate was rather large (i.e., >0.1 mg N kg^{-1} soil day^{-1} and $>10\%$ of the measured N mineralization rate).

Table 3. Details of the Data Sets of Soil Incubation Experiments Used for Model Validation

				Pool Size Estimate Method			Incubation Experiment						
No.[a]	Country	N	Soil Depth	Soil Texture	Soil Total C/N[b]	Microbial Measure[c] (element)	Temp	Moisture	Duration *Cmin*	Method[d] *Cmin*	Duration *Nmin*	Extraction Method *Nmin*
db1	Netherlands	36	0–15 cm	sand/silt/clay	CN[e]/CN	FE (C,N)	20°C	80% WFPS	2 h	GC	42 days	1 M KCl
db2	New Zealand	3	0–10 cm	NA[f]	CO/KJ	FE (C,N)	25°C	60% WFPS	10 days	KOH	56 days	2 M KCl
db3	New Zealand	2	0–10 cm	NA[f]	CO/KJ	FE (C,N)	25°C	60% WFPS	10 days	KOH	56 days	2 M KCl
											1 month/	
db4	Luxembourg	4	0–5 cm	NA[f]	CN/CN	FE (C,N)	20°C	"optimal"[g]	1 day	GC	42 days	0.5 M K_2SO_4
db5	Germany	4	0–10 cm	NA	CO[e]/CO	SIR (C)	22°C	−240 kPa	10 h	GC	–	–
db6	Germany (European)	88	0–15 cm	sand[h]	CN[e]/CN	SIR (C)	20°C	As in field 50–60%	8–18 h	GC	–	–
db7	Russia	17	0–10 cm	sand/silt/clay	DI/KJ	SIR (C)	22°C	WFPS	1 day	GC	–	–

WFPS: water filled pore space (fraction between 0 and 1); *Cmin*: soil respiration rates; *Nmin*: soil N mineralization rates.
[a]References are db1: this study; db2: *Ross et al.* [1999]; db3: *Ross et al.* [1996]; db4: *Kooijman et al.* [2008]; db5: *Blagodatskaya and Anderson* [1998]; db6: *Wirth* [2001]; and db7: *Ananyeva et al.* [2008].
[b]CN: CN analyzer, CO: combustion, DI: dichromate digestion, KJ: Kjeldahl digestion.
[c]FE: chloroform fumigation-extraction method, SIR: substrate-induced respiration method with added glucose (see Appendix B for conversion factors).
[d]GC: Gas chromatography, KOH: adsorbed in 0.1 M KOH and estimated by titration of excess alkali with 50 mM HCl after precipitation of K_2CO_3 by 1 M $BaCl_2$.
[e]Amount of inorganic C was subtracted to estimate organic C only.
[f]Texture was estimated based on the textural class, according to soil texture triangle of USDA.
[g]Gravimetric moisture content was 300% for organic and 50% for mineral soil samples.
[h]Clay content was approximated as 22% (average value of db1 and db7) of non-sand content.

2.4. Validating Soil Respiration and N Mineralization Rates

Prior to our validation, we determined the relationship between soil texture and respiration rates. Contrary to the assumption of CENTURY model that *Cmin*, expressed as a ratio to soil total C, is negatively related to the clay plus silt content, they were positively related in our validation data set (see Appendix C for more details). To avoid texture adversely affecting the modeled relations, we employed an arbitrarily chosen fixed value of sand and clay content (50% and 5%, respectively) for all sites.

We compared measured and predicted *Cmin* to test model performance for the different approaches of substrate consumption (LIN/MUL/MM) and C:N stoichiometry (INHin/INHorg/COin/COorg), and for different site-specific input values of microbial properties (constant/measured) (see Table 4 for an overview). First, for each approach of substrate consumption, we predicted *Cmin* with no site-specific microbial information (i.e., site-specific input values are soil total C and incubation temperature only) and no C:N stoichiometry effects. Here, the microbial fraction (C_B/C_{TOT}, where $C_{TOT} = C_B + C_{S1} + C_{S2}$) was set to 1% according to the initial value of CENTURY [*Metherell et al*., 1993]. Second, the constant microbial fraction was replaced with the measured microbial fraction. Third, we tested the four different approaches of the C:N stoichiometry effect (INHin/INHorg/COin/COorg) with measured microbial fraction. A constant microbial N:C ratio (NC_B) (0.14, the median value of a global data set [*Cleveland and Liptzin*, 2007]) was applied, and soil N pools were initiated such that the N:C ratio of the easily decomposable pool (NC_{S1}) is higher than that of the recalcitrant pool (NC_{S2}) (NC_{S1}: NC_{S2} equaling 11:8, as in CENTURY). In addition, for the subset for which NC_B had been measured (45 sites), the constant NC_B was replaced with measured NC_B values. Note that *Cmin* is affected by N:C ratios of substrates and microbes only when C:N stoichiometry effects are included. For all simulations, C_{S1} was assumed to be as twice large as C_B, and we assumed no reduction in decomposition due to soil moisture.

Subsequently, we tested model performance for *Nmin*. *Nmin* was predicted in the same way as for *Cmin* but with LIN model only (since model predictive ability for *Cmin* was better with LIN than with MUL or MM; see section 3). Validation was run with a constant NC_B (0.14) and with the site-specific measured NC_B value. See Table 4 for an overview.

Goodness of fit between observed and predicted *Cmin* and *Nmin* was quantified with Spearman's rank correlation coefficients (ρ) and normalized root mean square error (*nRMSE*). The latter quantifies the "average distance" of observed and predicted values in units of the observation range:

$$nRMSE = 100 \cdot \frac{\sqrt{\sum_{s=1}^{n} (obs_s - pre_s)^2 / n}}{obs_{max} - obs_{min}} \tag{12}$$

where obs_s is the log-transformed observed *Cmin* or *Nmin* of site *s*, pre_s is the log-transformed predicted *Cmin* or *Nmin* of site *s*, *n* is the number of sites, and obs_{max} and obs_{min} are the maximum and minimum values, respectively, of observed log-transformed *Cmin* or *Nmin*.

To evaluate model performance across models with different assumptions, median values and 95% confidence intervals of ρ and *nRMSE* were calculated from 1000-time bootstrapped sites (154 sites for *Cmin* and 45 sites for *Nmin*) [*Good*, 2005]. If fewer than 5% of the computed ρ or *nRMSE* for a model exceeded the median value of another model, we considered the change in the model predictive ability as significant ($P < 0.05$).

3. Results

3.1. Sensitivity of Modeled Soil Respiration to Microbial Substrate Consumption, Microbial Biomass, and Microbial Growth Efficiency

Figure 2 shows the sensitivities of modeled relative respiration rate, $Cmin/C_{TOT}$, for each type of substrate consumption kinetics given the 5th to 95th percentile of soil total C (C_{TOT}), microbial fraction (C_B/C_{TOT}), and MGE ($e_{i,m}$) from global studies. The patterns of relative respiration were contrasting among LIN, MUL, and MM models. With the LIN model, relative respiration was constant for all levels of C_{TOT} (Figure 2a), whereas relative respiration increased with increasing C_{TOT} with the MUL and MM models (Figures 2b and 2c, respectively). The sensitivity of relative respiration to C_{TOT} was stronger in the MUL model than in the MM model: relative respiration increased 19.3× with the MUL model and 2.9× with the MM model when C_{TOT}

Table 4. Overview of Model Assumptions to Predict Soil Respiration and N Mineralization Rates of the Validation Data Set and Their Goodness-of-Fit (in Normalized Root Mean Square Errors *nRMSE* and Spearman's Rank Correlation Coefficients ρ) With Observed Data

	Model Assumptions					Model Fit	
ID	Substrate Consumption (*c*)	Microbial Fraction (C_B/C_{TOT})	C:N Stoichiometry (*m*)	Microbial N:C ratio (NC_B)	Fig No.[a]	*nRMSE* (%)	ρ
			Soil Respiration				
LIN	LIN	1%[c]	none	–	S5a	45.4	0.66***
LIN_Cb	LIN	measured	none	–	S5b	21.3	0.78***
LIN_Cb_INHin	LIN	measured	INHin	0.14[d]	S5c	56.4	0.57***
LIN_Cb_INHorg	LIN	measured	INHorg	0.14	S5d	21.6	0.78***
LIN_Cb_COin	LIN	measured	COin	0.14	S5e	21.3	0.79***
LIN_Cb_COorg	LIN	measured	COorg	0.14	S5f	19.5	0.76***
MUL	MUL	1%	none	–	S5g	95.7	0.65***
MUL _Cb	MUL	measured	none	–	S5h	41.2	0.78***
MUL _Cb_INHin	MUL	measured	INHin	0.14	S5i	66.3	0.56***
MUL _Cb_INHorg	MUL	measured	INHorg	0.14	S5j	41.3	0.78***
MUL _Cb_COin	MUL	measured	COin	0.14	S5k	41.6	0.78***
MUL _Cb_COorg	MUL	measured	COorg	0.14	S5l	39.5	0.77***
MM	MM	1%	none	–	S5m	71.9	0.65***
MM _Cb	MM	measured	none	–	S5n	27.6	0.79***
MM _Cb_INHin	MM	measured	INHin	0.14	S5o	60.3	0.52***
MM _Cb_INHorg	MM	measured	INHorg	0.14	S5p	27.8	0.78***
MM _Cb_COin	MM	measured	COin	0.14	S5q	27.6	0.79***
MM _Cb_COorg	MM	measured	COorg	0.14	S5r	25.9	0.78***
			N Mineralization				
N	LIN	1%	none	0.14	S8a	29.0	ns
N_Cb	LIN	measured	none	0.14	S8b	31.0	ns
N_INHin	LIN	measured	INHin	0.14	S8c	27.6	ns
N_INHorg	LIN	measured	INHorg	0.14	S8d	31.0	ns
N_COin[b]	LIN	measured	COin	0.14	S8e	31.0	ns
N_COorg	LIN	measured	COorg	0.14	S8f	25.3	0.41**
N_nc	LIN	1%	none	measured	S8g	29.6	ns
N_Cb_nc	LIN	measured	none	measured	S8h	35.8	ns
N_INHin_nc	LIN	measured	INHin	measured	S8i	32.9	ns
N_INHorg_nc	LIN	measured	INHorg	measured	S8j	35.8	ns
N_COin_nc[b]	LIN	measured	COin	measured	S8k	35.8	ns
N_COorg_nc	LIN	measured	COorg	measured	S8l	22.2	0.35*

ns: not significant ($P > 0.05$);
*$P < 0.05$;
**$P < 0.01$;
***$P < 0.001$.
[a]Figure numbers corresponding to those in Figure S5 in Appendix D and Figure S8 in Appendix G.
[b]This assumption of N limitation does not affect N mineralization rates (but does affect respiration rates).
[c]Initial value of CENTURY [*Metherell et al.*, 1993].
[d]The median value of global data set [*Cleveland and Liptzin*, 2007].

increased from the 5th to the 95th percentile of its global values. Note that the sensitivity of the MM model changed with the choice of the half-saturation parameter values (km_{S1} and km_{S2}): the sensitivity of relative respiration increased to 3.8× when km_i values were doubled, whereas it decreased to 2.3× when km_i values were halved.

The effect of microbial biomass on relative respiration was strong, especially for the MUL model. Within the global 5th–95th percentile of microbial fraction (i.e., a 12.6× difference), relative respiration increased 6.5× for the LIN model (Figure 2d), 82.2× for the MUL model (Figure 2e), and 15.6× for the MM model (Figure 2f) when C_{TOT} was the global median value. The MUL model led to an unrealistic relative respiration (i.e., higher than its global range) whenever microbial fraction and C_{TOT} exceeded its global 75th percentile values (Figures 2b and 2e).

From the 5th to 95th percentile of the global MGE values (i.e., a 20.7× increase), relative respiration declined about 3× irrespective of the substrate consumption kinetics and C_{TOT} (Figures 2g–2i).

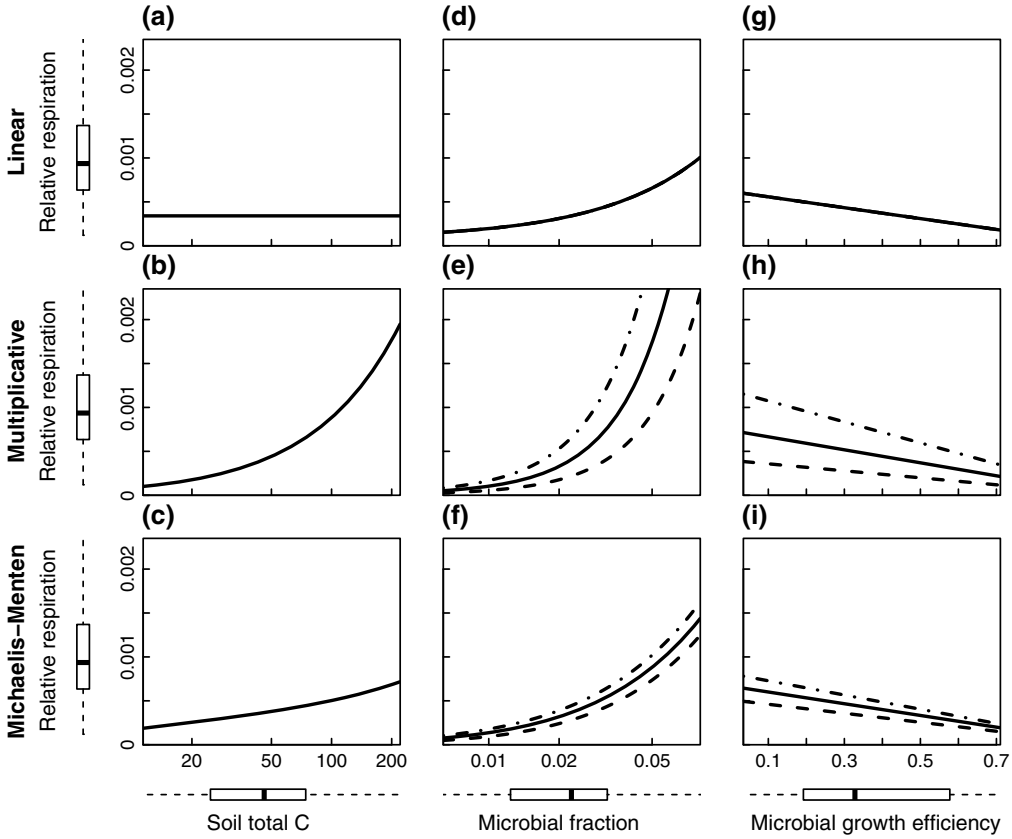

Figure 2. Sensitivity of relative respiration rate ($Cmin/C_{TOT}$, day^{-1}) to soil total C (C_{TOT}, g C kg^{-1} soil), microbial fraction (C_B/C_{TOT}), and microbial growth efficiency ($e_{i,m}$) for three model approaches of substrate consumption (a,d,g: linear (LIN), b,e,h: multiplicative (MUL), c,f,i: Michaelis-Menten (MM)). For the multiplicative and Michaelis-Menten models, the model behavior against microbial fraction and microbial growth efficiency depends on soil total C. Soil total C values were 24.8 (dashed line), 46.0 (solid line), and 74.3 (dot-dash-line), representing the 25th, 50th, and 75th percentiles of a global data set [*Cleveland and Liptzin*, 2007, $N = 155$]. Box plots show the 25th, 50th, and 75th percentiles of the global data set of soil total C and microbial fraction [*Cleveland and Liptzin*, 2007, $N = 144$], microbial growth efficiency (measured with mixed microbial community for litter [*Manzoni et al.*, 2008] and soil [*Six et al.*, 2006], $N = 112$), and relative respiration (this study, $N = 154$), with whiskers extending to the 5th and 95th percentiles. We assumed $C_B/C_{TOT} = 0.023$ for Figures 2a–2c and 2g–2i, and $e_{i,m} = 0.45$ for Figures 2a–2f.

3.2. Sensitivity of Soil Respiration and N Mineralization to Microbial C:N Stoichiometry Effects

Different approaches to modeling C:N stoichiometry effects led to opposing patterns of soil respiration for N-poor to N-rich conditions (Figures 3a–3c). When an inhibiting effect on decomposition was assumed (INHin and INHorg), relative respiration decreased with decreasing substrate N:C ratio (NC_i, for which $NC_{S1} = NC_{S2}$ was assumed) from a threshold value of NC_i onward (grey lines in Figures 3a–3c). In contrast, when N limitation was assumed to occur through an overflow of C (COin and COorg), relative respiration increased with decreasing NC_i (black lines in Figures 3a–3c). In both cases, when inorganic N triggered the effect (INHin and COin; dotted lines in Figures 3a–3c), the threshold values of NC_i where N limitation starts were lower, but the magnitude of change in relative respiration following the threshold was larger.

A higher microbial N:C ratio, NC_B, amplified the C:N stoichiometry effects on relative respiration (from Figures 3a to 3c), as the increasing demand of microbes for N increased the threshold value of NC_i, and therefore N limitation occurred at a less N-poor substrate.

The choice of the C:N stoichiometry effect had a less striking, but still substantial, effect on N mineralization (Figures 3d–3f). If there was no C:N stoichiometry effect (thick lines in Figures 3d–3f), relative N mineralization rates (i.e., $Nmin/C_{TOT}$) decreased with decreasing NC_i because a larger fraction of assimilated N was fixed by microbes and less N was released to the soil. As NC_i decreased further, N was eventually immobilized from

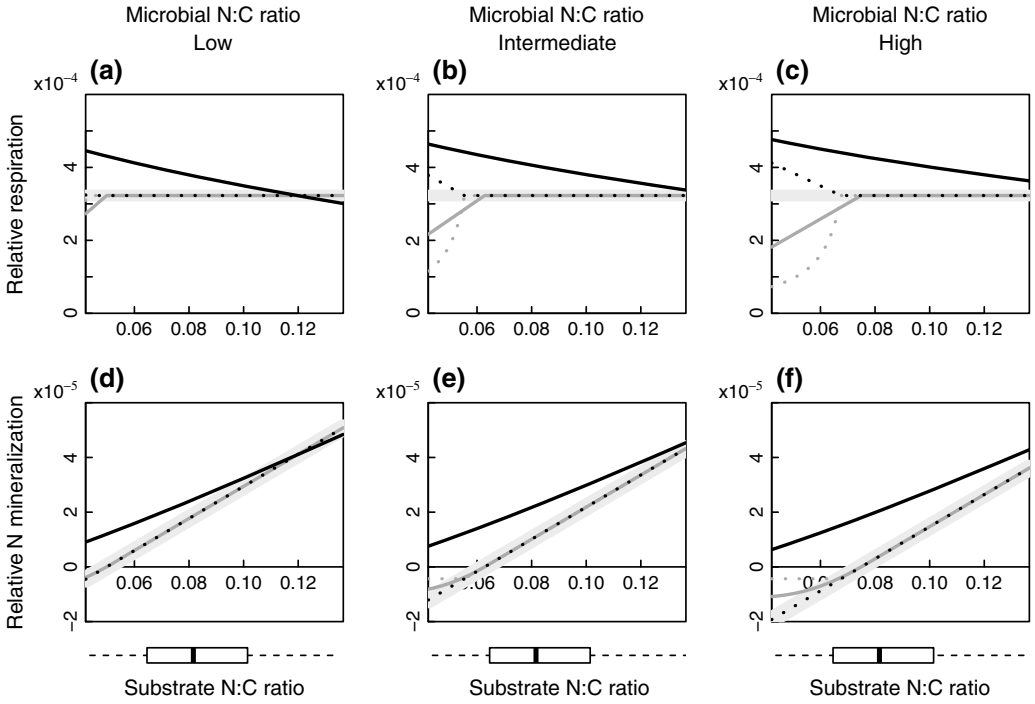

Figure 3. (a–c) Sensitivity of relative respiration rate ($Cmin/C_{TOT}$, day^{-1}) and (d–f) relative N mineralization rate ($Nmin/C_{TOT}$, g N g^{-1} C day^{-1}) against substrate N:C ratio (NC_i), with different approaches of the microbial C:N stoichiometry effects on C fluxes. The microbial C:N stoichiometry effect is described as INHin (dotted grey lines), INHorg (solid grey lines), COin (dotted black lines), and COorg (solid black lines), and no effect of C:N stoichiometry (thick grey lines). Sensitivity is shown for three different levels of microbial N:C ratio (NC_B); ($NC_B = 0.11$, left) low, ($NC_B = 0.14$, middle) intermediate, and ($NC_B = 0.17$, right) high levels, which corresponds to the 25th, 50th, and 75th percentiles of a global data set [*Cleveland and Liptzin*, 2007, $N = 134$]. Box plots show the 25th, 50th, and 75th percentiles of the global data set of NC_i [*Cleveland and Liptzin*, 2007, $N = 145$], with whiskers extending to the 5th and 95th percentiles. We used the linear model (LIN) and assumed $C_{TOT} = 46$, $C_B/C_{TOT} = 0.023$, and $e_{i,m} = 0.45$ (except for COorg, in which $e_{i,m}$ varies as a function of NC_i and NC_B).

inorganic N pools. This pattern still occurred when an inhibition effect of C:N stoichiometry was imposed (INHin and INHorg), but the magnitude of N immobilization was diminished (grey lines in Figures 3d–3f). Model behavior was quite different with COorg: relative N mineralization was less suppressed at lower NC_i, because C use efficiency was reduced by decreasing e, and therefore microbial N demands were kept relatively low at N-poor conditions (black solid lines in Figures 3d–3f).

Increasing NC_B decreased relative N mineralization for all models (from Figures 3d to 3f). However, the effect of increasing NC_B was limited for COorg, because a negative effect of high NC_B on relative N mineralization due to increased microbial demand was mitigated by a positive effect via decreasing MGE.

3.3. Model Validation for Soil Respiration Rates

The LIN model with minimal site-specific input values (soil total C and incubation temperature) predicted the rank order of *Cmin* reasonably well ($\rho = 0.66$) but not the magnitude of *Cmin* (*nRMSE* 45.4%) (Table 4; Figure S5a in Appendix D). Use of site-specific C_B data significantly improved *nRMSE* (21.3%, $P < 0.001$) and rank order ($\rho = 0.78$, $P < 0.01$) (Figure S5b; see Appendix E for the difference in model performance tested by bootstrapping). Including the INHin mechanism made model performance significantly ($P < 0.001$) worse (Figure S5c; $nRMSE = 56.4\%$), whereas there was a trend ($P = 0.089$) for the COorg mechanism to improve model predictions (Figure S5f; $nRMSE = 19.5\%$). Including the other mechanisms of C:N stoichiometry effects (INHorg [Figure S5d] and COin [Figure S5e]) did not make any significant change ($P > 0.10$) in model performance.

The MUL model made predictions of *Cmin* worse for all model settings (Table 4 and Figures S5g–S5l) because of model underestimation for organic-poor soils (bottom left side of the graph) and model overestimation for

organic-rich soils (top right side). The MM model gave slightly worse predictions than the LIN model (Table 4 and Figures S5m–S5r), mainly because of model underestimation for organic-poor soils.

With a subset of the sites for which microbial N data were available (45 sites), we also tested if site-specific NC_B data improved model performance for *Cmin*. No significant ($P > 0.05$) improvement was detected in *nRMSE* nor ρ after inclusion of measured NC_B (Appendix F).

3.4. Model Validation for Soil N Mineralization Rates

When NC_B was assumed to be constant, and when no C:N stoichiometry effect was assumed, model performance for *Nmin* was poor irrespective of whether C_B was kept constant (*nRMSE* = 29.0%, Figure S8a in Appendix G) or measured (*nRMSE* = 31.0%, Figure S8b). The poor performance was partly because many sites were falsely predicted to have net N immobilization. Including the INHin mechanism slightly improved the model performance in terms of *nRMSE* (27.6%, $P < 0.05$, Figure S8c) but not the rank order ($\rho = 0.14$, $P > 0.05$), because overestimation of N immobilization was corrected to some extent. Including the COorg mechanism significantly improved the model fit in terms of both *nRMSE* (25.3%, $P < 0.05$) and rank order ($\rho = 0.41$, $P < 0.001$) (Figure S8f). INHorg and COin did not cause any significant difference in model performance ($P > 0.05$).

When measured NC_B was used instead of constant NC_B (Figures S8g–S8l), model performance on *Nmin* was improved significantly only for COorg mechanism in terms of *nRMSE* (22.2%, $P < 0.05$, Figure S8j), yet the rank order remained unchanged ($\rho = 0.35$, $P > 0.05$).

4. Discussion

4.1. Important Model Elements to Improve Across-Site Predictions of Soil C and N Fluxes

Increasing model complexity potentially leads to improved model performance, yet at the expense of increasing efforts and uncertainty in defining input and parameter values. A challenge is to find an optimal complexity given the specific scope of the model and the availability of data. Our study identified the relative importance of components of model complexity (in terms of model structures on microbial processes and microbial parameters) in order to predict C and N fluxes across sites.

Microbial biomass had by far the strongest influence on predicted *Cmin* (Figures 2d–2f). Significant improvement of model predictive ability on *Cmin* when using site-specific microbial biomass data (Table 4) provides empirical evidence that microbial biomass counts for determining *Cmin*. From a model-structure perspective, the sensitivity of *Cmin* to microbial biomass is explained by the much higher (ca. 67×) decomposition coefficient for easily decomposable carbon (k_{S1}) than for recalcitrant carbon (k_{S2}), accounting for approximately 67% of total decomposition irrespective of the small size of the labile carbon pool (derived from equations in Appendix A, assuming 5% clay content and 45% silt content). Note that, even in the LIN model in which the microbial biomass was not explicitly included, partitioning of soil C pools was controlled by microbial biomass (see assumptions in section 2.2). Thus, the improved model fit by using measured microbial biomass does not per se justify the model structure of microbe-substrate relations or specific parameter values involved in our model but reflects the generic dependency of decomposition rate on the size of SOM fractions [*Ros*, 2012] and, therefore, the uncertainty in model performance due to initial fractionation of SOM in models [*Bruun and Jensen*, 2002; *Foereid et al*., 2012].

In contrast to the strong model sensitivity to microbial biomass, the impacts of different substrate consumption kinetics (LIN/MUL/MM) on predicted *Cmin* were minor, except that the MUL model causes unrealistically high predictions for C-rich soils (Figure 2). This implies that the LIN model is sufficient to describe across-site differences in steady-state *Cmin*. Second-order kinetics of decomposition may become important when predicting the temporal dynamics of C in non-steady conditions [*Treseder et al*., 2012; *Whitmore*, 1996] since dynamically changing microbial biomass could have large feedback effects on C cycling [*Allison et al*., 2010; *Wieder et al*., 2013], but that was not tested in our validation data set.

The assumptions employed for microbial C:N stoichiometry effects matter not only for the prediction of N fluxes but also for the prediction of C fluxes. Whether *Cmin* increases or decreases with increasing substrate N richness depends on the presumed mechanism of how microbes cope with N-limited conditions (i.e., INHin/INHorg/COin/COorg) (Figures 3a–3c). Model validation showed that using COorg resulted in the best model

performance for both *Cmin* and *Nmin*, whereas using INHin led to considerable underestimation in predicted *Cmin* and *Nmin* for N-poor soils (Table 4). In addition, decreasing *Cmin* at N-rich conditions (as in COin and COorg), instead of increasing *Cmin* (as in INHin and INHorg), is in accordance with observed patterns in fertilization experiments [*Butnor et al*., 2003; *Janssens et al*., 2010; but see *Lu et al*., 2011; *Ramirez et al*., 2010]. Strikingly, INHin is used in the majority of the existing SOM models that consider C:N stoichiometry effects [*Manzoni and Porporato*, 2009]. Another implication from the model validation was that the C:N stoichiometry mechanisms triggered by substrate N (INHorg, COorg) performed better than those triggered by mineral N (INHin, COin) when predicting *Cmin* (Table 4). Those substrate-driven mechanisms result in earlier emergence of N-limitation effects as a soil becomes N-poor (see tipping points in Figures 3a–3c). Importantly, SOM models adopting these mechanisms will project more rapid responses of soil C upon changed availability of C relative to N (e.g., CO_2 increase, N deposition) than conventional models (i.e., without C:N stoichiometry effects or with INHin mechanism), possibly leading to a considerable deviation in future predictions of global C cycles.

Interestingly, despite the importance of C:N stoichiometry mechanisms, including site-specific microbial C:N ratios did not clearly improve predictions of *Cmin* and *Nmin* (Appendix F). This is largely explained by the fact that the microbial C:N ratio is well constrained even across biomes [*Cleveland and Liptzin*, 2007]. Also, if there is a feedback mechanism of microbes to correct an imbalance between C and N (e.g., high N demand of N-rich microbes is mitigated by decreased MGE when substrate is relatively N-poor [COorg mechanism]), which is a plausible strategy evolved in N-poor environments, among-site variations of microbial C:N ratio will be masked by these feedbacks. Indeed, although model sensitivity to MGE was relatively minor compared to that to microbial biomass (Figures 2g–2i compared to Figures 2a–2c), our model fit did improve when MGE was assumed to be a function of substrate C:N ratios (COorg mechanism) (Table 4). This impact of variation in MGE on model performance reinforces the need for an explicit description of drivers of MGE in SOM models [*Frey et al*., 2013; *Manzoni et al*., 2012; *Sinsabaugh et al*., 2013].

4.2. The Importance and Challenges of Model Validation

Our study provided one of the first across-site validations of SOM models with various microbial processes for both *Cmin* and *Nmin*. Such across-site validations are a crucial step for evaluating the need for consideration of microbial processes and parameters in global soil models [*McGuire and Treseder*, 2010; *Ostle et al*., 2009; *Rastetter et al*., 2003; *Treseder et al*., 2012; *Wieder et al*., 2013]. When locally measured microbial biomass was imposed on our SOM model, across-site variations in C fluxes were predicted well (Table 4). Thanks to a recently developed global microbial biomass map [*Serna-Chavez et al*., 2013], it is now possible to incorporate microbial biomass also into global SOM models. Still, such estimates are available only for the contemporary climate. Moreover, in order to properly incorporate microbial biomass into global models, evaluation of their robustness to environmental drivers in space and time will remain needed. In addition, how microbial processes (for which we defined alternative descriptions) affect C fluxes at non-steady-state conditions needs to be examined with experimental data and validated in field conditions of multiple ecosystems. This highlights the need to continue our efforts to better understand the mechanisms and drivers of C dynamics, as well as to obtain more appropriate data sets for model parameterization.

Across-site model validation studies are even more critically needed for N compared to C. Soil N cycles are more complex compared to soil C cycles, coinciding with generally poorer model predictions for N than for C efflux [Table 4; also, see, e.g., *Kelly et al*., 2000; *Leirós et al*., 1999]. As a consequence, the current implications of N cycling in global models are highly uncertain. This is particularly problematic given the strong feedbacks of N cycling on CO_2 fluxes [*Thornton et al*., 2007]. Provided the importance of C:N stoichiometry effects, standardized flux and pool size measurements alone are likely to be insufficient to further enhance our understanding. Instead, one should aim at measuring gross rates of each process with, for example, isotopic approaches [*Schimel and Bennett*, 2004], although that is not easily realized in field conditions.

4.3. Implications to Improve Global Models

Our study provides important insights for improving SOM models as a crucial part of global models evaluating terrestrial C (and N) fluxes, such as Dynamic Global Vegetation models embedded in Earth system models. The need for including a mechanistic representation of microbial processes, which has been

discussed before [*Todd-Brown et al*., 2011; *Treseder et al*., 2012], was put forward in our study, yielding several vital indications for the required model complexity as follows.

First, microbial biomass, which differs considerably among sites, has to be better understood on global scales to improve model predictions. The recent progress in global databases of microbial biomass and activity [*Cleveland and Liptzin*, 2007; *Fierer et al*., 2009; *Serna-Chavez et al*., 2013; *Sinsabaugh et al*., 2008] allows for a more realistic initialization of microbial biomass and other microbial parameters for global SOM simulations for the contemporary climate. Such efforts should go hand in hand with efforts to improve model initialization of SOM fractionation in global models [*Pietsch and Hasenauer*, 2006].

Second, including the non-linear kinetics of microbial substrate consumption does not seem necessary to improve the model performance, unless capturing temporal fluctuation of fluxes is of main concern.

Finally, the microbial C:N stoichiometry mechanisms certainly need improved understanding and incorporation in global models. Given the increasing recognition on the importance of N feedbacks in global C models [*Esser et al*., 2011; *Gerber et al*., 2010; *Thornton et al*., 2007], rigorous efforts are needed to empirically test microbial feedbacks on C-N interactions (especially those concerning microbial growth efficiency) and to re-evaluate the approach of C:N stoichiometry effects in global SOM models. Detailed biologically realistic microbial models for small-scale applications may, in this context, allow testing of specific processes, eventually speeding up procedures of identifying and reducing model uncertainty, making SOM models more robust and better suited for global change predictions.

Concluding, our study showed that incorporating microbial processes in a simple SOM model considerably reduced prediction errors in soil C and N fluxes across different soil conditions: the predictive ability was improved from 45.4% to 19.5% *nRMSE* for soil respiration and from 29.0% to 22.2% *nRMSE* for soil N mineralization by including site-specific microbial biomass data and microbial N feedbacks on C via altered microbial growth efficiency. This highlights the need to better incorporate microbial mechanisms into global models. Future studies are needed to better understand spatial patterns and its drivers of microbial biomass based on the emerging global databases of microbes, as well as to re-evaluate the mechanisms of soil C-N interactions mediated by microbes. With such advancements, we envision improved predictions of global C and N fluxes for a current and projected climate.

Acknowledgments

This research was carried out in the framework of CARE project of the Dutch national research program Knowledge for Climate and the joint research program of the Dutch Water Utility sector. We thank Staatsbosbeheer, Veluwe national park, and PWN for the permission to sample soils; R. van Logtestijn, J. van Hal, and J. Weedon for their help in measuring microbial properties; W. Roling and M. Braster for their help in using TOC analyzer; H. Roelofsen and J. Runhaar for field sampling; and two anonymous reviewers for their constructive comments. Original data for the model validation is available as in Supporting Information Table S1.

References

Allison, S. D. (2012), A trait-based approach for modelling microbial litter decomposition, *Ecol. Lett.*, *15*(9), 1058–1070.

Allison, S. D., M. D. Wallenstein, and M. A. Bradford (2010), Soil-carbon response to warming dependent on microbial physiology, *Nat. Geosci.*, *3*(5), 336–340.

Ananyeva, N. D., E. A. Susyan, O. V. Chernova, and S. Wirth (2008), Microbial respiration activities of soils from different climatic regions of European Russia, *Eur. J. Soil Biol.*, *44*(2), 147–157.

Bardgett, R. D., C. Freeman, and N. J. Ostle (2008), Microbial contributions to climate change through carbon cycle feedbacks, *ISME J.*, *2*(8), 805–814.

Blagodatskaya, E. V., and T. H. Anderson (1998), Interactive effects of pH and substrate quality on the fungal-to-bacterial ratio and QCO2 of microbial communities in forest soils, *Soil Biol. Biochem.*, *30*(10-11), 1269–1274.

Blagodatsky, S. A., and O. Richter (1998), Microbial growth in soil and nitrogen turnover: A theoretical model considering the activity state of microorganisms, *Soil Biol. Biochem.*, *30*(13), 1743–1755.

Bruun, S., and L. S. Jensen (2002), Initialisation of the soil organic matter pools of the Daisy model, *Ecol. Model.*, *153*(3), 291–295.

Butnor, J. R., K. H. Johnsen, R. Oren, and G. G. Katul (2003), Reduction of forest floor respiration by fertilization on both carbon dioxide-enriched and reference 17-year-old loblolly pine stands, *Global Change Biol.*, *9*(6), 849–861.

Cleveland, C. C., and D. Liptzin (2007), C:N:P stoichiometry in soil: Is there a "Redfield ratio" for the microbial biomass?, *Biogeochemistry*, *85*(3), 235–252.

Del Grosso, S., D. Ojima, W. Parton, A. Mosier, G. Peterson, and D. Schimel (2002), Simulated effects of dryland cropping intensification on soil organic matter and greenhouse gas exchanges using the DAYCENT ecosystem model, *Environ. Pollut.*, *116*(Suppl. 1), S75–S83.

Esser, G., J. Kattge, and A. Sakalli (2011), Feedback of carbon and nitrogen cycles enhances carbon sequestration in the terrestrial biosphere, *Global Change Biol.*, *17*(2), 819–842.

Falkowski, P. G., T. Fenchel, and E. F. Delong (2008), The microbial engines that drive Earth's biogeochemical cycles, *Science*, *320*(5879), 1034–1039.

Fang, C., P. Smith, J. U. Smith, and J. B. Moncrieff (2005), Incorporating microorganisms as decomposers into models to simulate soil organic matter decomposition, *Geoderma*, *129*(3–4), 139–146.

Fierer, N., M. S. Strickland, D. Liptzin, M. A. Bradford, and C. C. Cleveland (2009), Global patterns in belowground communities, *Ecol. Lett.*, *12*(11), 1238–1249.

Foereid, B., P. H. Bellamy, A. Holden, and G. J. D. Kirk (2012), On the initialization of soil carbon models and its effects on model predictions for England and Wales, *Eur. J. Soil Sci.*, *63*(1), 32–41.

Frey, S. D., J. Lee, J. M. Melillo, and J. Six (2013), The temperature response of soil microbial efficiency and its feedback to climate, *Nat. Clim. Change*, *3*(4), 395–398.

Fujita, Y., P. M. van Bodegom, H. Olde Venterink, H. Runhaar, and J.-P. M. Witte (2013), Towards a proper integration of hydrology in predicting soil nitrogen mineralization rates along natural moisture gradients, *Soil Biol. Biochem.*, *58*, 302–312.
Gerber, S., L. O. Hedin, M. Oppenheimer, S. W. Pacala, and E. Shevliakova (2010), Nitrogen cycling and feedbacks in a global dynamic land model, *Global Biogeochem. Cycles*, *24*, GB1001, doi:10.1029/2008GB003336.
Good, P. I. (2005), *Permutation, Parametric, and Bootstrap Tests of Hypotheses*, Springer, New York.
IPCC (2007), *Contribution of Working Groups I, II and III to the Fourth Assessment Report of the Intergovernmental Panel on Climate Change*, edited by B. Metz et al., Cambridge Univ. Press, Cambridge, U.K., and New York.
Janssens, I. A., et al. (2010), Reduction of forest soil respiration in response to nitrogen deposition, *Nat. Geosci.*, *3*(5), 315–322.
Kelly, R. H., W. J. Parton, M. D. Hartman, L. K. Stretch, D. S. Ojima, and D. S. Schimel (2000), Intra-annual and interannual variability of ecosystem processes in shortgrass steppe, *J. Geophys. Res.*, *105*(D15), 20,093–20,100.
Kooijman, A. M., M. M. Kooijman-Schouten, and G. B. Martinez-Hernandez (2008), Alternative strategies to sustain N-fertility in acid and calcaric beech forests: Low microbial N-demand versus high biological activity, *Basic Appl. Ecol.*, *9*(4), 410–421.
Lawrence, C. R., J. C. Neff, and J. P. Schimel (2009), Does adding microbial mechanisms of decomposition improve soil organic matter models? A comparison of four models using data from a pulsed rewetting experiment, *Soil Biol. Biochem.*, *41*(9), 1923–1934.
Leirós, M. C., C. Trasar-Cepeda, S. Seoane, and F. Gil-Sotres (1999), Dependence of mineralization of soil organic matter on temperature and moisture, *Soil Biol. Biochem.*, *31*(3), 327–335.
Lu, M., X. Zhou, Y. Luo, Y. Yang, C. Fang, J. Chen, and B. Li (2011), Minor stimulation of soil carbon storage by nitrogen addition: A meta-analysis, *Agric. Ecosyst. Environ.*, *140*(1-2), 234–244.
Manzoni, S., and A. Porporato (2007), A theoretical analysis of nonlinearities and feedbacks in soil carbon and nitrogen cycles, *Soil Biol. Biochem.*, *39*(7), 1542–1556.
Manzoni, S., and A. Porporato (2009), Soil carbon and nitrogen mineralization: Theory and models across scales, *Soil Biol. Biochem.*, *41*(7), 1355–1379.
Manzoni, S., R. B. Jackson, J. A. Trofymow, and A. Porporato (2008), The global stoichiometry of litter nitrogen mineralization, *Science*, *321*(5889), 684–686.
Manzoni, S., J. A. Trofymow, R. B. Jackson, and A. Porporato (2010), Stoichiometric controls on carbon, nitrogen, and phosphorus dynamics in decomposing litter, *Ecol. Monogr.*, *80*(1), 89–106.
Manzoni, S., P. Taylor, A. Richter, A. Porporato, and G. I. Ågren (2012), Environmental and stoichiometric controls on microbial carbon-use efficiency in soils, *New Phytol.*, *196*(1), 79–91.
McGuire, K. L., and K. K. Treseder (2010), Microbial communities and their relevance for ecosystem models: Decomposition as a case study, *Soil Biol. Biochem.*, *42*(4), 529–535.
Metherell, A. K., L. A. Harding, C. V. Cole, and W. J. Parton (1993), CENTURY soil organic matter model environment. Technical documentation agroecosystem version 4.0., 247 pp.
Ostle, N. J., et al. (2009), Integrating plant–soil interactions into global carbon cycle models, *J. Ecol.*, *97*(5), 851–863.
Parton, W. J., D. S. Schimel, C. V. Cole, and D. S. Ojima (1987), Analysis of factors controlling soil organic-matter levels in Great-Plains grasslands, *Soil Sci. Soc. Am. J.*, *51*(5), 1173–1179.
Parton, W. J., et al. (1993), Observations and modeling of biomass and soil organic matter dynamics for the grassland biome worldwide, *Global Biogeochem. Cycles*, *7*(4), 785–809.
Parton, W., et al. (2007), Global-scale similarities in nitrogen release patterns during long-term decomposition, *Science*, *315*(5810), 361–364.
Pietsch, S. A., and H. Hasenauer (2006), Evaluating the self-initialization procedure for large-scale ecosystem models, *Global Change Biol.*, *12*(9), 1658–1669.
Porporato, A., P. D'Odorico, F. Laio, and I. Rodriguez-Iturbe (2003), Hydrologic controls on soil carbon and nitrogen cycles. I. Modeling scheme, *Adv. Water Resour.*, *26*(1), 45–58.
Ramirez, K. S., J. M. Craine, and N. Fierer (2010), Nitrogen fertilization inhibits soil microbial respiration regardless of the form of nitrogen applied, *Soil Biol. Biochem.*, *42*(12), 2336–2338.
Rastetter, E. B., J. D. Aber, D. P. C. Peters, D. S. Ojima, and I. C. Burke (2003), Using mechanistic models to scale ecological processes across space and time, *BioScience*, *53*(1), 68–76.
Ros, G. H. (2012), Predicting soil N mineralization using organic matter fractions and soil properties: A re-analysis of literature data, *Soil Biol. Biochem.*, *45*, 132–135.
Ross, D. J., K. R. Tate, and C. W. Feltham (1996), Microbial biomass, and C and N mineralization, in litter and mineral soil of adjacent montane ecosystems in a southern beech (Nothofagus) forest and a tussock grassland, *Soil Biol. Biochem.*, *28*(12), 1613–1620.
Ross, D. J., K. R. Tate, N. A. Scott, and C. W. Feltham (1999), Land-use change: Effects on soil carbon, nitrogen and phosphorus pools and fluxes in three adjacent ecosystems, *Soil Biol. Biochem.*, *31*(6), 803–813.
Schimel, D. S. (1994), Climatic, edaphic, and biotic controls over storage and turnover of carbon in soils, *Global Biogeochem. Cycles*, *8*(3), 279–293.
Schimel, J. P., and J. Bennett (2004), Nitrogen mineralization: Challenges of a changing paradigm, *Ecology*, *85*(3), 591–602.
Schimel, J. P., and M. N. Weintraub (2003), The implications of exoenzyme activity on microbial carbon and nitrogen limitation in soil: A theoretical model, *Soil Biol. Biochem.*, *35*(4), 549–563.
Serna-Chavez, H. M., N. Fierer, and P. M. van Bodegom (2013), Global drivers and patterns of microbial abundance in soil, *Global Ecol. Biogeogr.*, *22*, 1162–1172.
Sinsabaugh, R. L., et al. (2008), Stoichiometry of soil enzyme activity at global scale, *Ecol. Lett.*, *11*, 1252–1264.
Sinsabaugh, R. L., S. Manzoni, D. L. Moorhead, and A. Richter (2013), Carbon use efficiency of microbial communities: Stoichiometry, methodology and modelling, *Ecol. Lett.*, *16*(7), 930–939.
Six, J., S. D. Frey, R. K. Thiet, and K. M. Batten (2006), Bacterial and fungal contributions to carbon sequestration in agroecosystems, *Soil Sci. Soc. Am. J.*, *70*(2), 555–569.
Thornton, P. E., J. F. Lamarque, N. A. Rosenbloom, and N. M. Mahowald (2007), Influence of carbon-nitrogen cycle coupling on land model response to CO_2 fertilization and climate variability, *Global Biogeochem. Cycles*, *21*, GB4018, doi:10.1029/2006GB002868.
Todd-Brown, K., F. Hopkins, S. Kivlin, J. Talbot, and S. Allison (2011), A framework for representing microbial decomposition in coupled climate models, *Biogeochemistry*, *109*(1-3), 19–33.
Todd-Brown, K. E. O., J. T. Randerson, W. M. Post, F. M. Hoffman, C. Tarnocai, E. A. G. Schuur, and S. D. Allison (2013), Causes of variation in soil carbon simulations from CMIP5 Earth system models and comparison with observations, *Biogeosciences*, *10*(3), 1717–1736.
Treseder, K., et al. (2012), Integrating microbial ecology into ecosystem models: challenges and priorities, *Biogeochemistry*, *109*(1-3), 7–18.

Whitmore, A. P. (1996), Describing the mineralization of carbon added to soil in crop residues using second-order kinetics, *Soil Biol. Biochem.*, *28*(10–11), 1435–1442.

Wieder, W. R., G. B. Bonan, and S. D. Allison (2013), Global soil carbon projections are improved by modelling microbial processes, *Nat. Clim. Change*, *3*(10), 909–912.

Wirth, S. J. (2001), Regional-scale analysis of soil microbial biomass and soil-basal CO2-respiration in northeastern Germany, in *Sustaining the Global Farm – Selected Papers From the 10th International Soil Conservation Organization Meeting, May 24-29, 1999, West Lafayette*, edited by D. E. Stott, R. H. Mohtar, and G. C. Steinhardt, pp. 486–493, International Soil Conservation Organization in cooperation with the USDA and Purdue University, West Lafayette, Ind.

OPEN ACCESS Freely available online

PLOS ONE

Relationships between Nutrient-Related Plant Traits and Combinations of Soil N and P Fertility Measures

Yuki Fujita[1]*, Peter M. van Bodegom[2], Jan-Philip M. Witte[1,2]

1 Team Ecohydrology, KWR Watercycle Research Institute, Nieuwegein, The Netherlands, **2** Department of Systems Ecology, VU University Amsterdam, Amsterdam, The Netherlands

Abstract

Soil fertility and nutrient-related plant functional traits are in general only moderately related, hindering the progress in trait-based prediction models of vegetation patterns. Although the relationships may have been obscured by suboptimal choices in how soil fertility is expressed, there has never been a systematic investigation into the suitability of fertility measures. This study, therefore, examined the effect of different soil fertility measures on the strength of fertility–trait relationships in 134 natural plant communities. In particular, for eight plot-mean traits we examined (1) whether different elements (N or P) have contrasting or shared influences, (2) which timescale of fertility measures (e.g. mineralization rates for one or five years) has better predictive power, and (3) if integrated fertility measures explain trait variation better than individual fertility measures. Soil N and P had large mutual effects on leaf nutrient concentrations, whereas they had element-specific effects on traits related to species composition (e.g. Grime's CSR strategy). The timescale of fertility measures only had a minor impact on fertility–trait relationships. Two integrated fertility measures (one reflecting overall fertility, another relative availability of soil N and P) were related significantly to most plant traits, but were not better in explaining trait variation than individual fertility measures. Using all fertility measures together, between-site variations of plant traits were explained only moderately for some traits (e.g. 33% for leaf N concentrations) but largely for others (e.g. 66% for whole-canopy P concentration). The moderate relationships were probably due to complex regulation mechanisms of fertility on traits, rather than to a wrong choice of fertility measures. We identified both mutual (i.e. shared) and divergent (i.e. element-specific and stoichiometric) effects of soil N and P on traits, implying the importance of explicitly considering the roles of different elements to properly interpret fertility–trait relationships.

Citation: Fujita Y, van Bodegom PM, Witte J-PM (2013) Relationships between Nutrient-Related Plant Traits and Combinations of Soil N and P Fertility Measures. PLoS ONE 8(12): e83735. doi:10.1371/journal.pone.0083735

Editor: Ben Bond-Lamberty, DOE Pacific Northwest National Laboratory, United States of America

Received July 17, 2013; **Accepted** November 15, 2013; **Published** December 31, 2013

Funding: Knowledge for Climate (http://www.klimaatonderzoeknederland.nl/), Dutch Water Utility sector (B222044). The funders had no role in study design, data collection and analysis, decision to publish, or preparation of the manuscript.

Competing Interests: The authors have declared that no competing interests exist.

* E-mail: Yuki.Fujita@kwrwater.nl

Introduction

Soil nutrients, such as nitrogen (N) and phosphorus (P), constitute basic requirements for plants to support their life. In the short term, soil nutrients induce plastic responses of individual plants (e.g. as related to recruitment, growth, and reproduction). In the longer run, soil nutrients affect the species composition of a plant community, because each species has evolved to adapt to certain environments and therefore has contrasting requirements for nutrients. How and why plant community composition changes from fertile to unfertile soil has been a central concern of ecologists for many decades. A general trend derived from qualitative studies is that species with a rapid growth strategy dominate in fertile soils, whereas species with a conservative strategy dominate in infertile soils (for a review see [1]). In quantitative trait-based studies on a global scale, between-site variations of leaf traits were well explained by soil fertility if combined with climate factors (R^2 between 59 and 78% for specific leaf area and leaf N and P concentrations) [2]. Within a climatic region, however, the effects of soil fertility on leaf traits were moderate (e.g. 22–23% of between-site variance in an integrated leaf economy measure were explained by nutrient indicator value [3]; 31% and 50% of between-site variance in leaf N and P concentrations were explained by soil total P if combined with growth form [4]). Accordingly, the relatively weak relationship between soil fertility and plant traits remains an uncertain link in trait-based species distribution models [5].

Generally weak linkages between environmental factors and traits could be due to stochastic processes being more dominant than environmental filtering effects during the assembly of these plant communities [6,7]. However, these relatively weak relationships could also be the results of using suboptimal (or inappropriate) measure of soil fertility [3]. Soil fertility, or availability of nutrients for plants, is typically expressed as concentrations of dissolved N or P in soil, N mineralization rates for a certain period, soil total N or P, or soil C:N or C:P ratios. Although these soil fertility measures are generally correlated [2,8], it is likely that the choice of a fertility measure influences the strength of the correlation between soil fertility and plant traits (e.g. [9]). Nevertheless, whether the most relevant fertility measure was used to examine the relation with a specific plant trait has never been explicitly examined. For example, the two nutrient elements, N and P, both have pivotal yet different roles in how plants function. Previous studies showed that soil N and P have different degrees of contributions to each trait: specific leaf area was better predicted by soil N supply, whereas leaf N and P concentrations

showed stronger relationships with soil P [2,4]. This implies that element-specific mechanisms or stoichiometric effects (i.e. effects of relative availability of N and P) may play important roles in regulating these traits.

Furthermore, any measure of soil fertility reflects the nutrient status over a certain timescale. This timescale is implicitly (e.g. total N) or explicitly (e.g. N mineralization over 5 years) reflected in the way the measure is expressed. Measures from chemical soil bulk analysis at a certain moment, such as pool size and extractable amount of nutrients, provide only partial information about the nutrient availability for plants over a long time span [10]. Nutrient mineralization rates from soil could be a more relevant measure of nutrient availability for living plants as they reflect a major flow within soil nutrient cycles [11]. However, they fluctuate considerably over time and are controlled by abiotic factors such as temperature and soil moisture [12]. Thus, the timescale associated with soil fertility measures could influence the relationship between soil fertility and plant traits.

Moreover, since plants use soil nutrients in a multidimensional manner (e.g. different ratios of elements, at different timings and periods, etc.), certain combinations of soil fertility measures may better reflect plant trait variability. Hence, an aggregated measure derived from multiple fertility measures may better explain trait variability than a single fertility measure.

This study aims to investigate whether the relationships between soil fertility and nutrient-related plant traits can be improved by analyzing the mutual and divergent impacts of different soil fertility measures. To this aim, we tested (1) whether nutrient elements in soil (N or P) have specific or shared impacts on plot-mean plant traits (i.e. averaged or aggregated values of traits of all plants in each plot), (2) whether the timescale of a soil fertility measure is important in explaining plot-mean plant traits, and (3) whether use of an integrated soil fertility measure improves the fertility vs. trait relationships. Subsequently, we infer from our findings which fertility measure or combinations of fertility measures are the best suited to describe among-plots trait variations. Throughout the paper, we considered vascular plants only, since non-vascular species (i.e. mosses and lichens) do not directly take up nutrients from soils and are thus less relevant in the context of soil fertility–trait relationships.

Materials and Methods

Ethic Statement

We obtained permissions for soil and vegetation sampling in Hoge Veluwe national park (permission from Stichting het nationale park de Hoge Veluwe), Zuid-Kennemerland national park (permission from Provinciaal Waterleidingbedrijf Noord-Holland), and nature reserves owned by Staatsbosbeheer.

Site selection

We selected 36 sites in the Hoge Veluwe and Zuid-Kennemerland national parks and nature reserves owned by Staatsbosbeheer (dataset 1). Additionally, we used 47 sites of Olde Venterink et al. [11] (dataset 2) and 51 sites of Ordonez et al. [3] (dataset 3); these studies used almost the same methods to measure soil and plant properties (see Table 1 for a methodological overview). In total, we thus acquired information for 134 sites and 372 plant species in natural ecosystems in the Netherlands and Belgium, consisting of 104 grasslands, 17 shrub lands (including heath), and 13 forests. These sites cover the range of ecosystems typical in this region except for those influenced by brackish water. Vascular plant species were recorded in a plot size of 4 m^2 for herbaceous, 4, 9, or 25 m^2 for shrub (depending on the size of the woody species), and 100 m^2 for forest stands. Soil cores of 10 cm depth (datasets 1 and 3) or 15 cm depth (dataset 2) were taken within or next to the plot. Large roots were removed from the soil cores. For datasets 1 and 3, several soil cores were mixed to make a composite soil to eliminate the effects of local soil heterogeneity. In the peak growing season (July or August), above-ground standing biomass of vascular plants (datasets 1 and 2) or leaves of dominant vascular species (dataset 3) were harvested.

Soil fertility measures

Dissolved N ($N–NO_3$ + $N–NH_4$, mg N kg^{-1} soil) and dissolved P ($P–PO_4$, mg P kg^{-1} soil) were measured to indicate the short-term availability of N and P, respectively. Two different extraction methods were used to measure dissolved P: ammonium lactate-acetic acid (ALA) extraction and the Olsen extraction. Therefore, we converted the values estimated with the ALA extraction to be comparable to those with Olsen extraction, using an empirically derived relationship [13] (Olsen-P = 2.35+0.45 ·ALA-P). The potential influence of using two different extraction methods is tested in Fig. S1 in Appendix S1. Olsen extraction is meant for neutral to alkaline soils; however, this method was also used for some of our acid (pH<5) soils. The potential interference of these acid soils on our results is tested in Fig. S2 in Appendix S2.

As a longer-term indication of N availability, we measured in-situ N mineralization rates in the mid growing season ('summer Nmin') for 6 weeks (datasets 1 and 3) or 8 weeks (dataset 2) (see [14] for details about the method). The difference in dissolved N between the beginning and the end of the incubation period was considered as mineralized N from organic N. Mineralized N was expressed as rates per week (mg N kg^{-1} soil $week^{-1}$). Because denitrification in wet soil cores could have caused a considerable loss of N from the incubation tubes [14], we corrected for the N loss by adding modelled denitrification rates simulated by DAYCENT [15] to the measured N mineralization rates.

Additionally, to estimate nutrient availability for much longer terms, we used a modified version of a SOM model, CENTURY [14]. The CENTURY model simulates decomposition of soil organic C and associated flows of organic N and P. Soil total C, N, and P, soil texture, temperature, and moisture of the top soil were used as model input values. Soil temperature and moisture were simulated with a hydrological model SWAP [16]. The daily groundwater level of each site, required for the SWAP simulation, was estimated by temporal inter- and extrapolation of the observed groundwater levels in nearby wells (mostly within 30 m from the plot) using MENYANTHES software [17]. With the CENTURY model, cumulative net mineralization rates of N and P were estimated for the year of the sampling (from the first of January [mid-winter] until the end of August [end of summer], as plant traits were measured by then) ('annual Nmin', mg N kg^{-1} soil 243-day^{-1} and 'annual Pmin', mg P kg^{-1} soil 243-day^{-1}) and for the preceding five years (from September five years before the sampling year to August of the sampling year) ('5yr Nmin', mg N kg^{-1} soil 5-$year^{-1}$ and '5yr Pmin', mg P kg^{-1} soil 5-$year^{-1}$). Transformation processes of mineralized N and P (e.g., nitrification, denitrification, adsorption and precipitation of inorganic P) were not considered.

Finally, as very rough measures of soil fertility in the long time span, we used soil total N and P (% of total soil mass), soil N:C ratio, and soil P:C ratio.

Plant traits

N and P concentration in leaves (LNC and LPC, respectively; mg g^{-1}) were determined for dataset 3 only (Table 1). Nutrient concentrations were measured in each site for dominant species,

Table 1. Overview of methodology of soil and plant trait measurements for three datasets used in this study.

		Dataset 1	Dataset 2 [11]	Dataset 3 [3]
N. of sites		**36**	**47**	**51**
N. of combined soil cores per site		**3**	**1**	**5**
Soil fertility measurements				
Soil C	%	CNS analyzer*1*2	0.5 · Loss on ignition at 550°C	CNS analyzer*1
Soil N	%	CNS analyzer*1	Kjeldahl digestion	CNS analyzer*1
Soil P	%	HNO_3 + HCl digestion	Kjeldahl digestion	HNO_3 + HCl digestion
Dissolved N ($N–NO_3$ + $N–NH_4$)	mg N kg^{-1} dry soil	1 M KCl extraction	1 M KCl extraction	1 M KCl extraction
Dissolved P ($P–PO_4$)	mg P kg^{-1} dry soil	Olsen extraction (0.5 M $NaHCO_3$)	ALA extraction (0.1 M NH_4OH + 0.1 M lactic acid + 0.4 M acetic acid)	Olsen extraction (0.5 M $NaHCO_3$)
Summer N mineralization	mg N kg^{-1} dry soil $week^{-1}$	6 weeks in-situ incubation in May–July (d 15 cm x ø 4 cm)	8 weeks in-situ incubation in July–August (d 10 cm x ø 4.8 cm)	6 weeks in-situ incubation in June–August (d 15 cm x ø 6 cm)
Annual N and P mineralization	mg N (or mg P) kg^{-1} dry soil 243-day^{-1}	Simulated with CENTURY	Simulated with CENTURY	Simulated with CENTURY
5-year N and P mineralization	mg N (or mg P) kg^{-1} dry soil 5-$year^{-1}$	Simulated with CENTURY	Simulated with CENTURY	Simulated with CENTURY
Soil texture*3	clay/silt/sand in fraction	Laser particle sizer	Estimated*4	Estimated*4
Plant trait measurements				
LNC	mg g^{-1}	-	-	CNS analyzer*1
LPC	mg g^{-1}	-	-	HNO_3 + HCl digestion
WNC	mg g^{-1}	CNS analyzer*1	Kjeldahl digestion	-
WPC	mg g^{-1}	HNO_3 + HCl digestion	Kjeldahl digestion	-
IV_{nut}	-	Derived from species composition		
CSR	-	Derived from species composition		

*1CNS analyzer (Carlo Erba NA 1500, Rodana).
*2C in $CaCO_3$, determined with thermogravimetric analysis (TGA-601, Leco Corporation), was subtracted.
*3Used as model input values for CENTURY simulation.
*4Estimated based on top layer characteristics of the soil physical unit, derived from 1:50,000 soil map.
doi:10.1371/journal.pone.0083735.t001

and weighted averages (weighted by species' relative cover) were used as the plot-mean LNC and LPC. The dominant species were sampled until the cover sampled exceeded 50% of the total vascular plant cover. Note that the 50% of coverage being sampled is rather low compared to the recommended threshold of 80% [18], and therefore the LNC and LPC values in our study may slightly deviate from the true plot-mean values.

The entire above-ground plant biomass (i.e. all vascular plants of the community together) was sampled to determine whole-canopy N and P concentrations in each plot (WNC and WPC, respectively; mg g^{-1}) for datasets 1 and 2 (Table 1). Since WNC and WPC reflect the aggregated characteristics of the community, they are considered as plot-mean trait values. One plot in dataset 1, which did not have nutrient concentration data, was excluded from all analyses concerning WNC and WPC. Woody species were included in WNC and WPC when they were young seedlings less than one year old, so that WNC and WPC reflect the annual uptake of the nutrients. LNC, LPC, WNC, and WPC were log-transformed prior to analyses to correct for the right-skewed distributions.

Combinations of multiple plant traits are constrained by physiological trade-offs [19]; thus, integrative traits (e.g. nutrient use efficiency) or strategy types help to express trait variability in fewer dimensions. Here we used two types of integrative plant traits: one based on species occurrences in different habitats (i.e. indicator values for nutrients, IV_{nut} [20]), and the other based on life history traits (Grime's CSR strategy [21]).

IV_{nut} is comparable to the Ellenberg indicator value for nutrients, but is tailored for Dutch flora and has a continuous scale ranging from 1 (prevailing at nutrient poor sites) to 3 (prevailing at nutrient rich sites) [20]. Plot-mean IV_{nut} values were computed as arithmetic means of IV_{nut} for each site, rather than weighted means of IV_{nut} based on species abundance, as the former was shown to be sufficient for this trait with ordinal-scale values [22]. 26 species (out of total 372 species recorded in our study), for which IV_{nut} value was not available, were excluded from the calculation of plot-mean IV_{nut} values. The trait coverage (i.e. percentage of species with IV_{nut} values within each plot) ranged from 76% to 100% (median 94%).

The CSR scheme represents the adaptive strategy of plant species along gradients of resource availability, stress, and disturbance, expressed with three axes of primary components: C ('Competitors'), S ('Stress tolerators'), and R ('Ruderals'). Each species can be classified into one out of 19 classes with different combinations of strategy components, e.g. C, SR/R, or CSR. We retrieved CSR strategies from Hunt et al. [23] (313 species), supplemented by the BioFlor database [24] (35 species). For 11 species, we assigned the CSR strategy according to the method of

Hodgson et al. [25], using seven life-history traits of these species retrieved from the LEDA database [26]. The remaining 13 species, for which we could not attribute CSR strategy due to lack of trait information, were excluded from the calculation of plot-mean CSR values. For each species, scores of each primary component (C, S, and R) were determined from its proportional contribution to a specific strategy (e.g. C scores of C, CS, CSR strategy are 1, 0.5, and 0.33, respectively: cf. [27]). Subsequently, for each site, plot-mean scores of C, S, and R (again, not weighted average by species abundance) were calculated. The trait coverage ranged from 86% to 100% (median 100%).

Statistics

Variation partitioning. Soil fertility measures were correlated, especially strongly within the group of N-related measures and that of P-related measures (table S1). In order to examine the relative contribution of soil N and soil P to plant trait variation among sites, we partitioned the variance of each plant trait t ($\mathbf{T}t$, a vector of n plots) into unique and shared effects of the two groups of predictor variables; i.e. to N-related fertility measures (**N**, a matrix of n x p_N, where p_N is the number of N-related fertility measures, $p_N = 6$) and P-related fertility measures (**P**, a matrix of n x p_P, where p_P is the number of P-related fertility measures, $p_P = 5$) [28]. The fraction of variance explained was indicated by the coefficient of determination of linear regression analysis for $\mathbf{T}t$ regressed by $\boldsymbol{X}$, where $\boldsymbol{X}$ is either **N**, **P**, or **N**&**P**. In order to correct for the different number of fertility measures within each group, we used adjusted R^2, $R^2_{(\mathbf{T}t|\boldsymbol{X})\ \mathrm{adj}}$, according to [29]. The unique effects of **N** were calculated as the fraction of variance in $\mathbf{T}t$ explained by **N**&**P** minus the effects of **P** on $\mathbf{T}t$: $R^2_{(\mathbf{T}t|\mathbf{N}\&\mathbf{P})\ \mathrm{adj}} - R^2_{(\mathbf{T}t|\mathbf{P})\ \mathrm{adj}}$. Identically, the unique effects of **P** on $\mathbf{T}t$ were calculated as $R^2_{(\mathbf{T}t|\mathbf{N}\&\mathbf{P})\ \mathrm{adj}} - R^2_{(\mathbf{T}t|\mathbf{N})\ \mathrm{adj}}$. Shared effects of **N** and **P** on $\mathbf{T}t$ were calculated as $R^2_{(\mathbf{T}t|\mathbf{N})\ \mathrm{adj}} + R^2_{(\mathbf{T}t|\mathbf{P})\ \mathrm{adj}} - R^2_{(\mathbf{T}t|\mathbf{N}\&\mathbf{P})\ \mathrm{adj}}$. The analysis was performed in R [30].

Additionally, we tested if N-related fertility measures explain significantly more variance in plot-mean traits than P-related fertility measures, and vice versa, following the bootstrapping method described in [29] using R [30]. Bootstrapped adjusted R^2 was computed 1000 times, and the difference between the adjusted R^2 between groups, $D_i = R^2_{(\mathbf{T}t|\mathbf{N})\ \mathrm{adj\text{-}boot},i} - R^2_{(\mathbf{T}t|\mathbf{P})\ \mathrm{adj\text{-}boot},i}$, was calculated for each ith bootstrapping. p-values were calculated from the distribution of D_i, as the fraction of D_i that falls below zero (when the median of D_i was positive, i.e. variance explained by **N** was larger than that by **P**) or above zero (when the median of D_i was negative).

Hierarchical partitioning. In order to examine the most relevant timescale of soil fertility for explaining the variation of plant traits, we used the hierarchical partitioning method [31,32]. This method allows, within the hypothetical relationship between trait variance (response variable) and k fertility measures with different timescales (predictor variables), to quantify the independent contribution of a fertility measure S to the explained variance of a trait without being confounded by the other k-1 fertility measures. The hierarchical partitioning method computes the increase in goodness-of-fit when S is added to the model (in our case: a linear multivariate regression model of a trait regressed by fertility measures) compared to the model without S, and averages the increase over all possible models that include S as a predictor variable (i.e. 2^k models). In this way, the variation of a trait explained by S is divided into an independent effect of S and joint effect of S with other fertility measures. Negative values of a joint effect mean that the interactive effects of S and the other fertility measures on the trait are suppressive, rather than enhancing. An advantage of using the hierarchical partitioning over a one-model approach is that the averaging eliminates the problem of multicollinearity among predictor variables [32]. We conducted hierarchical partitioning separately for N-related and P-related fertility measures (i.e. $k = p_N$ or $k = p_P$), so that interactions of N and P do not obscure the effects of timescale. We used R^2 as the goodness-of-fit measure of the models. The analysis was performed in R [30] with the package 'hier.part' [33].

Foe each fertility measures, the statistical significance of their independent contribution to a plant trait was tested by randomizing the pairs of trait and fertility values for 1000 times [32] in R [30]. Z-scores were calculated from the generated distribution of randomized independent contributions, and statistical significance was determined based on the upper 95% confidence limit ($Z \geq 1.65$).

In addition, independent contributions were compared among fertility measures with different timescales by means of bootstrapping in R [30]. 134 plots were randomly selected with replacement, and the 95% confidence interval was computed from the distribution of independent contributions of 1000x bootstrapped 134 plots. Furthermore, the difference in independent effects between two fertility measures was computed for all combinations. When more than 95% of the difference was larger or smaller than zero, we considered that the two fertility measures had significantly ($p<0.05$) different magnitudes of independent effects.

Principal component regression. Since the soil fertility measures were strongly correlated, we extracted the main axes of variation by a Principal Component Analysis (PCA) in R [30], based on a correlation matrix to correct for differences in metrics among variables. We used six soil N measures, five soil P measures, and soil N:P ratio. All these variables were log-transformed prior to the analysis. We extracted the scores of sites along PCA axis 1 and 2 and related them to plot-mean values of each trait using linear regression.

Results

Relative contributions of soil N and P measures to plot-mean plant traits

Bivariate correlations between plant traits and soil fertility measures were often significant (table S2). All soil fertility measures together explained less than half of the among-site variation in leaf nutrient concentration (32.7% for LNC [Fig. 1A] and 42.8% for LPC [Fig. 1B]), in which a large part was attributed to the shared effects of soil N and P measures. There was no significant difference between soil N and P measures in their contribution to the total explained trait variance ($p = 0.42$ for LNC, $p = 0.30$ for LPC). P concentrations at the whole-canopy level were more strongly related to soil fertility measures than those on a leaf level (i.e. 65.9% of variance in WPC was explained, Fig. 1D). In contrast, the relationships between N concentrations and soil fertility were weak both on a whole-canopy level and on a leaf level (i.e. 31.0% of variance in WNC was explained, Fig. 1C). For both WPC and WNC, the shared effects of soil N and P measures were relatively small, and the contribution of soil P measures was larger than that of soil N measures (significant for WPC [$p<0.001$] but not for WNC [$p = 0.42$]).

55.5% of the variance in IV_{nut} was explained by soil fertility measures (Fig. 1E), of which less than half was attributed to the shared effects of soil N and P measures (18.2%). The contribution of soil P and N measures was not significantly different ($p = 0.33$).

Of the three components of the CSR strategy, soil fertility measures explained the variance in the S component to a largest extent (50.7%, Fig. 1G), followed by the C component (33.6%,

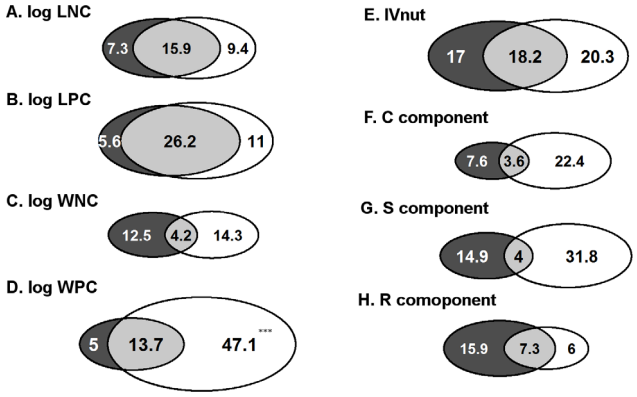

Figure 1. Partitioning of among-site plant trait variation. Trait variations (in percentage of variance) are divided into unique effects of soil N measures (dark grey), unique effects of soil P measures (white), and shared effects of both (light grey). Examined plot-mean plant traits are A: log-transformed leaf N concentration, LNC (mg/g) ($n = 51$), B: log-transformed leaf P concentration, LPC (mg/g) ($n = 51$), C: log-transformed N concentration of above-ground plant biomass, WNC (mg/g) ($n = 82$), D: log-transformed P concentration of above-ground plant biomass, WPC (mg/g) ($n = 82$), E: indicator value for nutrients, IV_{nut} ($n = 134$), F: C component ($n = 134$), G: S component ($n = 134$), and H: R component ($n = 134$). When the contribution of N or P measures to the total explained variance is significantly larger than the other, this is indicated by asterisks (***: $p<0.001$).
doi:10.1371/journal.pone.0083735.g001

Fig. 1F) and the R component (29.3%, Fig. 1H). Shared effects contributed to a small proportion of the explained variance (4.0% for S, 3.6% for C, and 7.3% for R). For the R component, the contribution of soil N measures was almost significantly ($p = 0.057$) larger than that of soil P measures, whereas for the C and S components, the contribution of soil P measures was considerably (but not significantly, $p = 0.16$ and $p = 0.21$, respectively) larger than that of soil N measures.

Effects of different timescales of soil fertility measures on plot-mean plant traits

Only few fertility measures had significant independent effects on LNC and WNC (i.e. dissolved P and soil total P for LNC [Fig. 2I], soil total N and annual Pmin for WNC [Fig. 2C and 2K]). The independent effects were not significantly ($p>0.05$) different among fertility measures with different timescales (Table S3).

For LPC, independent effects were significant for three out of six soil N measures (Fig. 2B) and for three out of five soil P measures (Fig. 2J). Longer-term measures (e.g. soil total N, soil total P) tended to have larger independent effects, but the differences with short-term measures were not very apparent (e.g. only dissolved N had slightly smaller effects than longer-term measures i.e. annual Nmin, 5yr Nmin, and soil total N, $p<0.05$, Table S3).

For WPC, all soil P measures had significant independent effects (Fig. 2L). Longer-term measures (e.g. 5yr Pmin and soil P:C ratio) tended to have larger independent effects, but the differences were not significant ($p>0.05$) except between 5yr Pmin and annual Pmin ($p<0.01$, Table S3).

For IV_{nut}, independent effects were significant for all fertility measures (Fig. 2E, Fig. 2M). The independent effects were not significantly ($p>0.05$) different among fertility measures with different timescales except between 5yr Pmin and annual Pmin ($p<0.05$, Table S3).

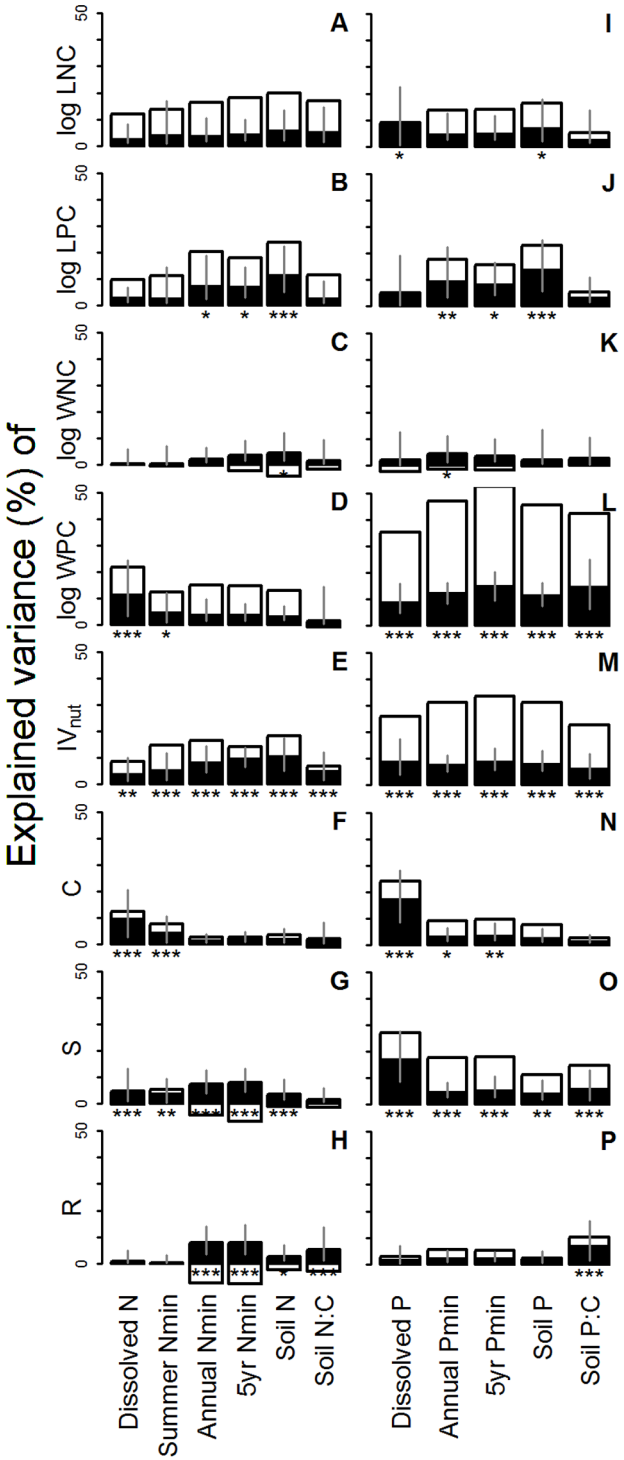

Figure 2. Hierarchical partitioning of among-site plant trait variation. Trait variations are divided into independent effects of a soil fertility measure (black bars) and its joint effects with other measures (white bars). All fertility measures (see Table 1 for specification) were log-transformed prior to the analysis. Examined plot-mean plant traits are A&I: log LNC, B&J: log LPC, C&K: log WNC, D&L: log WPC, E&M: IV_{nut}, F&N: C component, G&O: S component, and H&P: R component. See the caption of Figure 1 for the specification and sample number of each plant trait. Computation was done within each group of fertility measures (i.e. within soil N measures [A–H] and soil P measures [I–P]). Asterisks indicate that the independent effect was significant, based on Z-scores computed with randomization (*: $p<0.05$, **: $p<0.01$, ***:

$p<0.001$). 95% confidence intervals of independent effects, obtained by 1000-time bootstrapping, are shown.
doi:10.1371/journal.pone.0083735.g002

For the C component of the CSR strategy, independent effects were significant and stronger for shorter-term fertility measures (e.g. dissolved N, summer Nmin, dissolved P; Fig. 2F and Fig. 2N). In contrast, for the S component, almost all fertility measures had significant independent effects (Fig. 2G, Fig. 2O), but the difference was less apparent (although dissolved P had stronger independent effects than all other soil P measures, $p<0.05$, Table S3). The strong independent effects of dissolved P on the C and S components could be an artefact of using Olsen extraction methods for some of the acid soils (see Appendix S2 for details). For the R component, soil P measures hardly had significant independent effects, and timescale did not matter ($p>0.05$, Table S3) (Fig. 2P), whereas intermediate-term soil N measures (e.g. annual Nmin, 5yr Nmin) had significant and stronger ($p<0.01$) independent effects than shorter-term measures (e.g. dissolved N, summer Nmin) (Fig. 2H, Table S3).

Relations between integrated soil fertility measures and plot-mean plant traits

PCA analysis extracted major axes of variation in soil fertility measures. The first axis, explaining 59.8% of the variance, was related to overall nutrient availability of a site (i.e. high in both soil N and P), with the negative axis values representing fertile conditions (Fig. 3). The second axis, explaining 18.3% of the variance, separated relatively P-rich (positive axis values) from N-rich (negative axis values) sites (Fig. 3).

Most plant traits, except WNC and the R component, were significantly related to PCA axis 1 (Fig. 4A–H). PCA axis 2 was significantly related only to WPC, IV_{nut}, the S component, and the R component (Fig. 4I–P). Multiple regression analysis showed that both PCA axes had significant ($p<0.05$) effects for WPC, IV_{nut}, and the S component (and almost significant [$p<0.07$] effects for

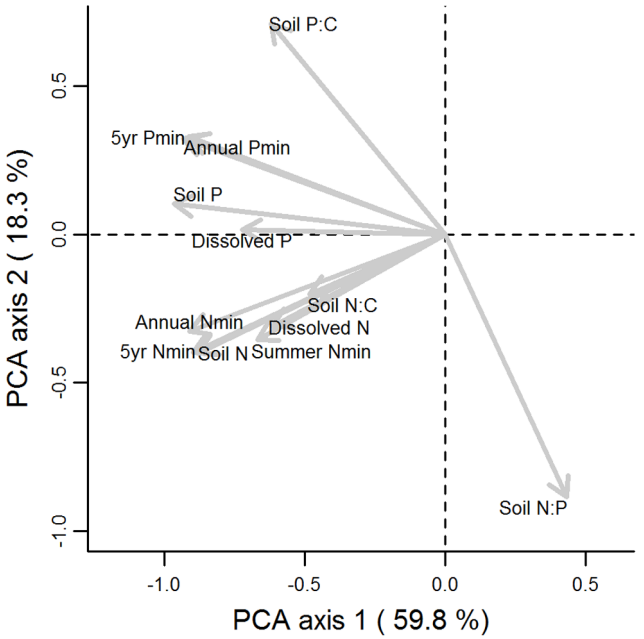

Figure 3. Principal Component Analysis (PCA) of 12 soil fertility measures for 134 plots.
doi:10.1371/journal.pone.0083735.g003

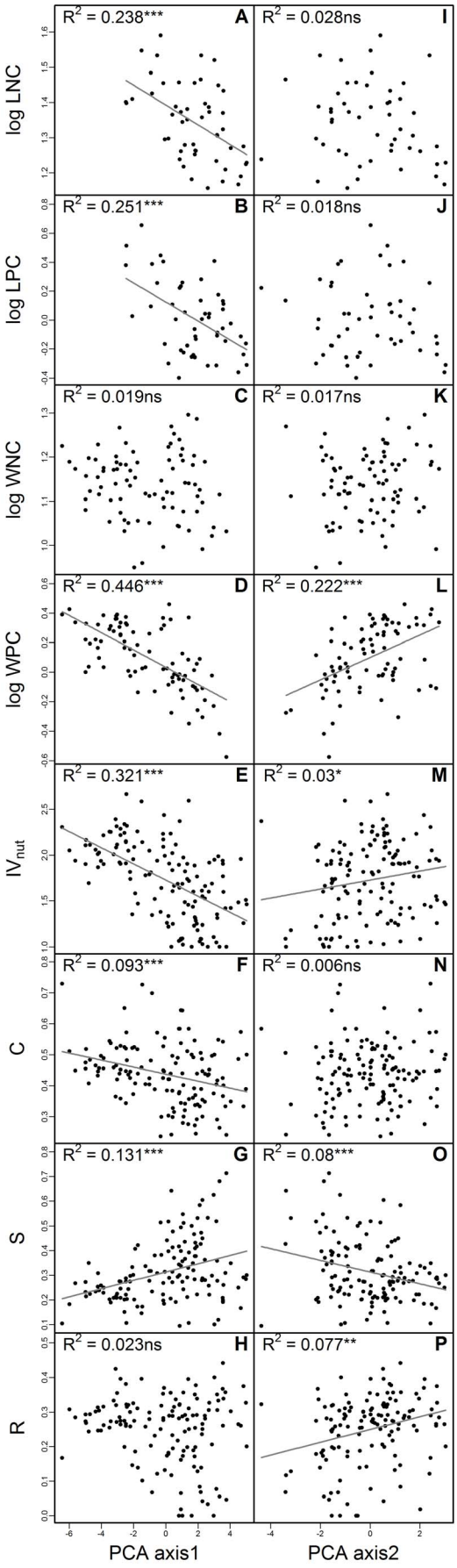

Figure 4. Relationships of the first and second PCA axis with plot-mean plant traits. R^2 and *p*-values of linear regression analysis are shown. Lines represent the regression model (only when $p<0.05$). See the caption of Figure 1 for the specification and sample numbers for each plant traits.
doi:10.1371/journal.pone.0083735.g004

the R component); this indicates that the two axes had complementary rather than redundant effects on these traits.

Discussion

Mutual and stoichiometric control of soil N and P on plant traits

In line with previous studies [2,4,5], we found that fertile soils are associated with plant communities composed of species with higher nutrient concentrations, and include more competitor rather than stress-tolerant types of species. However, we highlight the importance of considering both soil N and soil P concentrations in explaining trait variation among communities. Indeed, we found that soil N and P had a strong mutual (shared) effect on LNC and LPC while other traits tend to be related to unique effect of soil N or soil P.

There are several possible mechanisms that explain why LNC is related to both soil N and soil P (rather than only to soil N) and why LPC is related to both soil N and soil P (rather than only to soil P). Although leaf-level nutrient concentrations change plastically with changing concentrations of that element in the soil [34], LNC and LPC are strongly coupled with a 2/3-power law of scaling [35,36] due to the mutually dependent roles of N and P in photosynthesis. Consequently, rapid growth, which is associated with high LNC and high LPC [35], is realized only when both soil N and P availability for plants is high. This clarifies the observed pattern that the shared effects of soil N and P (i.e. overall fertility effects), rather than the unique effects of soil N and soil P, explain the large variation in LNC and LPC.

In contrast, the nutrient concentrations on a whole-canopy level (WNC and WPC) reflect the availability of single elements more strongly than on a leaf level, because plants store excess elements in non-leaf organs. This is reflected in a much larger variation in N:P ratio in non-leaf organs than in leaves [37]. The predictive power of soil P on WPC was especially strong, because plants can adjust P concentrations much more flexibly than N concentrations to the nutrient availability in the soil [38].

For IV_{nut}, the unique effects of single elements contributed to most of the explained variance, although the shared effect of soil N and P also accounted for a large part of the variance. For the CSR strategy, most of the explained variance was related to the unique effects of single elements, rather than to the shared effects of soil N and P. Here, the effects of N and P were highly different, indicating a stoichiometric control of soil N and P on the CSR strategy of vegetation. The unique effects of soil P were larger than those of soil N for the C and S components, in accordance with the findings of Ceulemans et al. [39] based on Olsen-extracted P availability and KCl-extracted N availability. Variance in the R component was least explained, reflecting that environmental drivers other than nutrient availability (i.e. disturbance) are the primary determinants of the distribution of ruderals [21].

To test whether the above-mentioned trends were merely an artefact of biased distribution of N- and P-limited ecosystems in our study, we conducted the same analyses for N-limited and P-limited plots separately (Appendix S3). When only N-limited plots were considered, contributions of soil N measures to plant trait variance tended to increase slightly (Fig. S3 left); however, other major trends (e.g. a stronger effect of soil P on WPC than that of soil N [$p = 0.094$], small shared effects on CSR strategy) remained. When only P-limited plots were considered, the contributions of soil P remained mostly unchanged or even decreased for some traits (Fig. S3 right). It is particularly notable that the stronger determinants for stress tolerators were N-related fertility measures in N-limited plots ($p<0.05$) and P-related fertility measures in P-limited plots ($p = 0.079$) (Fig. S3). Furthermore, signs of correlations between soil N measures and integrative plant traits (IV_{nut}, CSR strategy) reversed in P-limited plots compared to N-limited plots for most cases (e.g. stress tolerator increased as soil N availability increased in P-limited plots only; see Table S4 in comparison to Table S5 in Appendix S3). These reversed relationships imply that, under P-poor conditions, high soil N availability results in an extreme imbalance of soil N and P and therefore induces harsher environments for plant species. This emphasizes the importance of explicitly considering stoichiometric effects of nutrients on plant functioning.

Timescale has only minor impact on fertility–trait relationships

Contrary to previous results [2,10], we found no clear indication that the fertility–trait relationship is sensitive to the timescale of the soil fertility measure. Almost all soil fertility measures were closely correlated, and therefore the independent effects of a particular fertility measure were almost never outstandingly stronger than that of others.

It is more difficult to estimate the availability of soil P for plants than that of soil N; this is because various geochemical processes of soil inorganic P, such as adsorption and precipitation, are involved. These processes were not explicitly included in our soil P measures, possibly obscuring the impact of timescale on the fertility–trait relationships. To test this, we examined for a subset of our dataset (36 plots) whether adding extra measurements of soil P availability improved the fertility–trait relationships (Appendix S4). Neither summer gross P mineralization rates (i.e. increase in Olsen-extractable P [both inorganic and organic] in in-situ incubation experiments), oxalate-extractable P (i.e. an estimate of reducible amount of P, which includes P adsorbed on Al- and Fe-hydroxides and oxides [40]), nor the degree of phosphate saturation (i.e. the percentage of oxalate-extracted P over half of oxalate-extracted Al plus Fe, an index for soil capacity to release P [41]) were superior to other P fertility measures in explaining trait variations (Fig. S5 in Appendix S4). So, the virtual absence of timescale impacts on soil fertility–trait relationships was not likely due to the inadequacy of selected P measures.

Use of integrated soil fertility measures to explain community trait composition

There was no single fertility measure that dominantly explained plant trait variations; this indicates that plant traits are mutually controlled by multiple soil fertility measures, suggesting the usefulness of using integrated fertility measures. Indeed, the main axis of variation in fertility measures, overall fertility gradient (PCA axis 1), was related to almost all plant traits. However, the explanatory power of the PCA axis 1 (i.e. R^2 values in Fig. 4) was only slightly higher for LNC and LPC than that of the best single fertility measures (i.e. variance explained by a fertility measure, including both independent and joint effects, in Fig. 2). For the other traits, PCA axis 1 explained less than the best single fertility measures. The other integrated fertility measure, the relative availability of soil N and P (PCA axis 2), had small but complementary effects for some plant traits (i.e. WPC, IV_{nut}, S

component, R component). Similarly, including the type of nutrient limitation of plants (i.e. N- or P-limited) improved the relationship between overall fertility and several plant traits (WNC, WPC, IV_{nut}, R component) (Fig. S4 in Appendix S3). This means that the fertility–trait relationships are modulated by the type and magnitude of nutrient limitation, probably because the most influential factor of fertility is not identical for all sites but depends on which nutrient is actually limiting the plant growth of the site.

These findings imply that simultaneous consideration of overall fertility and N:P stoichiometry (either in soil or in plants) is a prerequisite for improving fertility–trait relationships. Note that the N:P stoichiometry effect cannot be assessed by individual fertility measures alone, but it can be explicitly tested by integrated fertility measures (i.e. PCA axis 2 in our case). This suggests the appropriateness of using integrated fertility measures as a starting point to explore which aspect of soil fertility has a relevant effect on the specific plant trait.

Wrong choice of fertility measure, or intrinsically moderate relationships between fertility and plant traits?

As in previous studies [2,4], variance of LNC was less strongly explained by fertility measures than that of LPC in our study, even if various types of fertility measures were considered (i.e. 32.7% explained by all fertility measures together, 19.9% by the best single measure [soil total N] and 23.8% by the best integrated measure [PCA axis 1]). Also, only a minor part of the variation was explained by soil fertility for WNC (31.0%, 3.2%, and 1.9%, respectively) and for R component (29.3%, 6.7%, and 7.7%, respectively). In contrast, several other plant traits could be well explained by fertility measures: 65.9%, 52.6%, and 44.6% for WPC, respectively, and 55.5%, 33.6%, and 32.1% for IV_{nut}, respectively. Reasonably good relationships between IV_{nut} or equivalent (e.g. Ellenberg indicator value for nutrients) and a single soil fertility measure have also been observed before (e.g. 49% explained by annual N mineralization rates [5], 35% explained by 'nitrification degree' [9], 29% explained by oxalate-extractable P [42]).

Thus, the moderate fertility–trait relationships of some plant traits are most likely not because of a wrong choice of fertility measure but because of the intrinsic nature of the relationships for these traits as explained earlier. Furthermore, environmental factors other than soil fertility also influence plant traits. For example, the occurrence of ruderal species (R component of CSR strategy) is primarily associated with disturbance rather than soil fertility [21], and LNC and LPC are weakly but consistently related with drought and oxygen stress [43]. Since plant traits are coordinated through physiological trade-offs and the coordination of the traits is strongly modulated by environmental factors [19,44], simultaneous consideration of multiple environmental factors is necessary to improve the prediction of these traits. Reasonably good relationships between fertility and IV_{nut} encourage the application of this relationship in species-distribution models to predict the functional composition of plant species. Also, other plant traits unexamined in our study, such as specific leaf area, may be considered for examining fertility–trait relationships. Specific leaf area was, however, not better related to soil fertility measures than LPC [4].

In conclusion, our study showed that among-site variations in nutrient-related plant traits are consistently, although moderately for some traits, related to soil fertility measures. Whether a trait has only a moderate relationship depends on the mechanism through which soil fertility and other factors regulate the trait variation. The timescale of the fertility measure has only negligible or minor effects on fertility–trait relationships, whereas the mutual and/or stoichiometric effects of N and P should be considered to improve the relationships. Since the relative importance of soil fertility measures is different among plant traits, a scan of integrated fertility measures will facilitate identification of influential fertility measures (or groups of fertility measures) for each specific plant trait separately.

Supporting Information

Table S1 Correlations among soil fertility measures.
(DOCX)

Table S2 Correlations between plot-mean plant traits and soil fertility measures.
(DOCX)

Table S3 Comparison of 1000x bootstrapped independent effects among soil fertility measures.
(DOCX)

Appendix S1 Testing the effects of using two extraction methods for dissolved P.
(DOCX)

Appendix S2 Testing the effects of using Olsen-P extraction for acid soils.
(DOCX)

Appendix S3 Fertility–trait relationships in N- and P-limited ecosystems.
(DOCX)

Appendix S4 Testing additional soil P measures for a subset of dataset.
(DOCX)

Acknowledgments

This research was carried out in the framework of CARE project of the Dutch national research program 'Knowledge for Climate' and the joint research programme of the Dutch Water Utility sector. We thank Staatsbosbeheer, Veluwe national park, and PWN for the permission to sample soils; H. Olde Venterink and J. Ordonez for the permission to use their database; F. Daniels, H. Roelofsen, and J. Runhaar for field sampling; and J.C. Douma and R.P. Bartholomeus for SWAP simulations.

Author Contributions

Conceived and designed the experiments: YF PMvB JPMW. Performed the experiments: YF. Analyzed the data: YF PMvB. Wrote the paper: YF PMvB JPMW.

References

1. Aerts R, Chapin FS, III (2000) The mineral nutrition of wild plants revisited: a re-evaluation of processes and patterns. Advances in Ecological Research 30: 1–67.
2. Ordonez JC, van Bodegom PM, Witte JPM, Wright IJ, Reich PB, et al. (2009) A global study of relationships between leaf traits, climate and soil measures of nutrient fertility. Global Ecology and Biogeography 18: 137–149.
3. Ordonez JC, van Bodegom PM, Witte JPM, Bartholomeus RP, van Hal JR, et al. (2010) Plant Strategies in Relation to Resource Supply in Mesic to Wet Environments: Does Theory Mirror Nature? American Naturalist 175: 225–239.
4. Ordoñez JC, Van Bodegom PM, Witte JPM, Bartholomeus RP, Van Dobben HF, et al. (2010) Leaf habit and woodiness regulate different leaf economy traits at a given nutrient supply. Ecology 91: 3218–3228.

5. Douma JC, Witte J-PM, Aerts R, Bartholomeus RP, Ordoñez JC, et al. (2012) Towards a functional basis for predicting vegetation patterns; incorporating plant traits in habitat distribution models. Ecography 35: 294–305.
6. Sonnier G, Shipley B, Navas M-L (2010) Quantifying relationships between traits and explicitly measured gradients of stress and disturbance in early successional plant communities. Journal of Vegetation science 21: 1014–1024.
7. Fukami T, Dickie IA, Paula Wilkie J, Paulus BC, Park D, et al. (2010) Assembly history dictates ecosystem functioning: evidence from wood decomposer communities. Ecology Letters 13: 675–684.
8. Cavender-Bares J, Kitajima K, Bazzaz FA (2004) Multiple trait associations in relation to habitat differentiation among 17 Floridian oak species. Ecological Monographs 74: 635–662.
9. Schaffers AP, Sykora KV (2000) Reliability of Ellenberg indicator values for moisture, nitrogen and soil reaction: A comparison with field measurements. Journal of Vegetation science 11: 225–244.
10. Van Duren IC, Pegtel DM (2000) Nutrient limitations in wet, drained and rewetted fen meadows: evaluation of methods and results. Plant and Soil 220: 35–47.
11. Olde Venterink H, Pieterse NM, Belgers JDM, Wassen MJ, de Ruiter PC (2002) N, P and K budgets along nutrient availability and productivity gradients in wetlands. Ecological Applications 12: 1010–1026.
12. Schaffers AP (2000) In situ annual nitrogen mineralization predicted by simple soil properties and short-period field incubation. Plant and Soil 221: 205–219.
13. Carmo Horta Md, Roboredo M, Coutinho J, Torrent J (2010) Relationship between Olsen P and ammonium lactate-extractable P in Portuguese acid soils. Communications in Soil Science and Plant Analysis 41: 2358–2370.
14. Fujita Y, van Bodegom PM, Olde Venterink H, Runhaar H, Witte J-PM (2013) Towards a proper integration of hydrology in predicting soil nitrogen mineralization rates along natural moisture gradients. Soil Biology and Biochemistry 58: 302–312.
15. Del Grosso S, Ojima D, Parton W, Mosier A, Peterson G, et al. (2002) Simulated effects of dryland cropping intensification on soil organic matter and greenhouse gas exchanges using the DAYCENT ecosystem model. Environmental pollution 116: S75–S83.
16. Van Dam JC, Groenendijk P, Hendriks RFA, Kroes JG (2008) Advances of modeling water flow in variably saturated soils with SWAP. Vadose Zone Journal 7: 640–653.
17. von Asmuth JR, Maas K, Knotters M, Bierkens MFP, Bakker M, et al. (2012) Software for hydrogeologic time series analysis, interfacing data with physical insight. Environmental Modelling & Software 38: 178–190.
18. Pakeman RJ, Quested HM (2007) Sampling plant functional traits: What proportion of the species need to be measured? Applied Vegetation Science 10: 91–96.
19. Wright IJ, et al. (2004) The worldwide leaf economics spectrum. Nature 428: 821–827.
20. Witte JPM, Wójcik RB, Torfs PJJF, De Haan MWH, Hennekens S (2007) Bayesian classification of vegetation types with Gaussian mixture density fitting to indicator values. Journal of Vegetation science 18: 605–612.
21. Grime JP, Hodgson JG, Hunt R (2007) Comparative plant ecology: a functional approach to common British species. KirkcudbrightshireUK: Castlepoint Press. 748 p.
22. Käfer J, Witte JPM (2004) Cover-weighted averaging of indicator values in vegetation analyses. Journal of Vegetation science 15: 647–652.
23. Hunt R, Hodgson JG, Thompson K, Bungener P, Dunnett NP, et al. (2004) A new practical tool for deriving a functional signiture for herbaceous vegetation. Applied Vegetation Science 7: 163–170.
24. Klotz S, Kühn I, Durka W (2002) BIOLFLOR - Eine Datenbank zu biologisch-ökologischen Merkmalen der Gefàβpflanzen in Deutschland. Schriftenreihe für Vegetationskunde 38. Bonn: Bundesamt für Naturschutz.
25. Hodgson JG, Wilson PJ, Hunt R, Grime JP, Thompson K (1999) Allocating C-S-R plant functional types: a soft approach to hard problem. OIKOS 85: 282–296.
26. Kleyer M, Bekker RM, Knevel IC, Bakker JP, Thompson K, et al. (2008) The LEDA Traitbase: a database of life-history traits of the Northwest European flora. Journal of Ecology 96: 1266–1274.
27. Willby NJ, Pulford ID, Flowers TH (2001) Tissue nutrient signatures predict herbaceous-wetland community responses to nutrient availability. New Phytologist 152: 463–481.
28. Borcard D, Legendre P, Drapeau P (1992) Partialling out the Spatial Component of Ecological Variation. Ecology 73: 1045–1055.
29. Peres-Neto PR, Legendre P, Dray S, Borcard D (2006) Variation partitioning of species data matrices: estimation and comparison of fractions. Ecology 87: 2614–2625.
30. R Development Core Team (2013) R: A language and environment for statistical computing. R Foundation for Statistical Computing, Vienna, Austria. URL http://www.R-project.org/. Accessed 2013 May 16.
31. Chevan A, Sutherland M (1991) Hierarchical Partitioning. The American Statistician 45: 90–96.
32. Mac Nally R (2002) Multiple regression and inference in ecology and conservation biology: further comments on identifying important predictor variables. Biodiversity & Conservation 11: 1397–1401.
33. Walsh C, Mac Nally R (2008) hier.part: Hierarchical Partitioning. R package version 1.0–3.
34. Garnier E, Cheplick GP (1998) Interspecific variation in plasticity of grasses in response to nitrogen supply. Population biology of grasses: Cambridge University Press, Cambridge. pp. 155–182.
35. Reich PB, Oleksyn J, Wright IJ, Niklas KJ, Hedin L, et al. (2010) Evidence of a general 2/3-power law of scaling leaf nitrogen to phosphorus among major plant groups and biomes. Proceedings of the Royal Society B: Biological Sciences 277: 877–883.
36. Niklas KJ, Owens T, Reich PB, Cobb ED (2005) Nitrogen/phosphorus leaf stoichiometry and the scaling of plant growth. Ecology Letters 8: 636–642.
37. Kerkhoff AJ, Fagan WF, Elser JJ, Enquist BJ (2006) Phylogenetic and growth form variation in the scaling of nitrogen and phosphorus in the seed plants. American Naturalist 168: E103–E122.
38. Güsewell S (2004) N:P ratios in terrestrial plants: variation and functional significance. New Phytologist 164: 243–266.
39. Ceulemans T, Merckx R, Hens M, Honnay O (2011) A trait-based analysis of the role of phosphorus vs. nitrogen enrichment in plant species loss across North-west European grasslands. Journal of Applied Ecology 48: 1155–1163.
40. Van Bodegom PM, Van Reeven J, Van Der Gon HACD (2003) Prediction of reducible soil iron content from iron extraction data. Biogeochemistry 64: 231–245.
41. Lookman R, Vandeweert N, Merckx R, Vlassak K (1995) Geostatistical assessment of the regional distribution of phosphate sorption capacity parameters (FeOX and AlOX) in northern Belgium. Geoderma 66: 285–296.
42. Ertsen ACD, Alkemade JRM, Wassen MJ (1998) Calibrating Ellenberg indicator values for moisture, acidity, nutrient availability and salinity in the Netherlands. Plant Ecology 135: 113–124.
43. Douma JC, Bardin V, Bartholomeus RP, van Bodegom PM (2012) Quantifying the functional responses of vegetation to drought and oxygen stress in temperate ecosystems. Functional Ecology 26: 1355–1365.
44. Westoby M, Falster DS, Moles AT, Vesk PA, Wright IJ (2002) Plant ecological strategies: Some leading dimensions of variation between species. Annual Review of Ecology and systematics 33: 125–159.

Soil Biology & Biochemistry 58 (2013) 302–312

Contents lists available at SciVerse ScienceDirect

Soil Biology & Biochemistry

journal homepage: www.elsevier.com/locate/soilbio

Towards a proper integration of hydrology in predicting soil nitrogen mineralization rates along natural moisture gradients

Yuki Fujita [a,*], Peter M. van Bodegom [b], Harry Olde Venterink [c], Han Runhaar [a], Jan-Philip M. Witte [a,b]

[a] KWR Watercycle Research Institute, P.O. Box 1072, 3430 BB Nieuwegein, The Netherlands
[b] Department of System Ecology, Vrije Universiteit, De Boelelaan 1085, 1081 HV Amsterdam, The Netherlands
[c] Institute of Integrative Biology, ETH Zurich, Universitätstrasse 16, 8092 Zurich, Switzerland

ARTICLE INFO

Article history:
Received 2 August 2012
Received in revised form
19 December 2012
Accepted 24 December 2012
Available online 9 January 2013

Keywords:
Nitrogen mineralization
Carbon decomposition
SOM model
Hydrology
Denitrification
In-situ incubation experiment
CENTURY
Soil moisture gradient

ABSTRACT

The controlling effects of soil moisture on soil nitrogen (N) supply to plants have been well established from lab experiments, and are often incorporated in soil organic matter (SOM) models, but rarely tested in the field along natural gradients of soil moisture. With a large dataset of *in-situ* incubation experiments across a wide range of natural ecosystems (mostly with shallow groundwater) in the Netherlands and Belgium, we tested whether and how soil moisture influences N mineralization rates (N_{min}) in natural soils, and what type of hydrological coupling (in terms of estimation of soil moisture and formulation of soil moisture effect) is suited to predict across-site variation of N_{min} with a SOM model, CENTURY. Our results show that soil moisture was related to a small (17%), but a larger than other site factors, proportion of the difference between measured and reference (i.e. simulated with no moisture effects) N_{min}, indicating that soil moisture has a subtle yet important influence on N_{min} of natural soils. Coupling CENTURY with a simple tipping-bucket hydrological module, a common way to estimate soil moisture in existing models, did not improve model performance on N_{min} compared to a model without soil moisture effects, irrespective of the formulation of moisture effect applied. Coupling of CENTURY model with a more detailed hydrological module improved the model performance, but only when an appropriate moisture function was applied. Our results also indicated that model performance largely improved if indirect moisture effects through N losses via denitrification were accounted for. With our best model, inclusion of soil moisture information improved the normalized residual variance from 28% to 18% of the observed range of N_{min}. We conclude that appropriate estimates of soil moisture and proper representation of its effects on mineralization are crucial to properly reflect between-site variation in soil N supply in natural ecosystems.

1. Introduction

The important role of soil nitrogen (N) supply is well recognized in global ecosystem studies, such as in modeling studies for the prediction of climate change effects on greenhouse gas emission (Hungate et al., 2003; Gärdenäs et al., 2011), as well as in studies to find generic relationships between environmental drivers and plant responses and occurrence (Ordonez et al., 2010). Soil organic matter (SOM) models are commonly used in these studies to assess soil N supply, as they enable making predictions of N mineralization rates (which is a large part of soil N supply) at regional scales with minimum input values.

A challenge in predicting N mineralization rates (N_{min}) at regional scales is that the moisture status of the soil, which is a predominant factor of SOM decomposition (Cook and Orchard, 2008; Liu et al., 2009) as well as N mineralization (Dessureault-Rompré et al., 2011), is difficult to estimate due to its high spatial and temporal variability. There are two issues that hamper our confidence in generic SOM models coupled with hydrological information. First, field studies validating such models along natural soil moisture gradients are lacking (Falloon et al., 2011; Moyano et al., 2012). Instead, the functions of soil moisture effects in SOM models have been derived from lab experimental data in which soil water content was manipulated (e.g. Linn and Doran, 1984; Walse et al., 1998; Paul et al., 2003). It is likely that these soils exhibit a different behavior than intact soils, because of altered soil physical characteristics and deviating responses of microbes to the non-ambient moisture conditions. Nevertheless,

* Corresponding author. Tel.: +31 (0)30 6069 707; fax: +31 (0)30 6061 165.
E-mail address: Yuki.Fujita@kwrwater.nl (Y. Fujita).

0038-0717/$ – see front matter © 2013 Elsevier Ltd. All rights reserved.
http://dx.doi.org/10.1016/j.soilbio.2012.12.013

whether these lab-based relationships hold under field conditions has been poorly explored on an across-ecosystem level.

Second, we have concerns about the current coupling of SOM models with hydrological modules. A number of SOM models have been coupled to a hydrological module to simulate SOM dynamics under various soil moisture conditions (e.g. CENTURY (Parton et al., 1993), APSIM (Probert et al., 1998), IBIS (Kucharik et al., 2000), RothC coupled with SOILCO2 (Herbst et al., 2008), MOMOS coupled with SAHEL (Pansu et al., 2010)). These coupled models have been only approximately validated on time-series responses of carbon and nitrogen to changing moisture conditions (Probert et al., 1998; Pansu et al., 2010), or on across-ecosystem variations in C, N, and biomass in climatically distinct locations (Parton et al., 1993; Kucharik et al., 2000), but never been studied across sites within one climatic region. Moreover, there has been no attempt to disentangle the source of false prediction in these models. Prediction of SOM dynamics is sensitive not only to accuracy of soil moisture estimates but also to formulation of moisture effects in SOM model (Rodrigo et al., 1997; Bauer et al., 2008; Falloon et al., 2011). Unraveling to what extent and under which conditions these factors contribute to the deviation of N_{min} prediction is a necessary step to build a robust SOM-hydrology model to predict soil N supply on a regional scale.

In order to improve the prediction of N_{min} in natural ecosystems, we studied the two sources of uncertainty in the current SOM-hydrology models. We aimed at examining 1) to what extent and in what direction soil moisture influences N_{min} in natural soils, and 2) what type of hydrological coupling (in terms of estimation of soil moisture and formulation of soil moisture effect) is suited to reflect between-site variation in N_{min}.

To address this aim, we simulated N_{min} by use of a commonly-used SOM model, CENTURY (Parton et al., 1987), for the *in-situ* incubated soil cores from 143 natural sites in the Netherlands and Belgium. This region is commonly associated with shallow groundwater table, allowing us to select ecosystems from a wide moisture range (but with a higher frequency of wet to moist conditions). First, we evaluated the importance of soil moisture for predicting N_{min} by comparing measured soil moisture with the unexplained variation of measured N_{min} by a null model (i.e. CENTURY with no soil moisture effect). Second, we tested the model performance (in terms of N_{min}) of CENTURY coupled with several hydrological modules which make estimates of soil moisture for each site. These hydrological modules vary in complexity of hydrological processes included and details of input values. Finally, we investigated the sensitivity of the model performance to the formulation of the moisture effects on decomposition.

2. Methods

2.1. Field measurements

We used an existing dataset of soil samples from 53 plots in the Netherlands (Ordonez et al., 2010) and one from 54 plots in the Netherlands and Belgium (Olde Venterink et al., 2002a). Additionally, we collected soil samples from 36 plots in the Netherlands. All samples were taken in natural ecosystems and measured with almost identical methods (see Table 1 for an overview of the three datasets). These 143 plots (generally measuring 2 × 2 m) cover all the major axes of variation in soil conditions, except salinity, that differentiate the ecosystems in this temperate region. The axes are clayish to sandy, alkaline to acid, wet to dry, and nutrient poor to rich conditions. Although the incubation experiments lasted only for a season (i.e. early summer), they cover the whole range of the natural moisture gradient in the region and therefore serve as a suitable validation dataset to test moisture effects on N_{min}.

N_{min} was measured with an *in-situ* soil incubation method. Paired soil cores of 10 or 15 cm depth were taken with PVC tubes from each plot. In order to eliminate the effect of small-scale soil

Table 1
Specification of data collection methods and input data estimation for three dataset. Total C, Total N, soil texture were used as site-specific input values for CENTURY, whereas other parameters were used for the hydrological modules to estimate θ.

	Dataset 1 (this study)	Dataset 2 (Ordonez et al., 2010)	Dataset 3 (Olde Venterink et al., 2002a)
Data collection methods			
Number of location	36	53	54
Number of combined soil cores	3	5	1
Soil depth	0–15 cm	0–15 cm	0–10 cm
Soil diameter	4 cm	6 cm	4.8 cm
Holes in soil cores	No	No	Yes[a]
Duration of incubation	6 weeks	6 weeks	8 weeks
Incubation period	May 2011–July 2011	July 2006–August 2006	June 1995–August 1995
Estimation of input values			
Total C (g C g^{-1} soil)	Measured with C/N analyzer	Measured with C/N analyzer	Estimated[b]
Total N (g N g^{-1} soil)	Measured with C/N analyzer	Measured with C/N analyzer	Measured with Kjeldahl digestion
Soil physical type[c]	1:50,000 soil map	1:50,000 soil map	1:50,000 soil map
Soil texture (clay/silt/sand fraction)	Measured with Laser particle sizer	Estimated[d]	Estimated[d]
Soil density (g cm^{-3})[e]	Measured	Estimated[f]	Estimated[f]
Bulk density (g cm^{-3})	Measured	Estimated[g]	Measured
θ_{sat} (cm^3 cm^{-3})	Estimated[h]	Estimated[h]	Estimated[h]
θ_{res}, α, and n[i]	Estimated[d]	Estimated[d]	Estimated[d]

[a] The PVC tubes had two small holes (ca. 5 mm in diameter, ca. 3.5 cm above soil surface) on the top side for ventilation. There was little risk of flooding event in those sites during the incubation period.
[b] Estimated as 0.5·SOM (measured by loss in ignition).
[c] Each site was labeled into one of the 23 distinct soil units ("eenheid" in Dutch) according to 1:50,000 maps. Each soil unit consists of several layers of soil element ("bouwsteen", 18 categories) characterized by grain size distribution and amount of SOM. The layer configuration and their physical properties were used in the hydrological modules.
[d] Estimated from "bouwsteen" of soil top layer, based on empirical analysis of Dutch soil (Wösten et al., 2001).
[e] Density of soil without pore space.
[f] Estimated as: (% SOM/147 + % Clay/275 + % Silt & Sand/266)$^{-1}$ (Heinen, 2006). SOM was approximated as twice the amount of soil total C.
[g] Estimated from SOM content and soil texture using the repro function of Dutch soil (Wösten et al., 2001).
[h] Estimated as 1-bulk density/soil density (Heinen, 2006).
[i] Parameter values of the curve of soil water content vs pressure head (van Genuchten, 1980).

heterogeneity, for the majority of the locations, several pairs of soil cores were taken within one plot and mixed to make a composite sample for subsequent analysis. For each pair, one soil core was transported to the lab to measure the initial nutrient concentrations. The other core was incubated for 6 or 8 weeks in the soil with caps on both sides of the PVC tubes, with two small holes on the side of PVC tubes for one dataset but no holes for the other datasets. The concentration of available N ($N{-}NH_4 + N{-}NO_3$) was measured with 1 M KCl extraction. The difference in available N between the initial and incubated soil samples divided by the period of incubation (mg N kg^{-1} d.w. soil $week^{-1}$) was considered as N_{min}. Note that this is not gross N mineralization rates but net N mineralization rates.

2.2. SOM model

We simulated N_{min} with the widely used SOM model, CENTURY (Parton et al., 1987; Metherell et al., 1993; Parton et al., 1993; Del Grosso et al., 2002). We only used the belowground part of CENTURY (i.e. active, slow, and passive SOM pools) to match the soil incubation which did not include surface litter or living plants. Each SOM pool consists of C and N, and C in different pools is associated with distinct decomposition rates. C decomposition rates are controlled by soil moisture, temperature, and soil texture. N mineralization is closely linked to C decomposition: mineralized amount of N is determined by C flows between pools, as well as C:N ratios of the originating and receiving pools. The formulation of the N mineralization process in CENTURY is functionally identical to those used in the majority of the other recent SOM models (Manzoni and Porporato, 2009). We used the model equations and parameter values of the daily version of CENTURY, DAYCENT (Del Grosso et al., 2002), unless specified otherwise. See Appendix I for the formulations of the model.

CENTURY model uses a function *Md* to represent the reduction effects of soil moisture on decomposition. *Md* ranges between 0 (complete reduction) and 1 (no reduction), reflecting negative effects of both dry conditions (f_d) and wet conditions (f_w):

$$Md = f_d \cdot f_w \quad (1)$$

We used different formulations of *Md*, depending on the type of the moisture estimates: Md_{null} when the moisture of the soil was assumed to be always optimum, Md_{imp} when the soil moisture was implicitly estimated (i.e. from regional weather data only), and Md_{exp} when the soil moisture was explicitly taken into account. See Table 2 for the overview of the different combinations of *Md* function and the moisture estimates.

2.2.1. Md for null model (Md_{null})

To calculate the reference N mineralization rates for each site, we made a null model in which soil moisture is always optimal ($Md_{null} = 1$) and therefore has no effect on decomposition (Fig. 1a).

2.2.2. Md as a function of regional weather data (Md_{imp})

CENTURY uses, if it is not coupled with a hydrological module, regional climatic data as a proxy for soil moisture conditions. Here, the amount of soil moisture is implicitly assumed to increase when precipitation exceeds potential evapotranspiration, and vice versa. Following version 4 of CENTURY (Metherell et al., 1993), the reduction effect of soil moisture on decomposition (Md_{imp}) is defined as the product of $f_{d,\ imp}$ (i.e. the reduction effect at dry conditions) and $f_{w,\ imp}$ (i.e. the reduction effect at wet soil conditions) (Fig. 1b):

$$f_{d,\ imp} = \frac{1}{1 + 30 \cdot \exp\left(-8.5 \cdot \frac{ppt}{pet}\right)} \quad (2)$$

Table 2
Overview of model configurations. Combinations of different soil moisture estimates and formulation of moisture effect (*Md*) resulted in eight model configurations (notated as: a1, b1, c1, c2, d1, d2, e1, e2). In addition, denitrification process was simulated for models with explicit soil moisture estimates, yielding six extra model configurations (c3, c4, d3, d4, e3, e4).

Soil moisture estimates					*Md* formulation	Denitrification	Notation[b]
Hydrological module	Expression of moisture	Spatial scale of input[a]	Inputs of hydrological module	Output of hydrological module			
None (Null model)	None	–	–	–	Md_{null}	N.A.[c]	a1
Implicit regional hydrological module	Implicit	Regional	*ppt*, *pet*	$\sum ppt/\sum pet$[d]	Md_{imp} (Eq (2) × Eq. (3))	N.A.[c]	b1
Explicit regional hydrological module (Tipping-bucket)	Explicit	Regional	*ppt*, *pet*, θ_{wp}, θ_{fc}	θ[e]	$Md_{exp,\ CENT}$ (Eq. (4) × Eq. (5))	No	c1
						Yes	c3
					$Md_{exp,\ ALT}$ (Eq. (8) × Eq. (9))	No	c2
						Yes	c4
Explicit local hydrological module (SWAP)	Explicit	Local	*ppt*, *pet*, pF- and k(θ)-curve parameters, groundwater level	θ[e]	$Md_{exp,\ CENT}$ (Eq. (4) × Eq. (5))	No	d1
						Yes	d3
					$Md_{exp,\ ALT}$ (Eq. (8) × Eq. (9))	No	d2
						Yes	d4
Locally measured soil moisture	Explicit	Local	Measured soil moisture	θ	$Md_{exp,\ CENT}$ (Eq. (4) × Eq. (5))	No	e1
						Yes	e3
					$Md_{exp,\ ALT}$ (Eq. (8) × Eq. (9))	No	e2
						Yes	e4

ppt: Precipitation (mm/day) of the closest weather station.
pet: Potential evapotranspiration (mm/day) according to Makkink (1957) of the closest weather station.
θ: Volumetric soil water content ($cm^3\ cm^{-3}$).
θ_{wp}: Volumetric soil water content at wilting point ($cm^3\ cm^{-3}$).
θ_{fc}: Volumetric soil water content at field capacity ($cm^3\ cm^{-3}$).
[a] Whether inputs for hydrological modules contain local information. Here soil physical parameters derived from 1:50,000 maps ($\theta_{w,\ p}$, θ_{fc}, pF-curve parameters) are considered as regional information.
[b] Notation of model configurations, used in Figs. 2 and 3.
[c] Denitrification can not be simulated, because soil moisture is not explicitly estimated.
[d] Ratio of *ppt* and *pet* during four weeks before the start of the incubation period.
[e] Average of seven days before the start of the incubation period.

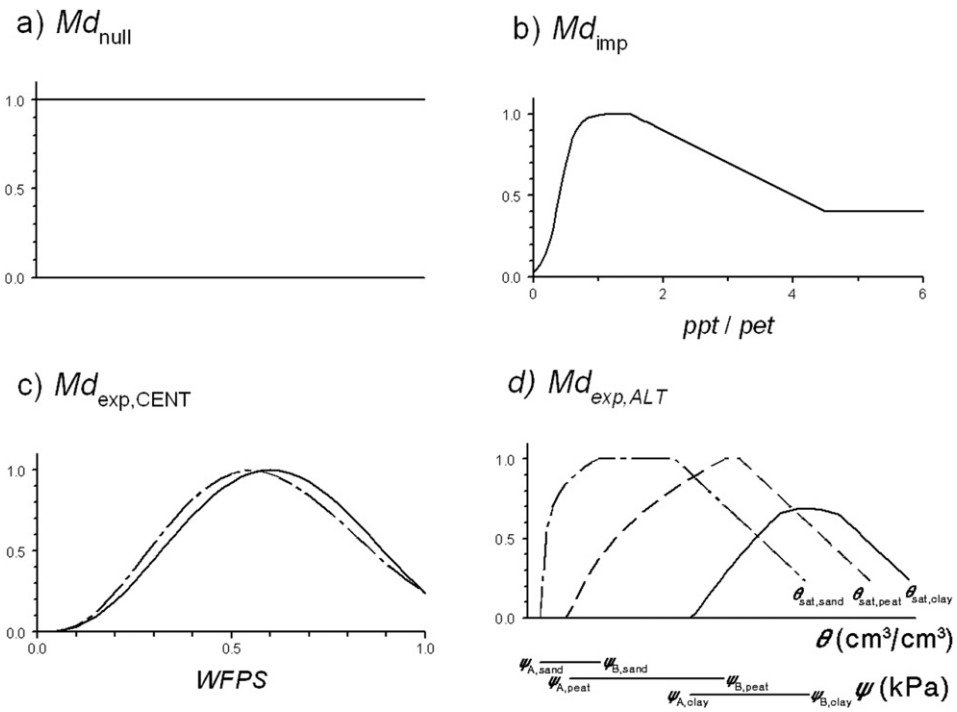

Fig. 1. Different formulations of soil moisture effects on decomposition (*Md*): (a) no moisture effects, $Md = Md_{null}$; (b) function of implicitly estimated moisture, $Md = Md_{imp}$; (c) function of explicitly estimated moisture according to CENTURY, $Md = Md_{exp,\,CENT}$; and (d) function of explicitly estimated moisture based on literature, $Md = Md_{exp,\,ALT}$. $Md_{exp,\,CENT}$ has two sets of parameter values, for coarse (sand content >70%, dashed line) and fine (≤70%, solid line) textured soils. Parameter values of $Md_{exp,\,ALT}$ varies depending on the site-specific soil physical characteristics. Three examples of distinct soil types are shown: clay-poor sand (dashed line), moderately heavy clay (solid line), and peaty sand (dotted line). ψ_B (−0.029 MPa) and ψ_A (−13.8 MPa) indicate the ψ where drought stress starts and ends, respectively. Oxygen stress starts when $\theta_{sat} - \theta$ becomes smaller than 0.2, and reaches at maximum when soil is saturated ($\theta = \theta_{sat}$).

$$f_{w,\,imp} = \begin{cases} 1 & \frac{ppt}{pet} < 1.5 \\ 1 - 0.2 \cdot \left(\frac{ppt}{pet} - 1.5\right) & 1.5 \le \frac{ppt}{pet} < 4.5 \\ 0.4 & 4.5 \le \frac{ppt}{pet} \end{cases} \quad (3)$$

where *ppt* is the monthly average precipitation (mm month^{-1}), and *pet* is the monthly potential evapotranspiration (mm month^{-1}). The *pet* is calculated as potential evapotranspiration of a reference lake (Linacre, 1977) multiplied with 0.75 (Metherell et al., 1993), which is roughly equivalent to potential evapotranspiration of a reference grassland according to Makkink (1957).

2.2.3. Md as a function of soil moisture according to CENTURY ($Md_{exp,\,CENT}$)

CENTURY uses, when it is coupled with a hydrological module, water filled pore space (WFPS; ranging between 0 and 1) in the top soil to define the moisture effects. The moisture reduction function, $Md_{exp,\,CENT}$, is a product of $f_{d,\,exp,\,CENT}$ and $f_{w,\,exp,\,CENT}$, which increases with increasing WFPS until the optimum and then decreases (Fig. 1c):

$$f_{d,\,exp,\,CENT} = \left(\frac{WFPS - b}{a - b}\right)^{d\frac{b-a}{a-c}} \quad (4)$$

$$f_{w,\,exp,\,CENT} = \left(\frac{WFPS - c}{a - c}\right)^{d} \quad (5)$$

$$WFPS = \theta/\theta_{sat} \quad (6)$$

where *a* is the water filled pore space where *Md* reaches the maximum, *b*, *c*, *d* are the other parameters defining the shape of the curves, θ is the volumetric water content (cm^3 cm^{-3}), and θ_{sat} is the saturated soil water content (cm^3 cm^{-3}). *a*, *b*, *c*, *d* equal 0.55, 1.70, −0.007, 3.22 for soils with a coarse texture (sand content >70%), and 0.60, 1.27, 0.0012, 2.84 for soils with a medium to fine texture (sand content ≤70%) according to DAYCENT (Del Grosso et al., 2002).

2.2.4. Alternative formulation of Md as a function of soil moisture ($Md_{exp,\,ALT}$)

The *Md* function in CENTURY, $Md_{exp,\,CENT}$, does not reflect the state-of-art knowledge of the relation between soil moisture and decomposition. Therefore, we have developed an alternative Md_{exp} function, $Md_{exp,\,ALT}$ (a product of $f_{d,\,exp,\,ALT}$ and $f_{w,\,exp,\,ALT}$), based on literature (Fig. 1d).

Reduction of decomposition under dry conditions is induced by hampered accessibility of microbes to substrates due to reduced solute diffusivity, as well as physiological responses of microbes to water stress causing reduced metabolic activity. It was found that the threshold values of soil moisture where biological activity ceases were nearly constant across biomes and climate (Manzoni et al., 2011) and across soil types (Myers et al., 1982) when expressed as matric potential (which is related to solute diffusivity), suggesting that accessibility to substrates plays a predominant role. We can calculate matric potential from θ and soil physical parameters according to the water retention curve defined by van Genuchten (1980):

$$\psi = 0.0981 \cdot \frac{1}{\alpha} \cdot \left[\left(\frac{\theta_{sat} - \theta_{res}}{\theta - \theta_{res}}\right)^{\frac{n}{n-1}} - 1\right]^{\frac{1}{n}} \quad (7)$$

where ψ is the matric potential (kPa), θ_{res} is the residual soil water content ($cm^3\ cm^{-3}$), α and n are the scaling parameters. θ_{res}, θ_{sat}, α, and n are site-specific soil physical parameters.

We assumed two thresholds of ψ where drought stress starts (ψ_B) and reaches the maximum (ψ_A). The decomposition rate reduces linearly from ψ_B to ψ_A on a log-scale (Davidson et al., 2000; Manzoni et al., 2011) as:

$$f_{d,\ exp,\ ALT} = \begin{cases} 1 & \psi_B \le \psi \\ 1 - \dfrac{\log(|\psi|) - \log(|\psi_B|)}{\log(|\psi_A|) - \log(|\psi_B|)} & \psi_A \le \psi < \psi_B \\ 0 & \psi < \psi_A \end{cases} \quad (8)$$

Manzoni et al. (2011) estimated from a large dataset of incubation experiments that ψ_A for mineral sieved soils is −13.8 MPa (pF 5.3). ψ_B is commonly set around field capacity (Rodrigo et al., 1997; Manzoni et al., 2011), which corresponds to a ψ of ca. −0.029 MPa (pF 2.5 (Koorevaar et al., 1983)).

Reduction of decomposition in wet conditions is associated with oxygen deficiency. Schjønning et al. (2003) showed that aerobic microbial activity decreases with decreasing soil gas content and relative gas diffusivity. They argued that soil gas phase rather than WFPS reflects the critical conditions for microbial activity in aeration limited soils, although most empirical studies related microbial responses in wet soils only to WFPS. Thus, we use the amount of gas in soil as a proxy of oxygen availability for microbes. We also assumed that a certain level of anaerobic decomposition occurs when soil pore is completely filled with water (i.e. $\theta = \theta_{sat}$).

$$f_{w,\ exp,\ ALT} = \begin{cases} 1 & \varphi_{gas\_th} \le \varphi_{gas} \\ \dfrac{\varphi_{gas}}{\varphi_{gas\_th}} \cdot (1 - m) + m & \varphi_{gas} < \varphi_{gas\_th} \end{cases} \quad (9)$$

where φ_{gas} is the soil gas content ($cm^3\ cm^{-3}$) which is equivalent to $\theta_{sat} - \theta$, φ_{gas_th} is the threshold of soil gas content where oxygen stress starts ($cm^3\ cm^{-3}$), and m is the level of anaerobic decomposition as a proportion to that of aerobic decomposition when soil is saturated (−). We set m as 0.24 to be comparable to the Md function of CENTURY ($Md_{exp,\ CENT}$), and φ_{gas_thr} as 0.2 $cm^3\ cm^{-3}$.

2.3. Soil moisture estimation with hydrological modules

Soil moisture conditions of the incubation soil cores were estimated with several hydrological modules, varying in the number and complexity of modeled processes, as well as in spatial scale of input values. See Table 2 for the summary of each module.

2.3.1. Implicit regional hydrological module

As the most approximate and implicit estimate of soil moisture conditions, we used the ratio between precipitation and potential evapotranspiration (according to Makkink, 1957) retrieved from the closest (within 50 km distance) weather station (http://climexp.knmi.nl). We disregarded site-specific information of plant and soil. For each site, the ratio of precipitation and potential evapotranspiration during four weeks before the start of the incubation period was used in combination with Md_{imp} (Eq. (2) × Eq. (3)).

2.3.2. Explicit regional hydrological module: tipping bucket model

A simple 'tipping-bucket' type of hydrological model included in CENTURY (Parton et al., 1993) was used to make an approximate but explicit estimate of soil moisture. This model calculates evaporation, transpiration, and for each soil layer, water content and percolation of water to the underlying layer. Upward water flow by capillary rise is neglected. We used this model except the state variables 'snow' and 'liquid snow', because the water dynamics related to snow do not influence the soil water during the period of our incubation experiment. Above-ground plant biomass, which this hydrological model uses to calculate potential transpiration rates, was arbitrarily chosen as 300 g m^{-2} for all plots. Site-specific soil parameters (volumetric soil water content at wilting point (θ_{wp}) and at field capacity (θ_{fc}), depth of each soil layer) were determined from the 1:50,000 soil map according to Wösten et al. (2001). The same climatic information as for the implicit regional hydrological module was used. For each site, a 7-day average value of θ in top 15 cm just before the start of the incubation period was used in combination with both formulations of Md_{exp} ($Md_{exp,\ CENT}$ (Eq. (4) × Eq. (5)) and $Md_{exp,\ ALT}$ (Eq. (8) × Eq. (9))).

2.3.3. Explicit local hydrological module: SWAP model

For a detailed estimate of soil water conditions, we used the Soil Water Atmosphere Plant model, SWAP (Van Dam et al., 2008), which is commonly used to simulate hydrology of vadoze zones in various environments. Daily groundwater levels since January of the measurement year was estimated by inter- and extrapolating the observed groundwater data in nearby wells (mostly within 30 m from the soil cores), using Menyanthes software (von Asmuth et al., 2012). The estimated daily groundwater level was used as a lower boundary condition in the SWAP simulation. We used the crop parameters of a reference grassland defined by Van Dam et al. (2008) to calculate the actual evapotranspiration rates of all plots. Site-specific soil physical properties (water retention and hydraulic conductivity curves (pF and k(θ) curves) described by Van Genuchten parameters θ_{res}, θ_{sat}, α, and n, depth of each soil layer) were derived from the 1:50,000 soil map according to Wösten et al. (2001). The same climatic information as for the implicit regional hydrological module was used. For each site, a 7-day average value of θ in top 15 cm just before the start of the incubation period was used in combination with both formulations of Md_{exp} ($Md_{exp,\ CENT}$ (Eq. (4) × Eq. (5)) and $Md_{exp,\ ALT}$ (Eq. (8) × Eq. (9))). Six plots were excluded from the analysis with this hydrological module because the groundwater data was not available.

2.3.4. Local field measurement of soil moisture

As the best possible estimate of soil moisture conditions, we used measured soil moisture content. Gravimetric water content (g water g^{-1} d.w. soil) of the soil in the incubation tube was measured by drying at 70 °C for 48 h. Because the PVC tubes were closed on both sides with caps, the moisture content of the majority of soil cores hardly fluctuated during the incubation period (see Appendix II for more details about the moisture fluctuation and its possible consequences on the results). We therefore used the moisture content at the end of incubation period for further calculations. For each site, θ ($cm^3\ cm^{-3}$) was calculated by multiplying the gravimetric water content with bulk density (g cm^{-3}), and used in combination with both formulations of Md_{exp} ($Md_{exp,\ CENT}$ (Eq. (4) × Eq. (5)) and $Md_{exp,\ ALT}$ (Eq. (8) × Eq. (9))).

2.4. Model simulation and analysis

N_{min} of the incubated soils (mg N kg^{-1} d.w. soil $week^{-1}$) were simulated with CENTURY. Site-specific input values included edaphic information (soil total C and N, soil texture), daily average temperature, and soil moisture of the incubated soil. Soil temperature in the incubation cores was assumed to fluctuate as in the ambient soil, and soil moisture was assumed to remain constant during the incubation period. Soil moisture was estimated using the different hydrological modules specified above. See Table 1 for

how input values were estimated for each dataset. For the following analyses, N_{min} were log transformed after adding 1, i.e. $ln(N_{min}+1)$.

First, we tested if and how soil moisture influences N_{min}. Since a direct comparison between measured N_{min} and measured soil moisture did not yield any consistent relationship due to large variations in other soil factors among plots (Appendix III), we first estimated the reference N_{min} (N mineralization rates assuming no moisture effect, simulated with the null model), and then compared the difference between the reference N_{min} and measured N_{min} (i.e. residuals from the 1:1 line) with the measured soil moisture. Measured soil moisture was expressed in ψ (kPa), WFPS (−), θ (cm^3 water cm^{-3} soil), gravimetric water content (g water g^{-1} d.w. soil), and φ_{gas} (cm^3 gas cm^{-3} soil). An outliner plot for which the lowest reference N_{min} was predicted was excluded from all the analysis because it violates the normality of the residual distributions. Two plots with unrealistically high φ_{gas} (>0.7 cm^3 cm^{-3}) were excluded from the analysis with φ_{gas}. Subsequently, the residuals were compared with other soil variables which were not used as input values of CENTURY but may influence N mineralization rates: soil pH-KCl, soil P:C ratio, soil N availability ($N{-}NH_4$ + $N{-}NO_3$ in the beginning of incubation period), and woodiness of above-ground vegetation (to evaluate impacts of woody vegetation on the quality of SOM, noting that CENTURY was originally parameterized for grasslands), approximated by the cover (in percentage) of non-herbaceous species among all vascular species. The residuals were regressed by the soil factors linearly and non-linearly (i.e. assuming an optimum value of the soil factor), and adjusted R^2 values (R^2_{ad}) were calculated. Non-linear regression models were considered only when the coefficient of the quadratic term was significantly ($p < 0.05$) different from zero.

Second, N_{min} were simulated with CENTURY in different model configurations, resulting from combinations of different soil moisture estimates (i.e. estimated with different hydrological modules) and *Md* functions. The emerging eight model configurations are: constant optimum soil moisture combined with Md_{null}, implicitly estimated soil moisture with Md_{imp}, explicitly estimated soil moisture (either with tipping-bucket, with SWAP, or with field measurement) combined with $Md_{exp,\ CENT}$ or $Md_{exp,\ ALT}$. See Table 2 for summary of all model configurations. First, for each model configuration, Spearman's correlation analysis with ties was applied between modeled and measured N_{min} to examine their predictive ability on rank order of N_{min} among plots. Subsequently, to compare the goodness of model fit among the model configurations, root mean square error (RMSE) was calculated as:

$$\mathrm{RMSE} = \sqrt{\frac{\sum_{i=1}^{n}(y_i - x_i)^2}{n}} \tag{10}$$

where y_i is log-transformed modeled N_{min} of plot i, x_i is log-transformed measured N_{min} of plot i, and n is the total number of plots. The percentage of the residual variance was expressed by the normalized RMSE (nRMSE):

$$\mathrm{nRMSE} = 100 \cdot \frac{\mathrm{RMSE}}{x_{max} - x_{min}} \tag{11}$$

where x_{max} and x_{min} are the maximum and minimum values of log-transformed measured N_{min}.

To examine if coupling with hydrology significantly improves the model performance, each model configuration was compared with the null configuration (i.e. null model) on the basis of Spearman's correlation coefficients ρ and nRMSE. For each model configuration, 143 pairs of modeled and measured N_{min} were randomly selected for 1000 times by bootstrapping. Values of ρ and nRMSE were calculated for each bootstrap of 143 pairs. Subsequently, for each model configuration, medians and 95% confidence intervals of ρ and nRMSE were determined. If the median of the null model fell outside the range of 95% confidence interval of another model configuration, we considered that this model configuration differed significantly from the null model in model performance.

It is likely that some of the wet soils, especially those with high organic matter content, lost N from the incubation tubes via denitrification (Olde Venterink et al., 2002b). Therefore, we additionally modeled nitrification and denitrification processes following DAYCENT (Del Grosso et al., 2002) to correct measured N_{min} for N loss via denitrification (see Appendix IV for the model formulations). Note that the estimates of denitrification rates were possible only for those six model configurations associated with explicit moisture estimates (i.e. tippint-bucket, SWAP, or measured soil moisture), because denitrification rates are calculated as a function of soil water content. Model performance for these extra six model configurations was evaluated in terms of ρ and nRMSE.

3. Results

3.1. Effects of soil moisture on N mineralization

The difference between the reference N_{min} (i.e. simulated by the null model) and the measured N_{min} was slightly but consistently related to factors which reflect soil moisture conditions. It was parabolically related to ψ (Fig. 2a, $R^2_{ad} = 0.049$, $P < 0.05$) and θ (Fig. 2c, $R^2_{ad} = 0.168$, $P < 0.001$), negatively related to WFPS (Fig. 2b, $R^2_{ad} = 0.045$, $P < 0.01$) and gravimetric water content (Fig. 2d, $R^2_{ad} = 0.152$, $P < 0.001$), and positively related to soil gas content (Fig. 2e, $R^2_{ad} = 0.058$, $P < 0.01$). Taken together, the reduction effect of wet conditions on measured N_{min} was indicated by any expression of soil moisture, whereas that of dry conditions was only implied by ψ and θ.

The residuals were related to soil pH (Fig. 2f, $R^2_{ad} = 0.138$, $P < 0.001$) in a way that the model underestimated N_{min} the most at an intermediate pH. The residuals were only slightly and negatively related to soil P:C ratio (Fig. 2g, $R^2_{ad} = 0.075$, $P < 0.001$) and to available N in soil (Fig. 2h, $R^2_{ad} = 0.051$, $P < 0.01$). Percentage of woody species had a parabolic influence on the residuals (Fig. 2i, $R^2_{ad} = 0.105$, $P < 0.001$), but this seems to be a pseudo-relation caused by a strong negative correlation between percentage of woody species and soil moisture (i.e. Spearman's correlation coefficient with θ was −0.63, $P < 0.001$).

3.2. Comparison of predictive ability of models coupled differently with hydrology

Model performance to predict N_{min} was compared among different model configurations (i.e. CENTURY models coupled with different hydrological modules and formulations of *Md*; Table 2). Compared to the null model ($\rho = 0.56$, nRMSE = 28%, Fig. 3-a1), CENTURY coupled with implicit regional hydrological module did not significantly ($P > 0.05$ tested with bootstrapping, Fig. 4) improve model performance ($\rho = 0.56$, nRMSE = 26.4%; Fig. 3-b1). Coupling CENTURY with the tipping-bucket did not improve model performance either, irrespective of the *Md* function applied (with $Md_{exp,\ CENT}$: $\rho = 0.53$, nRMSE = 27.1%, Fig. 3-c1, with $Md_{exp,\ ALT}$: $\rho = 0.46$, nRMSE = 26.2%, Fig. 3-c2). Coupling CENTURY with the SWAP significantly ($P < 0.01$) improved model performance when $Md_{exp,\ ALT}$ was applied in terms of nRMSE (21%) but not in rank order ($\rho = 0.54$ ($P = 0.66$), Fig. 3-d2), whereas model performance significantly ($P < 0.05$) worsened when $Md_{exp,\ CENT}$ function was applied in terms of rank order ($\rho = 0.43$, Fig. 3-d1). Finally, coupling CENTURY with measured soil moisture significantly ($P < 0.01$)

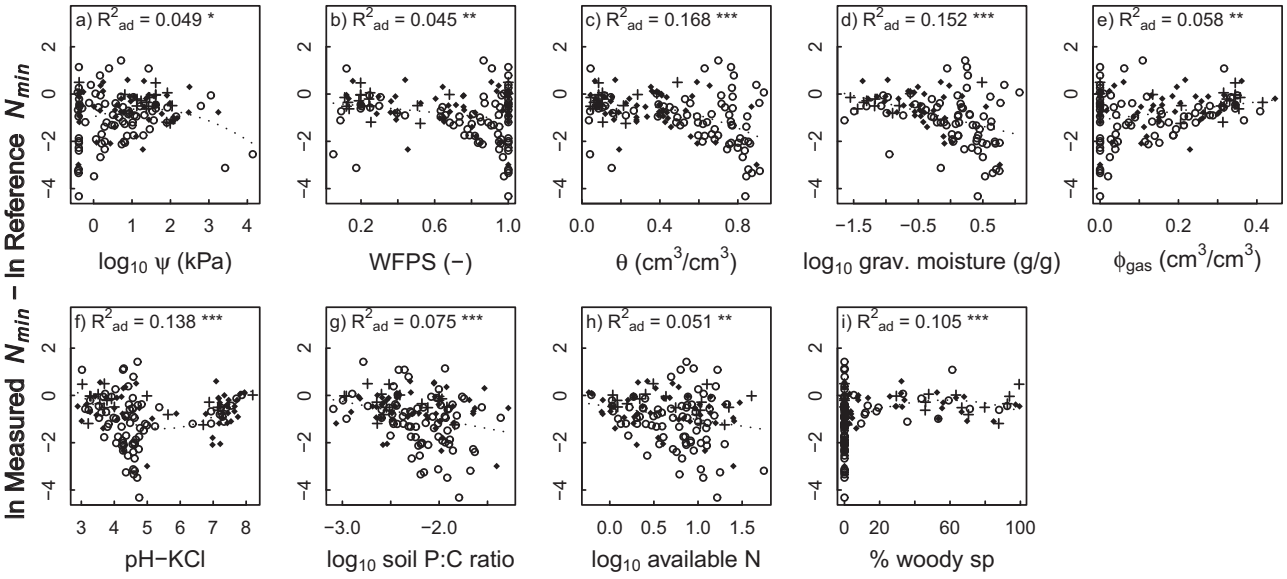

Fig. 2. Difference between measured and reference N mineralization rates (N_{min}, mg N kg^{-1} d.w. soil $week^{-1}$) plotted against soil moisture and other site factors. N_{min} was log-transformed prior to the analysis, as $ln(N_{min} + 1)$. The reference N_{min} were simulated with the null model (no moisture effect on decomposition). Soil moisture was expressed as: (a) matric potential ψ (kPa), (b) water filled pore space WSFP (−), (c) volumetric water content θ ($cm\ cm^{-3}$), (d) gravimetric soil moisture (g water g^{-1} d.w. soil), and (e) soil gas content φ_{gas} ($cm\ cm^{-3}$). The other site factors compared were (f) soil pH-KCl, (g) soil P:C ratio, (h) soil available N ($N{-}NH_4 + N{-}NO_3$) (mg N kg^{-1} d.w. soil), and (i) cover of woody species in above-ground vegetation (%). Zero on the *y*-axis means that measured N_{min} are perfectly predicted by the null model, whereas negative values on the *y*-axis indicate overestimation of N_{min} by the null model (i.e. N_{min} in the field were suppressed by other factors than those already included as input variables of the null model (soil C, soil N, soil texture, and temperature)). Adjusted R^2 values (R^2_{ad}) and *P*-values of the regression models are shown. Different symbols represent wetness of the site, approximated with average indicator values for moisture of the occurring plant species in the plot, F_m. F_m is comparable to Ellenburg indicator value for moisture, but it is on a continuous scale which ranges from 1 (aquatic sites) to 4 (extremely dry sites) (Witte et al., 2007). Symbols depict: wet ($F_m < 2.5$, open circles), moist ($2.5 \leq F_m < 3.5$, filled circles), and dry ($3.5 \leq F_m$, crosses).

improved model performance in terms of nRMSE irrespective of *Md* function applied (with $Md_{exp,\ CENT}$: nRMSE = 21.7%, Fig. 3-e1, with $Md_{exp,\ ALT}$: nRMSE = 21.9%, Fig. 3-e2), although rank order did not change significantly ($\rho = 0.55$ and $\rho = 0.58$, respectively).

For the model configurations with an explicit estimate of soil moisture, we corrected measured N_{min} with estimated N loss via denitrification. The correction for N loss significantly improved model performance for the model configurations with measured soil moisture irrespective of *Md* function (with $Md_{exp,\ CENT}$: $\rho = 0.66$ ($P < 0.05$), nRMSE = 18.2% ($P < 0.001$), Fig. 3-e3, with $Md_{exp,\ ALT}$: $\rho = 0.68$ ($P < 0.05$), nRMSE = 17.7% ($P < 0.001$), Fig. 3-e4). With the SWAP, model performance improved by correcting for N loss when $Md_{exp,\ ALT}$ was applied ($\rho = 0.62$ ($P = 0.18$), nRMSE = 18.4% ($P < 0.001$), Fig. 3-d4) but less when $Md_{exp,\ CENT}$ was applied ($\rho = 0.55$ ($P = 0.53$), nRMSE = 19.9% ($P < 0.001$), Fig. 3-d3). With the tipping-bucket, the correction for N loss did not result in significant improvement in model performance (Fig. 3-c3, c4).

4. Discussion

4.1. Moisture–decomposition relationships in natural soils

For the first time, our study explicitly examined some of the primary sources of uncertainty in the current SOM model with a large (143 sites) incubation dataset from a wide range of ecosystems. The test for the first source of uncertainty, i.e. soil moisture–decomposition relationships under field conditions, was made feasible by estimating 'reference' N mineralization rates (i.e. rates when no moisture effects exists) of multiple sites differing in soil characteristics with the aid of a process-based model. Soil moisture was related to a significant portion (17%) of the discrepancy between the measured and the reference N mineralization rates, which was higher than other site factors (i.e. soil pH, soil P:C ratio, woodiness of vegetation). Furthermore, the negative effects of wet soil conditions on N mineralization rates were consistent but weak, whereas those of dry soil conditions were hardly evident. These results imply that moisture is a relevant factor to predict between-site difference in N mineralization rates for natural soils, but that the relationship observed in lab experiments may not be readily applicable to natural soils. A similarly weak effect of soil wetness conditions was indicated by multivariate regression analysis of 74 Dutch natural ecosystems (Schaffers, 2000). Other studies with fewer plots in dry ecosystems showed more apparent moisture effects on respiration but only in dry conditions (with four Amazonian forests and pastures (Davidson et al., 2000), four temperate forests (Davidson et al., 1998), and17 temperate forests and shrubs (Reichstein et al., 2003)).

Several reasons may explain the obscured influence of soil moisture on N mineralization rates in our study. First, it is likely that the history of the prevailing soil moisture conditions in the area is already reflected in other model input values (e.g. soil total C, soil C/N ratio), making the inclusion of soil moisture information partly redundant. Second, microbial communities in natural soils are likely adapted to the prevailing soil moisture conditions (Groffman and Tiedje, 1991), in contrast to communities suddenly exposed to deviating soil moisture conditions in lab experiments. This may underlie the less profound responses of natural soils to wet or dry conditions. Thirdly, our analysis on soil moisture effects holds true only if no other site factors have influence on net N mineralization rates in a moisture-dependent manner. Lower rates of measured N mineralization at intermediate pH and higher amount of soil available N imply that denitrification, which is related to these site factors and is a moisture-dependent process, might be a confounding factor obscuring the true relationship between moisture and N mineralization. We will discuss the consequences of denitrification on our results later in the Discussion.

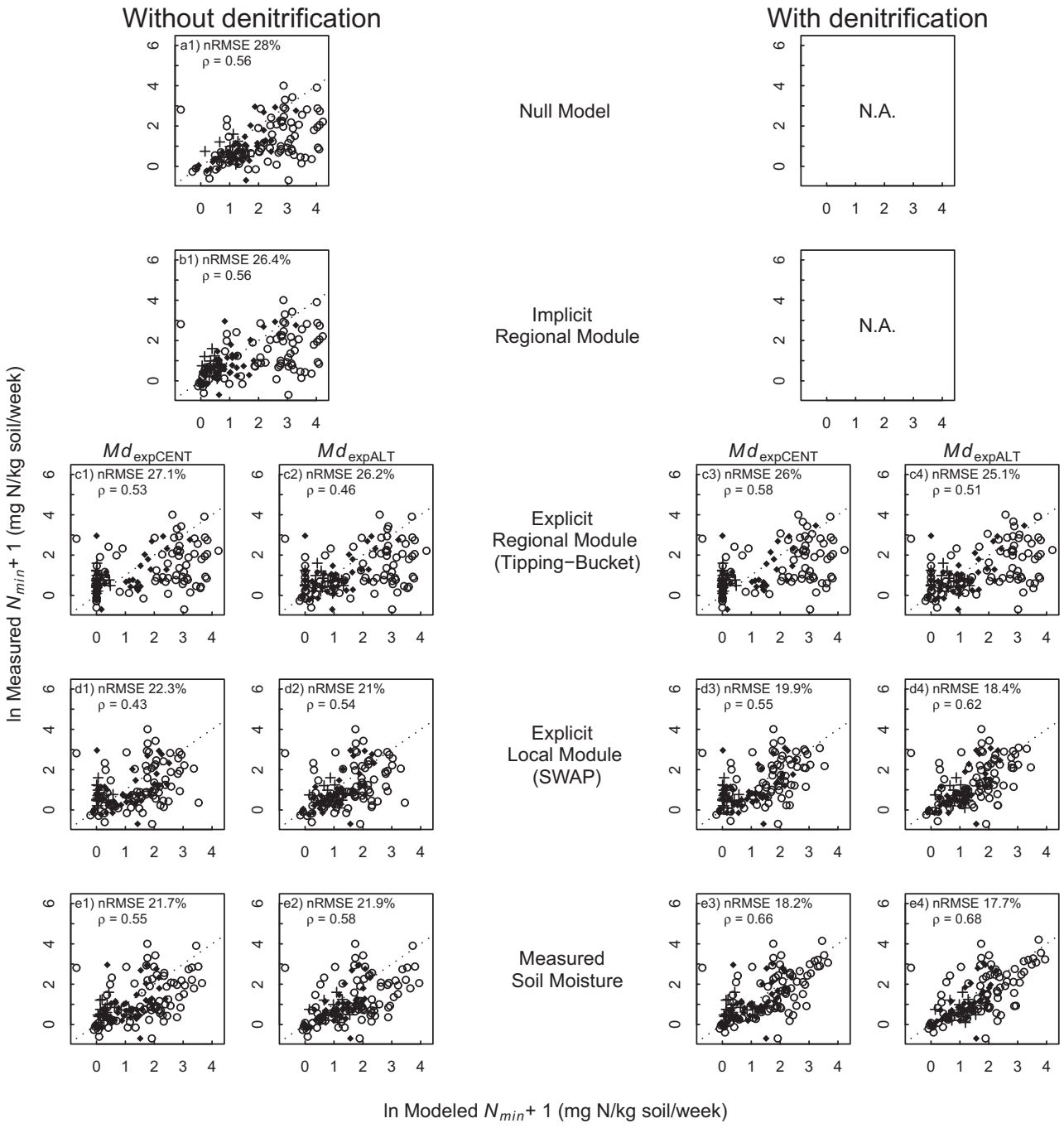

Fig. 3. Comparisons of measured and modeled N mineralization rates (N_{min}, mg N kg^{-1} d.w. soil $week^{-1}$). To model N_{min}, CENTURY was coupled to different hydrological modules: a) null model (i.e. soil moisture is always optimum), b) implicit regional hydrological module (i.e. soil moisture was approximated with *ppt*/*pet*), c) explicit regional hydrological module (i.e. soil moisture was simulated by a simple tipping-bucket model), d) explicit local hydrological module (i.e. soil moisture was simulated by a detailed local hydrological model SWAP), and e) measured soil moisture in the incubation soil cores. For the models with explicit soil moisture estimates (c–e), results for two different formulations of *Md* ($Md_{exp,\ CENT}$ (c1, d1, e1) and $Md_{exp,\ ALT}$ (c2, d2, e2)) are shown. Additionally, the measured N_{min} were corrected for the N loss by adding modeled denitrification rates. This correction was possible only for models with explicit soil moisture estimates (c3, c4, d3, d4, e3, e4) because denitrification is calculated as a function of soil moisture. See Table 2 for the notation of the model configurations. Data is shown for 143 plots except for d), for which six plots were excluded due to the insufficient input values for the hydrological module. The 1:1 lines of modeled and measured N_{min} (dotted line) are shown, as well as normalized RMSE (i.e. residual variance in %) and Spearman's correlation coefficient ρ. Symbols are identical to Fig. 2.

4.2. Importance of proper representation of soil moisture

A second source of uncertainty in the current SOM model, i.e. coupling with hydrological modules, was revealed to cause significant differences in model performance. Coupling with an explicit regional hydrological module (a simple tipping-bucket model) did not improve model performance at all irrespective of the choice of the *Md* function, simply because this module was not able to reproduce the site moisture conditions (Appendix V). This is striking, because many existing models are coupled with a tipping-bucket kind of hydrological module (e.g. CENTURY, APSIM). We should stress that our study region is located in the lowlands and thus often subject to the influence of groundwater. In such areas, a proper moisture estimate of the top soil is possible only with local

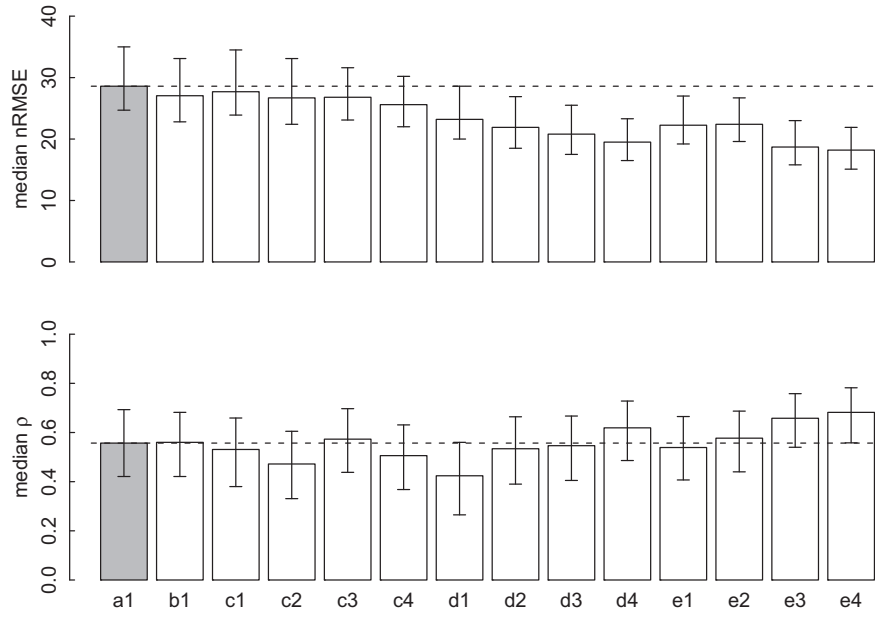

Fig. 4. Median and 95% confidence intervals of normalized root mean square means (nRMSE) and spearman's correlation coefficient (ρ) of modeled and measured N mineralization rates, calculated from 143 plots randomly chosen with bootstrapping for 1000 times. See Table 2 for the notations of the model configurations. Dotted lines show the level of the null model (a1) (i.e. no moisture effects are considered). A smaller nRMSE value and a larger ρ value than the null model means that the model performance improved by including hydrological information.

information of groundwater, as in the SWAP model (Appendix V). In addition, even when groundwater-independent plots ($N = 30$) were separately examined, model predictability was slightly worse for those coupled with the tipping-bucket than those coupled with the SWAP (results not shown). These findings highlight the necessity of proper choice of hydrological model to achieve a realistic representation of top soil moisture and consequently a proper prediction of N supply in top soils.

4.3. Different formulation of moisture effects (Md) on decomposition

The formulation of the moisture function *Md* caused additional deviations in our model predictions. This is consistent with modeling studies that pointed out a high sensitivity of model outputs to different formulations of the water-related reduction function in SOM models (Rodrigo et al., 1997; Bauer et al., 2008). In our case, model performance was generally poorer when using $Md_{\mathrm{exp,\ CENT}}$ than $Md_{\mathrm{exp,\ ALT}}$. The poor performance of $Md_{\mathrm{exp,\ CENT}}$ may be attributed to its use of WFPS to represent moisture threshold values, which simulated too strong water stress for some dry soils. The reduction in aerobic microbial activities at dry conditions is mainly driven by solute diffusivity (Manzoni et al., 2011), whereas there is no generic relationship between WFPS and diffusivity. This coincides with the wide variation of observed optimum WFPS values for the highest N mineralization or respiration rates, e.g. ranging 0.57–0.78 with 28 wetland soils (Sleutel et al., 2008), 0.4–0.9 with 42 soils (Dessureault-Rompré et al., 2011), 0.4–0.9 with 90 soils (Moyano et al., 2012), and 0.8–0.9 with 9 soils (Stanford and Epstein, 1974). Thus, WFPS is less suited to reflect moisture conditions for decomposition across soil types (Schjønning et al., 2003; Castellano et al., 2011), unless WFPS is scaled to the soil-specific optimum values (Dessureault-Rompré et al., 2011) or field capacity (Castellano et al., 2011).

It is worth mentioning that the relation between soil moisture and N mineralization rates was particularly scattered in our wet soils, and also that knowledge from lab experiments in wet conditions is scarcer than that in dry conditions. No 'universal' expression of soil moisture has been found to reflect oxygen stress (i.e. before alternative electron acceptors kick in) across soil types (Schjønning et al., 2011), although gas diffusivity has a potential to play the role (Schjønning et al., 2003, 2011). Furthermore, it has been poorly clarified to which level mineralization rates drop under anaerobic conditions when other electron acceptors than oxygen are involved. Factors influencing anaerobic decomposition (e.g. the amount of other electron acceptors, redox status, and abundance and composition of anaerobic microbes) are highly site-specific, making across-site predictions of anaerobic N mineralization a challenge. Clearly, more research is needed to elucidate the processes and factors governing anaerobic decomposition across soil types, and replace the empirically-based formulation of oxygen stress in our model with a kinetics-based formulation.

4.4. N loss via denitrification from incubated soils

The *in-situ* incubation and soil extraction approach, as used in this study and in many others, yield net change in the extractable N during a period, which can be a result of various processes (Hart et al., 1994). Theoretically, only a minimal degree of denitrification should occur in the incubation tubes, because of different peaks of nitrification and denitrification rates along soil moisture gradient (Bateman and Baggs, 2005). However, within an incubation tube of 10–15 cm height, vertical moisture gradient may facilitate coupled nitrification–denitrification processes (Olde Venterink et al., 2002b). Denitrification rates are typically in the range of 0–1 mg N kg soil^{-1} day^{-1} in riparian ecosystems (Hefting et al., 2004). This is in the same order of magnitude as modeled N denitrification rates in our soil samples (median 0.02 and 95th percentile 1.3 mg N kg soil^{-1} day^{-1}). Our model performance was largely improved if measured N mineralization rates were corrected with N loss via denitrification, but only when the model was coupled with realistic moisture estimates (i.e. SWAP output or

measured soil moisture). This amplifies the need for a proper coupling of SOM models with hydrological modules to predict N flows across ecosystems.

4.5. Validity of a coupled SOM-hydrology model to predict soil N supply across natural ecosystems

Despite the important role of soil N supply in ecosystem functioning, global models have been poorly validated on N fluxes in soils. For example, the CENTURY model has been frequently validated for C accumulation and net primary production (e.g. Schimel, 1994; Gilmanov et al., 1997; Kelly et al., 1997) but only rarely for N. N mineralization rates predicted by CENTURY model matched reasonably well with observed rates of 44 soils on a global scale (R^2 = 0.62 with a simplified CENTURY model (Ordonez et al., 2009)), but less when validated with a time-series data of a steppe ecosystem (R^2 = 0.33 with DAYCENT (Kelly et al., 2000)), or they needed an adjustment of a parameter value to match with incubation data of three forest soils (Kirschbaum and Paul, 2002). Although a methodological drawback in *in-situ* incubation measurements was suggested (as explained in the previous section about denitrification), our study shows that the N module of CENTURY model produces fairly good estimates of N mineralization rates in terms of both rank order among plots and absolute magnitude on an across-ecosystem level within a climatic region, particularly when the local soil moisture status and its effects are properly reflected. Moreover, the model performance was not biased by the ecosystem types (Appendix VI). This supports the applicability of the model to predict soil N supply on a large spatial scale once hydrology is taken care of.

4.6. Conclusions

Despite the apparent importance of soil moisture on soil N supply and the prevailing coupling of SOM and hydrological modules in existing models, field scale observation has been critically lacking to examine the necessity and appropriateness of such coupling. Our study emphasized that a detailed representation of local soil moisture is needed in SOM models to improve the prediction of soil N supply. A simple representation of soil moisture, for instance with a tipping-bucket kind of hydrological module, can worsen model performance, particularly in ecosystems with shallow groundwater. At least two sources of uncertainty hamper the successful prediction of soil N supply: (1) a lack of generic understanding of the moisture effects on SOM decomposition in natural soils, and (2) difficulties in accurately estimating the moisture status of soils. With our best estimates of soil moisture and a better formulation of the moisture–decomposition relationship, inclusion of hydrological information in a SOM model improved the residual variance of modeled N mineralization rate from 28% to 18% (of the observed range). To build a model which can generically reflect the moisture effects on soil N supply, we advocate a more kinetics-based formulation of moisture–decomposition relationship, better coupling with hydrological module especially in groundwater dependent systems, as well as validation of coupled SOM-hydrology models in other climate than the temperate region of our study. Such a robust model will broaden our capacity to make future projections of soil nutrient dynamics.

Acknowledgments

This research was carried out in the framework of CARE project of the Dutch national research program Knowledge for Climate and the joint research program of the Dutch Water Utility sector. We thank Staatsbosbeheer, Veluwe national park and PWN for allowing us to use their field sites; H. Roelofsen, F. Daniels, A. and J. Vrielink for their help in field measurements; J. van Hal, R. van Logtestijn, and R. Broekman for lab measurements; J. Ordoñez for the permission to use her database; R. Bartholomeus and B. Douma for SWAP simulations; and I. Leunk for MENYANTHES simulations.

Appendix A. Supplementary data

Supplementary data related to this article can be found at http://dx.doi.org/10.1016/j.soilbio.2012.12.013.

References

Bateman, E.J., Baggs, E.M., 2005. Contributions of nitrification and denitrification to N_2O emissions from soils at different water-filled pore space. Biology and Fertility of Soils 41, 379–388.
Bauer, J., Herbst, M., Huisman, J.A., Weihermüller, L., Vereecken, H., 2008. Sensitivity of simulated soil heterotrophic respiration to temperature and moisture reduction functions. Geoderma 145, 17–27.
Castellano, M.J., Schmidt, J.P., Kaye, J.P., Walker, C., Graham, C.B., Lin, H., Dell, C., 2011. Hydrological controls on heterotrophic soil respiration across an agricultural landscape. Geoderma 162, 273–280.
Cook, F.J., Orchard, V.A., 2008. Relationships between soil respiration and soil moisture. Soil Biology and Biochemistry 40, 1013–1018.
Davidson, E.A., Belk, E., Boone, R.D., 1998. Soil water content and temperature as independent or confounded factors controlling soil respiration in a temperate mixed hardwood forest. Global Change Biology 4, 217–227.
Davidson, E.A., Verchot, L.V., Henrique Cattânio, J., Ackerman, I.L., Carvalho, J.E.M., 2000. Effects of soil water content on soil respiration in forests and cattle pastures of eastern Amazonia. Biogeochemistry 48, 53–69.
Del Grosso, S., Ojima, D., Parton, W., Mosier, A., Peterson, G., Schimel, D., 2002. Simulated effects of dryland cropping intensification on soil organic matter and greenhouse gas exchanges using the DAYCENT ecosystem model. Environmental Pollution 116, S75–S83.
Dessureault-Rompré, J., Zebarth, B.J., Georgallas, A., Burton, D.L., Grant, C.A., 2011. A biophysical water function to predict the response of soil nitrogen mineralization to soil water content. Geoderma 167–168, 214–227.
Falloon, P., Jones, C.D., Ades, M., Paul, K., 2011. Direct soil moisture controls of future global soil carbon changes: an important source of uncertainty. Global Biogeochemical Cycles 25, GB3010.
Gärdenäs, A.I., Ågren, G.I., Bird, J.A., Clarholm, M., Hallin, S., Ineson, P., Kätterer, T., Knicker, H., Nilsson, S.I., Näsholm, T., Ogle, S., Paustian, K., Persson, T., Stendahl, J., 2011. Knowledge gaps in soil carbon and nitrogen interactions – from molecular to global scale. Soil Biology and Biochemistry 43, 702–717.
Gilmanov, T.G., Parton, W.J., Ojima, D.S., 1997. Testing the 'CENTURY' ecosystem level model on data sets from eight grassland sites in the former USSR representing a wide climatic/soil gradient. Ecological Modelling 96, 191–210.
Groffman, P.M., Tiedje, J.M., 1991. Relationships between denitrification, CO_2 production and air-filled porosity in soils of different texture and drainage. Soil Biology and Biochemistry 23, 299–302.
Hart, S.C., Nason, G.E., Myrold, D.D., Perry, D.A., 1994. Dynamics of gross nitrogen transformations in an old-growth forest: the carbon connection. Ecology 75, 880–891.
Hefting, M., Clément, J.C., Dowrick, D., Cosandey, A.C., Bernal, S., Cimpian, C., Tatur, A., Burt, T.P., Pinay, G., 2004. Water table elevation controls on soil nitrogen cycling in riparian wetlands along a European climatic gradient. Biogeochemistry 67, 113–134.
Heinen, M., 2006. Application of a widely used denitrification model to Dutch data sets. Geoderma 133, 464–473.
Herbst, M., Hellebrand, H.J., Bauer, J., Huisman, J.A., Šimůnek, J., Weihermüller, L., Graf, A., Vanderborght, J., Vereecken, H., 2008. Multiyear heterotrophic soil respiration: evaluation of a coupled CO_2 transport and carbon turnover model. Ecological Modelling 214, 271–283.
Hungate, B.A., Dukes, J.S., Shaw, M.R., Luo, Y., Field, C.B., 2003. Nitrogen and climate change. Science 302, 1512–1513.
Kelly, R.H., Parton, W.J., Crocker, G.J., Grace, P.R., Klír, J., Körschens, M., Poulton, P.R., Richter, D.D., 1997. Simulating trends in soil organic carbon in long-term experiments using the century model. Geoderma 81, 75–90.
Kelly, R.H., Parton, W.J., Hartman, M.D., Stretch, L.K., Ojima, D.S., Schimel, D.S., 2000. Intra-annual and interannual variability of ecosystem processes in shortgrass steppe. Journal of Geophysical Research D: Atmospheres 105, 20093–20100.
Kirschbaum, M.U.F., Paul, K.I., 2002. Modelling C and N dynamics in forest soils with a modified version of the CENTURY model. Soil Biology and Biochemistry 34, 341–354.
Koorevaar, P., Menelik, G., Dirksen, C., 1983. Elements of Soil Physics. Elsevier, Amsterdam.
Kucharik, C.J., Foley, J.A., Delire, C., Fisher, V.A., Coe, M.T., Lenters, J.D., Young-Molling, C., Ramankutty, N., Norman, J.M., Gower, S.T., 2000. Testing the performance of a dynamic global ecosystem model: water balance, carbon balance, and vegetation structure. Global Biogeochemical Cycles 14, 795–825.

Linacre, E.T., 1977. A simple formula for estimating evaporation rates in various climates, using temperature data alone. Agricultural Meteorology 18, 409–424.
Linn, D.M., Doran, J.W., 1984. Effect of water-filled pore space on carbon dioxide and nitrous oxide production in tilled and nontilled soils. Soil Science Society of America Journal 48, 1267–1272.
Liu, W., Zhang, Z., Wan, S., 2009. Predominant role of water in regulating soil and microbial respiration and their responses to climate change in a semiarid grassland. Global Change Biology 15, 184–195.
Makkink, G.F., 1957. Testing the Penman formula by means of lysimeters. Journal of the Institution of Water Engineers 11, 277–288.
Manzoni, S., Porporato, A., 2009. Soil carbon and nitrogen mineralization: theory and models across scales. Soil Biology and Biochemistry 41, 1355–1379.
Manzoni, S., Schimel, J.P., Porporato, A., 2011. Responses of soil microbial communities to water-stress: results from a meta-analysis. Ecology 93, 930–938.
Metherell, A.K., Harding, L.A., Cole, C.V., Parton, W.J., 1993. CENTURY Soil Organic Matter Model Environment. Technical Documentation Agroecosystem Version 4.0, pp. 247.
Moyano, F.E., Vasilyeva, N., Bouckaert, L., Cook, F., Craine, J., Curiel Yuste, J., Don, A., Epron, D., Formanek, P., Franzluebbers, A., Ilstedt, U., Kätterer, T., Orchard, V., Reichstein, M., Rey, A., Ruamps, L., Subke, J.A., Thomsen, I.K., Chenu, C., 2012. The moisture response of soil heterotrophic respiration: interaction with soil properties. Biogeosciences 9, 1173–1182.
Myers, R.J.K., Campbell, C.A., Weier, K.L., 1982. Quantitative relationship between net nitrogen mineralization and moisture content of soils. Canadian Journal of Soil Science 62, 111–124.
Olde Venterink, H., Pieterse, N.M., Belgers, J.D.M., Wassen, M.J., de Ruiter, P.C., 2002a. N, P and K budgets along nutrient availability and productivity gradients in wetlands. Ecological Applications 12, 1010–1026.
Olde Venterink, H., Davidsson, T.E., Kiehl, K., Leonardson, L., 2002b. Impact of drying and re-wetting on N, P and K dynamics in a wetland soil. Plant and Soil 243, 119–130.
Ordonez, J.C., van Bodegom, P.M., Witte, J.P.M., Bartholomeus, R.P., van Hal, J.R., Aerts, R., 2010. Plant strategies in relation to resource supply in mesic to wet environments: does theory mirror nature? American Naturalist 175, 225–239.
Ordonez, J.C., van Bodegom, P.M., Witte, J.P.M., Wright, I.J., Reich, P.B., Aerts, R., 2009. A global study of relationships between leaf traits, climate and soil measures of nutrient fertility. Global Ecology and Biogeography 18, 137–149.
Pansu, M., Sarmiento, L., Rujano, M.A., Ablan, M., Acevedo, D., Bottner, P., 2010. Modeling organic transformations by microorganisms of soils in six contrasting ecosystems: validation of the MOMOS model. Global Biogeochemical Cycles 24, GB1008.
Parton, W.J., Schimel, D.S., Cole, C.V., Ojima, D.S., 1987. Analysis of factors controlling soil organic-matter levels in great-plains grasslands. Soil Science Society of America Journal 51, 1173–1179.
Parton, W.J., Scurlock, J.M.O., Ojima, D., Gilmanov, T.G., Scholes, R.J., Schimel, D.S., Kirchner, T., Menaut, J.-C., Seastedt, T., Garcia Moya, E., Kamnalrut, A., Kinyamario, J.I., 1993. Observations and modeling of biomass and soil organic matter dynamics for the grassland biome worldwide. Global Biogeochemical Cycles 7, 785–809.
Paul, K.I., Polglase, P.J., O'Connell, A.M., Carlyle, J.C., Smethurst, P.J., Khanna, P.K., 2003. Defining the relation between soil water content and net nitrogen mineralization. European Journal of Soil Science 54, 39–47.
Probert, M.E., Dimes, J.P., Keating, B.A., Dalal, R.C., Strong, W.M., 1998. APSIM's water and nitrogen modules and simulation of the dynamics of water and nitrogen in fallow systems. Agricultural Systems 56, 1–28.
Reichstein, M., Rey, A., Freibauer, A., Tenhunen, J., Valentini, R., Banza, J., Casals, P., Cheng, Y., Grünzweig, J.M., Irvine, J., Joffre, R., Law, B.E., Loustau, D., Miglietta, F., Oechel, W., Ourcival, J.M., Pereira, J.S., Peressotti, A., Ponti, F., Qi, Y., Rambal, S., Rayment, M., Romanya, J., Rossi, F., Tedeschi, V., Tirone, G., Xu, M., Yakir, D., 2003. Modeling temporal and large-scale spatial variability of soil respiration from soil water availability, temperature and vegetation productivity indices. Global Biogeochemical Cycles 17, 1104.
Rodrigo, A., Recous, S., Neel, C., Mary, B., 1997. Modelling temperature and moisture effects on C–N transformations in soils: comparison of nine models. Ecological Modelling 102, 325–339.
Schaffers, A.P., 2000. In situ annual nitrogen mineralization predicted by simple soil properties and short-period field incubation. Plant and Soil 221, 205–219.
Schimel, D.S., 1994. Climatic, edaphic, and biotic controls over storage and turnover of carbon in soils. Global Biogeochemical Cycles 8, 279–293.
Schjønning, P., Thomsen, I.K., Moldrup, P., Christensen, B.T., 2003. Linking soil microbial activity to water- and air-phase contents and diffusivities. Soil Science Society of America Journal 67, 156–165.
Schjønning, P., Thomsen, I.K., Petersen, S.O., Kristensen, K., Christensen, B.T., 2011. Relating soil microbial activity to water content and tillage-induced differences in soil structure. Geoderma 163, 256–264.
Sleutel, S., Moeskops, B., Huybrechts, W., Vandenbossche, A., Salomez, J., De Bolle, S., Buchan, D., De Neve, S., 2008. Modeling soil moisture effects on net nitrogen mineralization in loamy wetland soils. Wetlands 28, 724–734.
Stanford, G., Epstein, E., 1974. Nitrogen mineralization – water relations in soil. Soil Science Society of America Proceedings 38, 103–107.
Van Dam, J.C., Groenendijk, P., Hendriks, R.F.A., Kroes, J.G., 2008. Advances of modeling water flow in variably saturated soils with SWAP. Vadose Zone Journal 7, 640–653.
van Genuchten, M.T., 1980. Closed-form equation for predicting the hydraulic conductivity of unsaturated soils. Soil Science Society of America Journal 44, 892–898.
von Asmuth, J.R., Maas, K., Knotters, M., Bierkens, M.F.P., Bakker, M., Olsthoorn, T.N., Cirkel, D.G., Leunk, I., Schaars, F., von Asmuth, D.C., 2012. Software for hydrogeologic time series analysis, interfacing data with physical insight. Environmental Modelling & Software 38, 178–190.
Walse, C., Berg, B., Sverdrup, H., 1998. Review and synthesis of experimental data on organic matter decomposition with respect to the effect of temperature, moisture, and acidity. Environmental Reviews 6, 25–40.
Witte, J.P.M., Wójcik, R.B., Torfs, P.J.J.F., De Haan, M.W.H., Hennekens, S., 2007. Bayesian classification of vegetation types with Gaussian mixture density fitting to indicator values. Journal of Vegetation Science 18, 605–612.
Wösten, J.H.M., Veerman, G.J., de Groot, W.J.M., Stolte, J., 2001. Waterretentie- en doorlatendheidskarakteristieken van boven- en ondergronden in Nederland: de Staringreeks, Alterra-rapport. Alterra, Wageningen, pp. 86.

A probabilistic eco-hydrological model to predict the effects of climate change on natural vegetation at a regional scale

Jan-Philip M. Witte, Ruud P. Bartholomeus, Peter M. van Bodegom, D. Gijsbert Cirkel, Remco van Ek, Yuki Fujita, Gijs M. C. M. Janssen, et

Landscape Ecology

ISSN 0921-2973
Volume 30
Number 5

Landscape Ecol (2015) 30:835-854
DOI 10.1007/s10980-014-0086-z

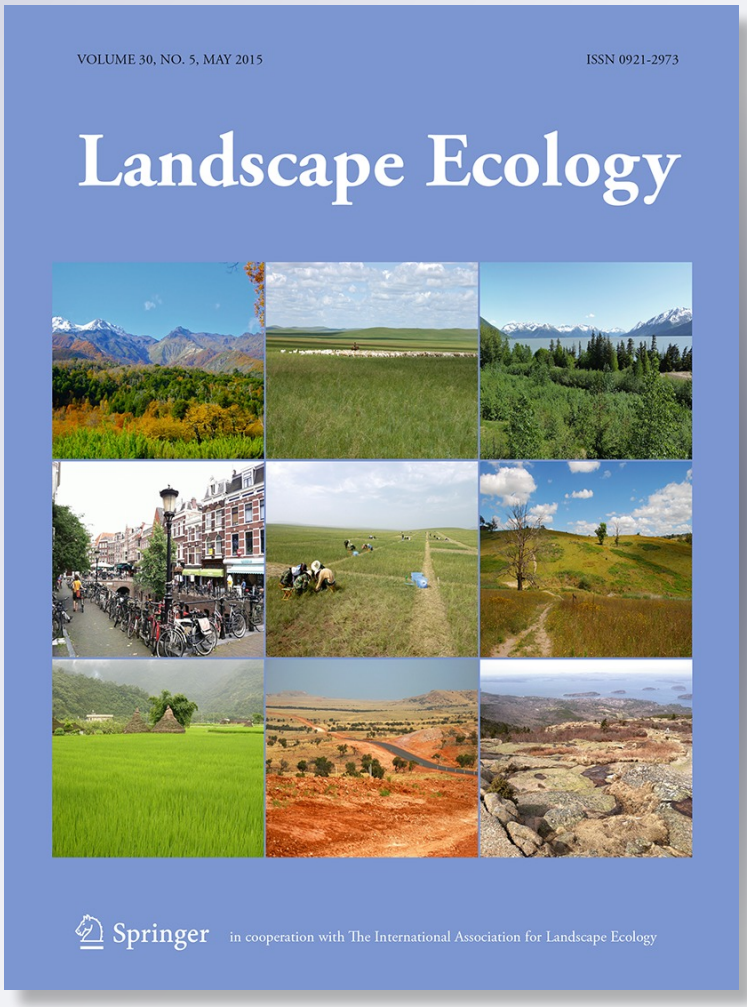

Springer

Landscape Ecol (2015) 30:835–854
DOI 10.1007/s10980-014-0086-z

RESEARCH ARTICLE

A probabilistic eco-hydrological model to predict the effects of climate change on natural vegetation at a regional scale

Jan-Philip M. Witte · Ruud P. Bartholomeus · Peter M. van Bodegom · D. Gijsbert Cirkel · Remco van Ek · Yuki Fujita · Gijs M. C. M. Janssen · Teun J. Spek · Han Runhaar

Received: 31 March 2014 / Accepted: 16 August 2014 / Published online: 29 August 2014

Abstract Climate change may hamper the preservation of nature targets, but may create new potential hotspots of biodiversity as well. To timely design adequate measures, information is needed about the feasibility of nature targets under a future climate. Habitat distribution models may provide this, but current models have certain drawbacks: they apply indirect empirical relationships between habitat and vegetation, they often disregard spatially explicit information about groundwater, and they are designed for too coarse spatial scales. We introduce a model that explicitly takes into account spatial effects through groundwater and that can easily be adapted to new scientific approaches and the needs of end-users. It combines (spatially explicit) data sources, transfer functions derived from mechanistic models, and robust relationships between habitat factors and plant characteristics. Outputs are maps showing the occurrence probabilities of vegetation types and their associated conservation values, both on a spatial scale that fits the needs of nature managers and spatial planners. The model was applied to a catchment of 270 km^2 to forecast, on a 25 m resolution, the effects of a national climate scenario (related to IPCC A2 and A1B). Computation time was a couple of minutes on a standard PC. Severe loss was predicted for wet and mesotrophic species-rich grasslands, while vegetation of dry and acidic soils appeared to profit. The results were not univocal though, and could probably not have been foreseen on the basis of expert judgement and logic alone, especially because of edaphic factors and spatial hydrological relationships.

Keywords Habitat distribution model · Hydrology · Mechanistic modelling · Oxygen stress · Transfer functions · Plant traits

Electronic supplementary material The online version of this article (doi:10.1007/s10980-014-0086-z) contains supplementary material, which is available to authorized users.

J.-P. M. Witte (✉) · R. P. Bartholomeus · D. G. Cirkel · Y. Fujita · H. Runhaar
KWR Watercycle Research Institute, P.O. Box 1072, 3430 BB Nieuwegein, The Netherlands
e-mail: flip.witte@kwrwater.nl

J.-P. M. Witte · P. M. van Bodegom
Systems Ecology, Department of Ecological Science, VU University Amsterdam, De Boelelaan 1085, 1081 HV Amsterdam, The Netherlands

R. van Ek · G. M. C. M. Janssen
Deltares, P.O. Box 85467, 3508 AL Utrecht, The Netherlands

T. J. Spek
Provincie Gelderland, P.O. Box 9090, 6800 GX Arnhem, The Netherlands

Introduction

Global warming will affect the amount and temporal distribution of both precipitation and evapotranspiration

on earth (Karl et al. 1995; Solomon et al. 2007; Dai 2011; Trenberth et al. 2014). Droughts are expected to set in quicker and to be more intense, whereas precipitation is expected to become more concentrated in intensive showers. These meteorological changes will alter the water balance of soils, as well as the distribution of water through the landscape (Easterling et al. 2000; Weltzin et al. 2003; Porporato et al. 2004; Fay et al. 2008; Knapp et al. 2008; Witte et al. 2012; Karlsson et al. 2014). It is evident that such hydrological changes, in concert with temperature rise, will affect habitat factors that are essential to plant growth, such as soil acidity and the availability of moisture, oxygen, and nutrients in the root zone of plants (Easterling et al. 2000; Weltzin et al. 2003; Porporato et al. 2004; Knapp et al. 2008; Levine et al. 2008; Bartholomeus et al. 2011). For this reason it is questionable whether nature targets, for example those formulated under the European Habitat Directive and the Water Framework Directive, are still attainable in future climatic conditions. At present, focus in nature management is on the conservation of existing distribution patterns of ecosystems and species. This is generally done by carrying out measures such as the planning of ecological networks, the creation of hydrological buffers against desiccation, and nutrient management like sod-cutting. Climate change may, however, also ask for a more flexible approach, not only aiming at the conservation of existing patterns, but taking the opportunity to exploit potential future hotspots of biodiversity as well.

To design adequate measures and spatial plans, and to avoid ineffective ones, policy makers, nature managers, and spatial planners require information about the feasibility of nature targets under a future climate. Because the empirical basis for climate change impacts in the recent past, across transects that cover different climate zones, is too narrow, it is inevitable that models are used for this purpose. The evaluation of climate change effects on vegetation composition has predominantly been done with rather correlative habitat distribution models (HDMs) (e.g. Thomas et al. 2004). In recent years, however, the application of HDMs for climate projections has been criticized for a variety of reasons (as reviewed in Pearson and Dawson 2003; Guisan and Thuiller 2005; Botkin et al. 2007; Bartholomeus et al. 2011; Van Bodegom et al. 2012): they are based on measurements from the current climate, assuming steady state conditions; the applied relationships between environmental factors and vegetation are usually indirect and highly correlative; they do not account for no-analogue combinations of environmental conditions. Another drawback of correlative HDMs is a lack of good predictor variables at a fine spatial scale, implying that in practice they seem to be designed for predicting species and vegetation patterns on coarse spatial scales (Early et al. 2008), such as a whole country (e.g. Buckley et al. 2010) or a continent (e.g. Bakkenes et al. 2002).

Conservationists, however, are in need of information on the scale that fits their vegetation targets, thus a site scale typically ranging from approximately 100–10,000 m^2. The combination of a fine spatial scale, a detailed vegetation typology and climate projections create a need for a more mechanistic way of modelling, taking explanatory factors into account that directly impact plant performance, such as the availability of soil moisture for transpiration. By explicitly modelling (the dynamics in) habitat factors, such models are more suitable to forecast climate change effects on vegetation. This, however, requires a larger number of input parameters, which usually goes at the cost of the model accuracy and applicability (Baird 1999; Guisan and Zimmermann 2000; Douma et al. 2012c). To fulfil the data hunger of mechanistic models, a well-designed field campaign, including an accurate description of local soil properties, will certainly be useful to forecast climate change effects for a particular case study (e.g. Van Oene et al. 1999). However, such an approach is only feasible for a limited number of carefully selected sites and difficult to generalise. Moreover, we may expect that important climate change effects in groundwater-fed ecosystems, which often harbour high conservation values, will be related to the distribution of groundwater, since climate induced hydrological changes in recharge areas will impact the water supply of discharge areas (Witte et al. 2012; Karlsson et al. 2014). This necessitates an approach that explicitly links groundwater flow to vegetation responses.

In summary, neither correlative HDMs, nor mechanistic models of single sites fulfil the needs of policy makers, nature managers, and spatial planners who want to anticipate on climate change by taking timely measures. The aim of this paper therefore is to present, building on previous work by Witte et al. (2004) and Douma et al. (2012c), the model PROBE (PRObability-Based Ecological target model), which can predict

vegetation distribution under a changing climate. It explicitly takes into account spatial effects through hydrology, yet needs a relatively limited amount of input values. The model optimally combines available (spatially explicit) data sources, transfer functions (to speed-up the calculations) derived from mechanistic models, and empirical relationships between soil and vegetation characteristics. For both practical and theoretical reasons, PROBE simulates vegetation types instead of plant species. Of course modelling vegetation types has its shortcomings, especially in the face of climate change. In the Discussion section we will go into these drawbacks.

In this paper we will describe PROBE, and demonstrate the model for a small catchment within The Netherlands. We will comment upon the simulated ecological effects of climate change and their consequences for nature conservation and spatial planning. Finally, we will discuss the pros and cons of our modelling approach, as well as possibilities for improvements.

Model description

General approach

PROBE estimates vegetation patterns assuming steady state conditions, meaning that vegetation is in equilibrium with long-term (30 years) weather conditions and groundwater levels. Central to our model (Fig. 1) is that the ecological amplitudes of vegetation types can be described by mean plot values of plant characteristics, as was demonstrated by (Witte et al. 2007; Douma et al. 2012a). This starting point is in accordance with the assembly theory, which states that the environment acts as a filter, which over time removes species that are not adapted to the local conditions (Keddy 1992). An essential second feature of PROBE is that it computes occurrence probabilities of vegetation types, thus accounting for the fact that vegetation types may partly share the same habitat requirements and that the abundance of vegetation types is locally unpredictable as "this is determined by the order of species arrival (Drake 1991), species interactions and other historical events (Van der Maarel and Sykes 1993)" (Douma et al. 2012a).

Supported by an overwhelming number of publications (e.g. Tilman 1985; Ellenberg 1992; Grime 2001), a basic assumption of PROBE is that vegetation composition can largely be explained by the following environmental drivers: 'light', 'salinity', 'moisture regime', 'nutrient availability' and 'acidity'. Of these drivers, most competition for light in Dutch nature reserves is controlled for by nature management, like mowing or grazing. We accounted for this by imposing a known vegetation structure (i.e. short herbaceous, or tall and woody). Salinity was disregarded because PROBE currently only produces results for inland vegetation, outside the influence of seawater.

While one of the central themes in current community ecology involves the application of traits-based approaches (McGill et al. 2006; Van Bodegom et al. 2012 and references therein), current relationships between environmental drivers and functional traits are weak (see e.g. Fujita et al. 2013b for nutrients and Douma et al. 2012b for moisture), or even lacking (acidity). For the current model version, we therefore used the indicator values for Dutch species of Witte et al. (2007) to describe the vegetation characteristics in relation to environmental drivers. This indicator list describes the preference of each species on an ordinal and continuous scale towards moisture regime (*F*, ranging from 1.0 = open water to 4.0 = completely dry), nutrient availability (*N*, ranging from 1.0 = nutrient poor to 3.0 = very nutrient rich) and acidity (*R*, ranging from 1.0 = acid to 3.0 = alkaline). Hence, we describe vegetation type amplitudes with PROBE by mean plot values of indicator values (*mF*, *mN* and *mR*). Note: since the indicator scales are continuous (in contrast to the discrete scales of indicator classes of for instance Ellenberg 1992), the lengths of these scales have no substantive meaning.

Geographical input to PROBE are raster maps with geographical data on climate, hydrology, soil, and land use ("Geographical input" section). For each grid cell, which size may vary depending on the application (e.g. 10 m or 250 m), the model goes through four successive steps to translate geographical input into vegetation types (Fig. 1). In Step 1 proxies of environmental drivers (hereafter: site factors) are simulated with the help of transfer functions ("Step 1 and 2: simulation of site factors and indicator values" section). Site factors implemented are transpiration stress *TS* (m H_2O 10 $days^{-1}$) (Bartholomeus et al. 2011), root respiration stress *RS* (kg O_2 m^{-2} 10 $days^{-1}$) (Bartholomeus et al. 2012), phosphorus mineralization rate *Pmin* (mg P kg $soil^{-1}$ $year^{-1}$) and

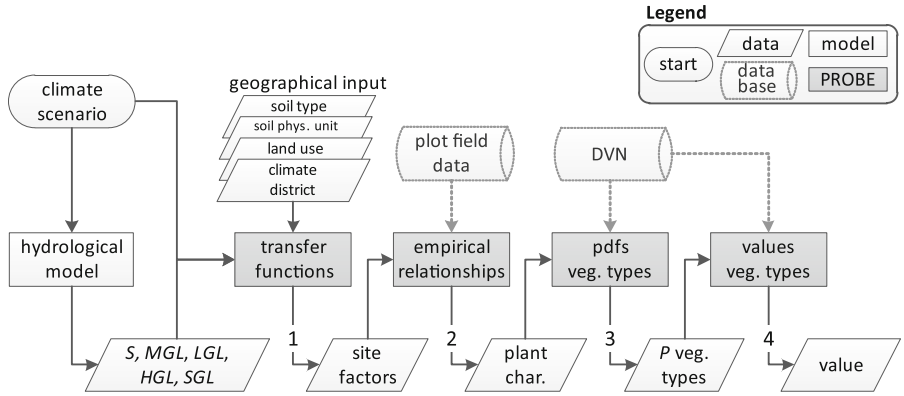

Fig. 1 Schematic representation of PROBE, which computes, per grid cell, the effects of climate change in four successive steps: (1) geographical data and the output of a transient hydrological model (seepage intensity *S* and mean, lowest, highest, and spring groundwater level (resp. *MGL*, *LGL*, *HGL* and *SGL*)) are input to transfer functions to obtain site factors; (2) which are translated to plot mean plant characteristics with the aid of empirical relationships from vegetation plots; (3) this combination of characteristics is input to probability density functions (pdfs) that are derived from a large data base with classified vegetation relevés (DVN) to simulate the Bayesian occurrence probabilities of vegetation types; (4) which are weighted according the conservation value they represent, after which the results are summed to yield the conservation value of the grid cell

soil acidity pH (−). In step 2 these site factors are related to mean indicator values ("Step 1 and 2: simulation of site factors and indicator values" section), which are used in step 3 to predict the Bayesian occurrence probability *p* of each vegetation type ("Step 3: from indicator values to vegetation types" section). Finally, in step 4 a conservation value is ascribed to the grid cell on the basis of the occurrence probabilities of all simulated vegetation types ("Step 4: from vegetation types to conservation value" section).

The generic model set-up allows PROBE to be adapted to the vegetation typology desired by the end-user, as well as to local information on soil and climate. Here we present one possible model schematization.

Geographical input

PROBE uses a land use map, basically stored in a 25 m grid (Hazeu 2005), to identify nature areas, as well as to distinguish between different vegetation structures. Since all site factors depend on soil type, the soil map of the Netherlands also serves as input. Transpiration stress *TS* and root respiration stress *RS* depend on, amongst others, soil physical properties (water retention and unsaturated hydraulic conductivity curves), which are deduced from a map of 21 soil physical units (Wösten et al. 2001). Both soil maps are vector based and commonly available on a 1:50,000 scale. To serve as input for PROBE, they have to be converted to a raster by classifying each grid cell to the soil type with the highest surface area.

TS, *RS* and *Pmin* are affected by temperature, precipitation and reference evapotranspiration. To account for spatial variation in these meteorological variables within the Netherlands, we used a national map with 14 climate districts from Pulles (1985). In case of shallow groundwater levels, capillary flow to the rooting zone is an important source of water supply which, via its effects on soil moisture content, acts upon *TS*, *RS*, *Pmin* and *pH*. In groundwater-fed ecosystems, *pH* can also be influenced by upwelling of alkaline groundwater. To reflect these influences of shallow groundwater, PROBE requires the following hydrological input variables, to be generated by a dynamic transient hydrological model: average seepage intensity *S* (m days^{-1}) and four groundwater level characteristics (all in m below soil surface): mean groundwater level through the year *MGL*, average lowest groundwater level *LGL*, average highest groundwater level *HGL*, average groundwater level in springtime (1 April) *SGL*. To properly reflect climate conditions, these averages should be based on daily values from a simulation period of 30 years (Bartholomeus et al. 2008).

Step 1 and 2: simulation of site factors and indicator values

We have derived process-based relationships between site factors and vegetation characteristics, i.e. relationships that can also be applied outside their calibration range as is required for climate projections. These relationships have been implemented in PROBE, as is described below.

Moisture regime

In groundwater-fed ecosystems, the moisture regime is usually described by mean groundwater levels, or the period and degree that the groundwater level exceeds a certain threshold value (Bartholomeus et al. 2012 and references therein). Because these proxies affect plant performance indirectly, their relationships with plant characteristics are only valid for specific climatic and edaphic conditions. Therefore we used two process-based and climate versatile proxies for moisture regime: *TS*, which accounts for periods of drought, when soil moisture availability does not meet vegetation's transpiration demand, and *RS* that accounts for periods with insufficient oxygen in the root zone for respiration at a potential rate (Bartholomeus et al. 2011). Both measures include the physiological response of the vegetation to climate change, meaning that the demand for water and oxygen increases with temperature. *TS* and *RS* relate to the annual maximum stress (defined as transpiration and respiration deficit respectively) of reference grassland not adapted to drought, nor to waterlogging, in a 10-days period, averaged across 30 years (Bartholomeus et al. 2011). *TS* and *RS* have appeared to correlate well with observed vegetation characteristics and to be more robust in extrapolations than indirect proxies for moisture regime (Bartholomeus et al. 2012). Since the computation of *TS* and *RS* is time-consuming, and therefore practically unfeasible for thousands to millions of grid cells that we want to process with PROBE, we developed groundwater to stress transfer (GTST) software, which generates a transfer function for *TS* and one for *RS* for each combination of climate scenario, climate district and soil physical unit (Bartholomeus and Witte 2013). Underlying these transfer function are runs of the soil–water-atmosphere-plant model SWAP (Kroes et al. 2008; Van Dam et al. 2008) for automatically generated plots (30 years, time-step of 1 day). From each plot, both groundwater level characteristics (*MGL*, *LGL* and *HGL*) and stresses (*TS* and *RS*) are simulated. After running thousands of plots, GSTS empirically relates *TS* and *RS* to *MGL*, *LGL* and *HGL*.

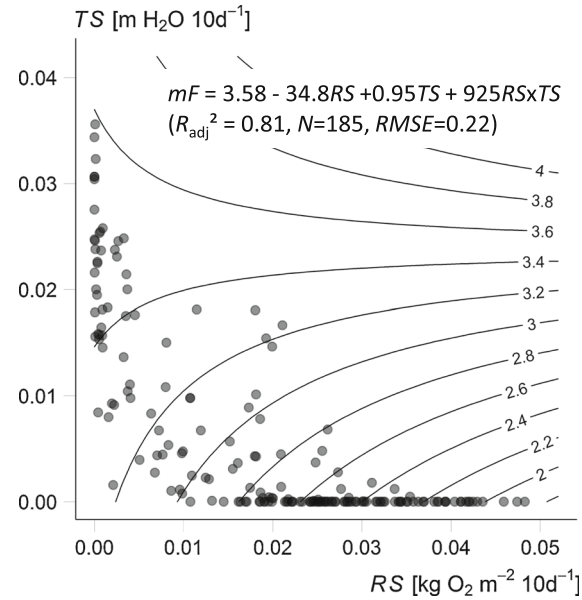

Fig. 2 Empirical relationship between simulated root respiration stress *RS*, simulated transpiration stress *TS*, and 'observed' mean moisture indicator value *mF*. Each plot represents a vegetation plot

After applying the transfer functions to known *MGL*, *LGL* and *HGL*, climate and soil variables, PROBE translates *TS* and *RS* to a mean moisture indicator value *mF* with the aid of a relationship that we derived from 185 vegetation plots where soil texture and groundwater levels were measured (Fig. 2). These plots were distributed near groundwater observation wells over different types of ecosystems throughout the country (data presented in Bartholomeus et al. 2011).

Nutrient availability

According to inter-comparisons of different soil proxies (Ordoñez et al. 2009; Fujita et al. 2013b), nutrient availability for plants is best approximated by the mineralization rate of phosphorus, *Pmin*. The transfer functions of *Pmin* were generated within the framework of GTST, by coupling of SWAP with the soil organic matter model CENTURY (Parton et al.

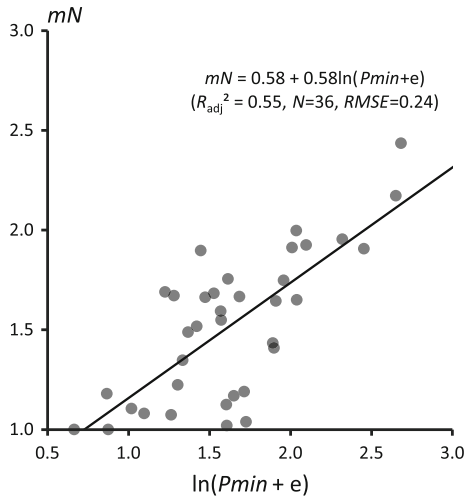

Fig. 3 Empirical relationship between simulated mineralization rate *Pmin* (e is the base of the natural logarithm) in the topsoil (0–10 cm), and mean nutrient indicator value *mN*. Data from Fujita et al. (2013b)

1993) that we adapted to groundwater-dependent sites (Fujita et al. 2013a). For each run (again: 30 years for each scenario), monthly averaged SWAP output of moisture content and soil temperature in the upper 10 cm soil layer served as input to CENTURY. For each combination of climate scenario, climate district, and soil physical unit the transfer function describes *Pmin* in dependency of *RS* (which in turn is a function of *MGL*, *LGL* and *HGL*).

On the basis of field data of Fujita et al. (2013b) we found a reasonable fit between *Pmin* and mean nutrient indicator value *mN* (Fig. 3). After applying *Pmin* derived from the transfer functions to the *Pmin*-*mN* relationship, the simulated *mN* in a 250 grid showed significant agreement with 'observed' *mN* in vegetation plots throughout the country ("Model plausibility" section). The explained variance was low though (20 %), presumably partly due to a lack of data to properly parameterize the units of the soil physical map (for details, Van Ek et al. 2014). Therefore we initialized PROBE with a knowledge system (WATERNOOD) developed in the commission of the Dutch water boards to provide water managers with information on hydrological requirements of vegetation types and help them to predict the effects of water management measures on vegetation (De Haan et al. 2010). Inputs to WATERNOOD (in fact a collection of transfer functions) are soil type, land use, *LGL*, groundwater level in springtime *SGL* and seepage intensity *S*. However, WATERNOOD, with its correlative relationships and for the current climate, cannot be used for climate projections. Therefore, after initialization of *Nm* with WATERNOOD (details: see Van Ek et al. 2014), the transfer functions from GTST in combination with the empirical relationship between *Pmin* and *Nm* (Fig. 3) were used to simulate a change in indicator value ΔNm resulting from a climate projection.

Acidity

We found a strong relationship between soil-pH and mean acidity indicator value *mR* (Cirkel et al. 2014) but were not able to use this because we could not yet simulate soil acidity in a process-based manner. For this reason we applied the decision rules of WATERNOOD to compute *mR*, both for the current and the future climate (for details, see Van Ek et al. 2014). These rules were based on pH measurements in soils and on model simulations with SMART (Kros et al. 1995). Input variables to determine *mR* are soil type, land use, *LGL* and *S*.

Step 3: from indicator values to vegetation types

Using the indicator values from Step 2, PROBE computes the occurrence probability *P* of each vegetation type. For this purpose, PROBE utilizes probability density functions (pdfs) describing the Bayesian occurrence probability of vegetation types in dependency of plant traits or indicator values (Witte et al. 2007). Bayes' theorem meets the second Kolmogorov axiom, which means that the sum of *P* for each grid cell is always 100 %. The method used to generate pdfs with the aid of Gaussian Mixture Models (Witte et al. 2007) is applicable to any vegetation classification system, as long as a large database of vegetation plots (relevés) is available. Moreover, the method can use indicator values, functional traits, or a combination thereof to generate pdfs. These pdfs are non-parametric, i.e. they do not assume a priori any particular distribution of data points in the 3-D space. To acquire reliable pdfs, a minimum of 10 relevés per indicator value per vegetation type was set as a minimum (hence, a minimum of 30 relevés when using three indicator values).

We used a national database (DVN, Database Vegetation of the Netherlands) to calculate the density functions. This database contains 35,000 relevés, taken all over the country in the period 1928-1988. DVN had been used for the standard work of vegetation types in the Netherlands (Schaminée et al. 1995b, 1996; 1998; Stortelder et al. 1999). On the basis of their species composition, relevés of DVN were classified into vegetation types ("Model application" section). Additionally, indicator values *mF*, *mN*, and *mR* were computed for each relevé, based on their species composition. Thus, the position of each classified relevé was obtained in a three dimensional space of indicator values. Combining all relevés from a vegetation type thus allows fitting the pdfs of vegetation types as a function of indicator values (Witte et al. 2007).

Step 4: from vegetation types to a conservation value

Maps of different vegetation types can be difficult to interpret, particularly if this has to be done by non-specialists like policymakers and spatial planners. But even for experts it may be extremely difficult to give an opinion about multiple vegetation maps, especially when they are asked to give an overall judgement about the consequences of a particular climate projection.

For this reason PROBE offers the possibility to merge maps of the various vegetation types into one map, showing the conservation values of the model area. To this end, for each grid cell the occurrence probability P is multiplied by the conservation value V of the vegetation type, upon which the results of all vegetation types are summed (value cell $= \Sigma(P \times V)$). There are numerous ways to assess the conservation value of vegetation, ranging from simply counting the number of species or red list species, to more elaborate methods that take account of species rarity, distinctiveness of species, species abundance, species rarity on a national and international scale, etc. PROBE does not prescribe any particular valuation method; users have the freedom to use the system they prefer and even to score vegetation types according to their own preferences. However, on the basis of a double-blind consultation of vegetation experts we advise the following three methods (Witte et al. 2011b): counting the number of red list species (Van der Meijden et al. 2000), or using the more detailed methods of Hertog and Rijken (1992) or Witte (1998). PROBE obtains a value V for each vegetation type as the mean conservation value of the relevés in DVN ascribed to this vegetation type (Witte et al. 2011b).

Model plausibility

Elements of the PROBE model (SWAP, CENTURY, WATERNOOD, oxygen stress module) have been validated in different climates. Unfortunately, we were not able to validate the full model. For that purpose, data on species composition and site conditions for a wide range of soils, and hydrological and climatic conditions would be needed. Lacking such a database, we restricted ourselves to a plausibility analysis for the current climate. This plausibility was assessed by comparing indicator values simulated with PROBE with those observed in 3,458 well-located relevés in nature reserves all over the Netherlands (Van Ek et al. 2014). PROBE was fed by hydrological input from a national hydrological model (De Lange et al. 2014) which has a spatial resolution of 250 m. Likewise, for this validation PROBE also used a resolution of 250 m. Note that relevés measure on average approximately 4 m^2, which is a factor 15,625 smaller than these grid cells. In spite of this huge difference in spatial scale, and the fact that the national hydrological model tended to simulate too deep groundwater levels in wet and moist reserves (Witte et al. 2011a), there was a very significant agreement ($p < 0.001$) between simulated and observed indicator values: for *mF*, Pearson's R^2 amounted 52 % and the Nash–Sutcliffe coefficient *NS* was 24 %; for *mN* these figures were $R^2 = 41$ %, $NS = 38$ %; and for *mR* they were $R^2 = 50$ % and $NS = 20$ %. Compared to Pearson's R^2 *NS* was relatively low, which, at least partly, could be ascribed to the systematic underestimation of groundwater levels in wet and moist nature reserves.

Model application

Study area

We applied the model to the 'Baakse beek', a small catchment of 270 km^2, typical for the eastern and southern Pleistocene cover landscape, which occupies about half of the Netherlands (Fig. 4). A number of

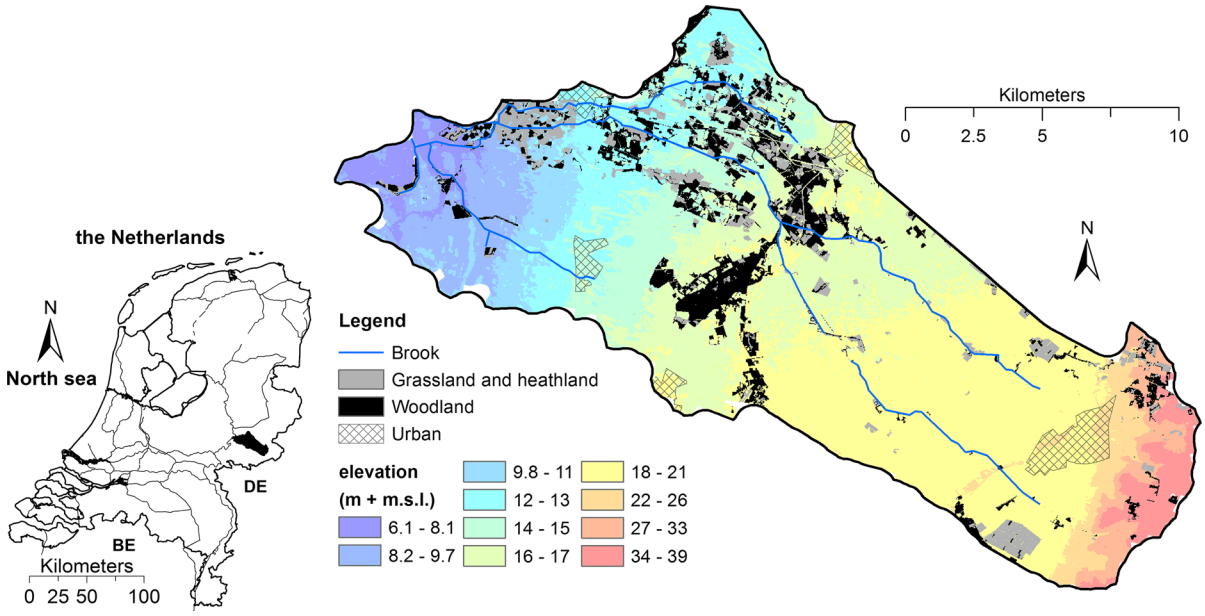

Fig. 4 Overview of the Baakse beek catchment with its nature areas (part of the current NEN) in *grey* and *black*. PROBE results can be used to determine future extensions and adaptations of the NEN

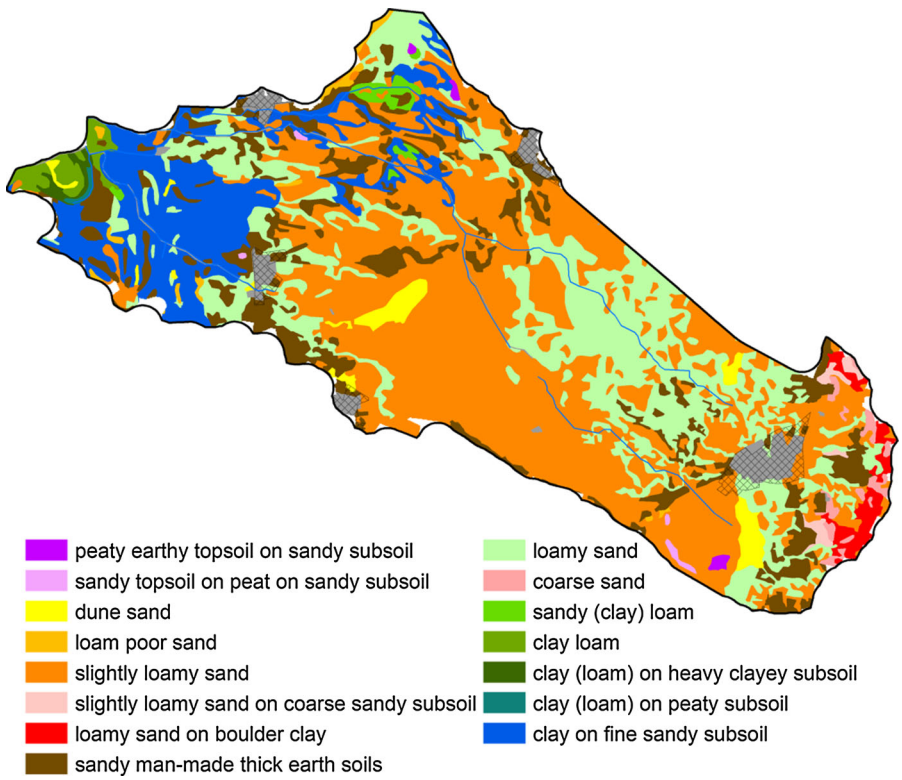

Fig. 5 Soil physical units of the Baakse beek catchment

small brooks spring from the eastern more elevated part of the area (20 to 40 m +m.s.l.) from which they flow to the outlet of the catchment in the west (7 m +m.s.l.). Major soil physical units are 'loamy sand', 'slightly loamy sand', and 'clay on fine sandy subsoil' (Fig. 5). Mean annual precipitation in the area is ca. 850 mm, mean reference evapotranspiration according to Makkink ca. 550 mm, and mean temperature ca. 10 °C. Like in the rest of the Netherlands, there is a precipitation surplus in winter and a precipitation deficit in summer.

Most of the area is used for intensive dairy farming, which implies that pasture and maize fields dominate the flat landscape. About 13 % of the area is designated nature, with coniferous woodland on soils that are dry (i.e. groundwater level below ca. 2 m minus soil surface), deciduous woodlands in former estates in the north-west, and small reserves with mesotrophic meadows, hayfields and heathlands scattered over the catchment. Over the last 20 years, nature restoration has become important in the area. For the implementation of the national ecological network (NEN), agricultural land will have to be converted to nature, but the total area and the spatial zonation are still subject of debate between the provincial government and various stakeholders. We used PROBE to generate maps on a 25 m resolution that may help spatial planners to design the NEN in an optimal way for nature conservation, especially in the face of climate change. Currently, land purchases by nature organizations are often based on general evaluations that are strongly based on the current state of the land and not on future change (Bakker et al. in review for Landscape Ecology). Maps such as the ones produced by PROBE can help policymakers and nature organizations in aiming at feasible nature targets, and direct their land-purchasing activities to those areas with the highest potential for nature development.

Climate projection

In 2006, based on general circulation model simulations published in the Fourth Assessment Report of the IPCC (Solomon et al. 2007), the Royal Netherlands Meteorological Institute (KNMI) issued four climate scenarios which include changes in temperature, precipitation, and reference evapotranspiration (Van den Hurk et al. 2006). Here, we focus on the warmest and driest W+ scenario in 2050. This scenario, which may be considered as a worst-case one for wetlands, is related to the IPCC A2 and A1B scenarios and comprises a +2 °C global temperature increase, and a strong change of wind circulation, which induces warmer and moister winter seasons and increases the likelihood of dry and warm summertime situations (Table 1).

Table 1 Effects of climate change on temperature, precipitation *Pr*, and reference evapotranspiration *ET* in the Netherlands for the warm and dry climate scenario W+ (Van den Hurk et al. 2006)

Variable	Summer (JJA)	Winter (DJF)
Mean temperature K	+2.8	+2.3
Mean *Pr* %	−19.0	+14.2
Wet day frequency %	−19.3	+1.9
Pr on wet day %	+0.3	+12.1
Reference *ET* %	+15.2	

Hydrological input

To generate the hydrological input for PROBE, we used a dynamic regional hydrological model (Van Ek et al. 2012) which consists of the following three coupled procedures: MODFLOW (Harbaugh et al. 2000) to simulate the distributed flow of groundwater, METASWAP (van Walsum and Groenendijk 2008) for the vertical flow between groundwater table and root zone (i.e. percolation and capillary rise), and the crop growth model WOFOST for the actual evapotranspiration in dependency of moisture, temperature and atmospheric CO_2 (van Walsum and Supit 2012). Spatial and temporal resolution was 25 m and 1 days, respectively; model accuracy of characteristic groundwater levels was 0.20 m *RMSE* (root mean square of errors). To characterize the hydrology of the Baakse beek for the current climate (1981–2010), the model was fed with 30 years of daily values on precipitation and temperature, wind speed, relative humidity, and solar radiation to compute reference evapotranspiration according to Penman–Monteith. For the 2050 climate, we transformed these time series to the 2050-climate of W+, using transformation software supplied by the KNMI (Bakker and Bessembinder 2007). This software accounts for shifts in precipitation from summer to winter, and of intensified rainfall and drought events. With the aid of a digital elevation model (Van der Sande et al. 2010; original resolution

Table 2 Alliances selected for PROBE, including their conservation value *V*. 09AA–1232 have a short vegetation structure, 37AB–42AB a tall one

Code	Name	Habitat description	*V*
09AA	*Caricion nigrae*	Poor fens and dune slacks	197
09BA	*Caricion davallianae*	Rich fens and dune slacks	399
11AA	*Ericion tetralicis*	Wet heath	218
12AA	*Polygonion avicularis*	Short vegetation on nutrient-rich dynamic soils	18
14AA	*Corynephorion canescentis*	Pioneer vegetation on acidic sandy soils	76
14BA	*Thero-Airion*	Grasslands on acidic sandy soils	79
14BB	*Plantagini-Festucion*	Grasslands on non-calcareous sandy soils	113
14BC	*Sedo-Cerastion*	Short veg. on calcareous sandy soils (alluvial)	194
14CA	*Tortulo-Koelerion*	Pioneer veg. on calcareous sandy soils (coastal dunes)	122
14CB	*Polygalo-Koelerion*	Grasslands on calcareous sandy soils (coastal dunes)	219
15AA	*Mesobromion erecti*	Grasslands on calcareous loamy soils	396
16AA	*Junco-Molinion*	Mesotrophic wet grasslands	315
16AB	*Calthion palustris*	Eutrophic wet grasslands	134
16BA	*Alopecurion pratensis*	Alluvial hay meadows on moist calcareous clay soils	90
16BB	*Arrhenatherion elatioris*	Hay meadows on dry sandy clay and sandy clay	93
16BC	*Cynosurion cristati*	Pastures on moist soils	64
20AA	*Calluno-Genistion pilosae*	Dry heath (inland mainly)	94
20AB	*Empetrion nigri*	Dry heath (coastal dunes)	171
1232	12BA *Lolio-Potentillion anserinae* +29AA *Bidention tripartitae* + 32AA *Filipendulion* + 32BA Epilobion *hirsute*	Wet eutrophic vegetations (grassland, tall herb, pioneer)	59
37AB	*Carpino-Prunion*	Shrubs on moist to dry slightly to non-calcareous soils	71
37AC	*Berberidion vulgaris*	Shrubs on dry calcareous soils	165
38AA	*Salicion albae*	Alluvial forests on dynamic wet eutrophic sites	51
3639	36AA *Salicion cinereae* + 39AA *Alnion glutinosae*	Mesotrophic wet shrubs and forests	83
40AA	*Betulion pubescentis*	Oligotrophic wet forests	98
42AA	*Quercion roboris*	Dry acidic forests	65
43AA	*Alno-Padion*	Mesotrophic to eutrophic moist forests	151
43AB	*Carpinion betuli*	Mesotrophic forests on moist calcareous soil	211

of 0.5 m scaled up to 25 m by arrhythmic averaging), simulated groundwater levels were expressed in m below soil surface. With an *RMSE* of the soil surface of 0.10 m, the *RMSE* of the characteristic groundwater levels, relative to soil surface, becomes 0.22 m.

Vegetation typology and valuation system

In most European countries it is common practice to classify the vegetation according to the French-Swiss school of Braun-Blanquet, also known as 'phytosociology'. For this paper we used a national phytosociological standard work (Schaminée et al. 1995a, 1995b, 1996, 1998; Stortelder et al. 1999) that is commonly used in the Netherlands, both for scientific and planning purposes. In this standard work 242 vegetation types are distinguished on the level of associations, grouped into 89 alliances. An advantage of the associations is that they are reasonably homogeneous in terms of site conditions. However, we considered the association level too detailed for climate change projections on the basis of merely four environmental drivers (i.e. moisture, nutrients, acidity and light). Hence, we went one level higher to describe the vegetation at the more heterogeneous level of alliances. From the 89 alliances of the standard work, we selected 31 ones to represent terrestrial vegetation of inland nature reserves in the Netherlands (Supplementary material I). Some alliances with similar habitat requirements were merged, leaving a total of

27 vegetation units, 19 with a short vegetation structure, and 8 of woodlands (Table 2).

In a validation procedure, where a randomly chosen half of DVN was used for the calibration of pdfs and the other half for the validation of predicted alliances, we showed that the percentage of correctly classified relevés was 75 % for alliances with a short vegetation structure and 82 % for alliances of woodlands (Supplementary material II).

We gave each unit a conservation value on the basis of the method of Hertog and Rijken (1992) (Table 2). This method takes account of the number of species, species abundance and species value (which depends on species rarity on a national and international scale, degree of threat, vulnerability, and distinctiveness). For our selection the scale runs from the lowest valued alliance 12AA *Polygonion avicularis* with 18 points, to the highest valued 09BA *Caricion davallianae* with 399 points (Table 2).

Results

While originally (before ca. 1950) being wet and frequently flooded in winter and spring, nowadays the agricultural land that covers the major part of the area is well drained, with a *SGL* of on average 0.6–1.5 m–s.s. (Fig. 6A1). Especially in the western part there are some areas that are still relatively wet. Nature areas are chiefly located on the more elevated soils, with a *SGL* deeper than about 1 m–s.s. (compare Figs. 4, 6A1). These soils were originally less profitable for agriculture and thus left for forestry, recreation and nature conservation. The W+ scenario will result in a drop of groundwater levels (*MGL, LGL, HGL, SLG*), especially in areas where groundwater levels are deep (Fig. 6A2). In some parts levels hardly change though, particularly in those with a shallow groundwater table (e.g. the west of the catchment). Upward seepage *S* of bicarbonate enriched groundwater (Fig. 6B1) is an important source of pH buffering in mesotrophic, often very species-rich, ecosystems. In general, *S* decreases in the W+ scenario, though in the lower western part of the catchment *S* increases (Fig. 6B2).

The results of PROBE had to support both the definition of feasible nature targets under a future climate, and the design of a climate versatile NEN. For the latter reason we predicted vegetation patterns for the whole of the catchment for the hypothetical situation that the whole area is managed as nature conservation area. These maps can thus be considered as habitat suitability maps, indicating where we may expect the highest potential for vegetation development under optimal vegetation management, but with current water management.

The well-drained situation of the catchment is reflected in high occurrence probabilities and corresponding areas for alliances of dry soils, particularly of 20AA *Calluno-Geniston pilosae* (Table 3) and 42AA *Quercion roboris* (Table 4). In general, alliances of wet and moist conditions suffer from the W+ scenario whereas alliances of drier soils profit. However, through the flow of groundwater locally different results emerge, as we will demonstrate for four alliances (Fig. 7). A univocal response to climate change shows 14AA *Corynephorion canescentis* (Fig. 7A), with an increase in area of 60 %, largely at the cost of 20AA *Calluno-Geniston pilosae* (Table 3: 3 % of the 19,441 ha of 20AA is converted to 14AA). Severe loss is expected for alliances of wet, nutrient poor to moderately nutrient rich and weakly acid sites: 16AA *Junco-Molinion* (Fig. 7B) and 16AB *Calthion palustris* (Fig. 7C), with a decrease in area of 25 and 18 % respectively. In decalcified soils these species-rich and valuable vegetation types (Table 3) often depend on upwelling groundwater (Cirkel et al. 2013). They are known for their high susceptibility to small changes in hydrology, which may provoke both internal eutrophication and acidification. It appears that that *Junco-Molinion* (16AA) may transform to 11AA *Ericion tetralicis* (more acidic), 16AB *Calthion palustris* (more nutrient-rich), but also to 09AA (comparable conditions, slightly wetter). Cells with 16AB *Calthion palustris*, in turn, may particularly shift to 16BC *Cynosurion cristati* (drier and richer). There is, however, not only loss for these two alliances (see the small green spots in Fig. 7B2 and Fig. 7C2 and the column numbers of Table 2). For instance (Table 2), 6 % of the cells with 09AA *Caricion nigrae* in the current climate transform to 16AA *Junco-Molinion* in the W+ climate, and 2 % with 16AA *Junco-Molinion* shift to 16AB *Calthion palustris*. The simulated area of 11AA *Ericion tetralicis* (Fig. 7D1) drops by 13 %, with a mixed pattern of loss and gain (Fig. 7D2). Loss is predicted in the well-drained area, where this alliance transforms into the drier 20AA *Calluno-Geniston pilosae* and 20AB *Empetrion nigri.* Presumably as a result of acidification, gain is especially predicted in the wetter western part, particularly at the cost of 16AA *Junco-Molinion.*

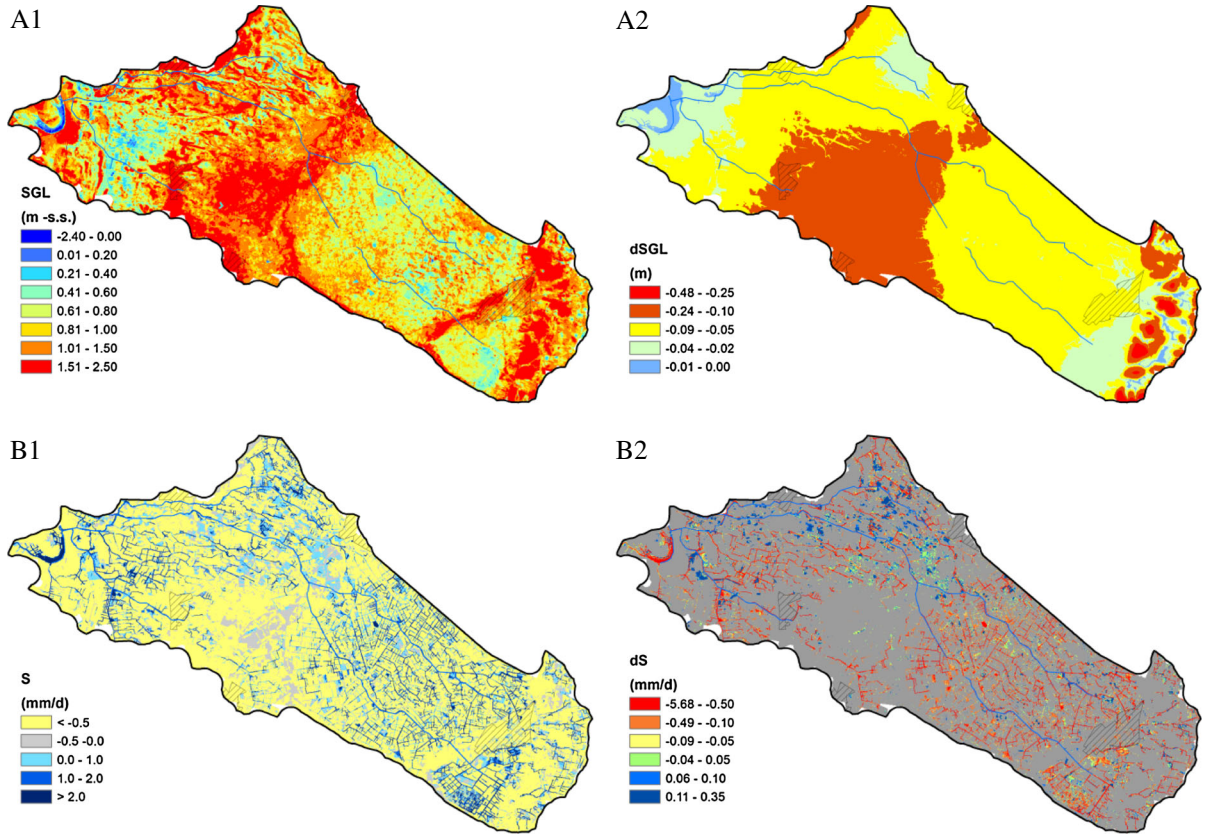

Fig. 6 Spring groundwater level *SGL* (**A**) and seepage intensity *S* (**B**) in the current climate (*left*) and change in both entities as a result of the W+ scenario (2050) (*right*). Figure B2 only shows the change where $S > 0$ in the current climate

Integrating all 19 alliances with a short vegetation structure into one conservation value map reveals that the current potential hotspots of biodiversity particularly lie in the western part of the catchment (Fig. 7A1). The W+ scenario poses a serious threat on the potential conservation value of the catchment, although a local increase in conservation value can be observed throughout the catchment, particularly in the west and at the foot of the elevated part of the catchment (Fig. 8A2). Managed as woodland, current conservation values appear to be lower than when managed as a short vegetation (compare Figs. 8A1, B1). Focusing on current nature reserves with their current vegetation structure, we see a loss of conservation values (Fig. 8B2), almost without exceptions. Presently, potential high conservation values are chiefly found outside current reserves, though for some reserves high values are predicted, which matches the actual situation (Van Ek et al. 2012).

Discussion

Advantages, shortcomings and plans for improvements of PROBE

Current habitat distribution models have certain drawbacks: they apply indirect empirical relationships between habitat and vegetation, they disregard effects of groundwater flow, and they are designed for too coarse spatial scales. For this reason we developed PROBE, which can predict vegetation distribution under a changing climate at a spatial scale that is relevant for regional planners and nature managers. To this end, PROBE combines available (spatially explicit) data sources, transfer functions (to speed-up the calculations) derived from mechanistic models, and robust relationships between soil and plant characteristics.

Thanks to the use of transfer functions, the computation time of a scenario is about three minutes for

Table 3 Changes in the area (computed as the sum of *P*) of alliances with a short vegetation structure, as well as the percentage shift in the area from the current climate (C) to the W+ climate in 2050

Area (ha)				% Transformation													
	C	W+	%	09AA	09BA	11AA	12AA	14AA	14BA	14BB	14CB	16AA	16AB	16BA	16BC	20AA	20AB	1232
09AA	86	113	31	**75**		16						6	1				1	
09BA	62	67	9	1	**78**	2							11		2	1	4	
11AA	766	665	−13	1	2	**73**										22	2	
12AA	124	115	−7			2	**59**		1	2			3	2	3	25	1	3
14AA	1,007	1,615	60					**100**										
14BA	36	41	14					1	**97**	1						2		
14BB	174	207	19						2	**85**						13		
14CB	26	26	−1								**96**					1		
16AA	368	275	−25	9		12	1					**64**	6		2	2	3	
16AB	714	583	−18	1		1	2			1		2	**75**	5	8	4		1
16BA	327	340	4				1			3			1	**88**		6		
16BC	481	454	−6				3			4		1	1	2	**80**	8		1
20AA	19,441	19,202	−1					3								**97**		
20AB	528	427	−19		1	6		4				2				11	**75**	
1232	71	82	15	1								1		4	2			**91**

Alliances predicted in <20 cells not shown. Example: the area of 09AA increases with 31 % to 113 ha; from the area of from 86 ha in C, 75 % remains 09AA and 16 and 6 % are replaced by 11AA and 16AA in W+

the Baakse beek catchment (with numerous input and output maps consisting of more than 1.5 million grid cells each) on a standard PC (2.50 GHz, 4 Gb RAM). Because of its ability to quickly produce results, PROBE was used to analyse eight scenarios in a national study to the availability of fresh water in the Netherlands (Ter Maat et al. 2014). Another advantage of PROBE is its flexibility, allowing: (1) the prediction of vegetation types according to any classification system (see e.g. Van der Knaap et al. (this issue), and Witte et al. 2007 for the prediction of ecotopes and associations, respectively); (2) the (combined) use of various lists of plant characteristics, from indicator values to functional plant traits; (3) the adaptation to local environmental drivers by constructing tailor-made transfer functions.

For a number of reasons we did not model plant species, but vegetation types instead (Witte et al. 2008; Laughlin et al. 2012; Douma et al. 2012c). First, a species approach would require information about the physiological amplitude of species, based on measurements in the close vicinity of plant individuals, while in practice such data are very scarce and we have to rely on realized amplitudes from field observations. Second, we would have to include competition for nutrients, light and water in our model. And third, given the importance of stochastic processes, functional similarity of species and intraspecific variation, it is practically impossible to predict the species occurrence with sufficient certainty. While vegetation maps may be an important means to convey the message to policy makers, a disadvantage of the use of vegetation classification is that any classification may lose its validity, since species within one vegetation unit may respond differently to climate change. For this reason, rather coarse vegetation units, such as alliances, may be preferred and should be considered as reference points in a multi-dimensional trait space. On the other hand, since PROBE generates occurrence probabilities, it is capable of computing new combinations of vegetation types. Moreover, this drawback may partly be resolved by calibrating PROBE on an international data base of vegetation relevés and by using an international vegetation typology.

Fig. 7 Potential occurrence probability *P* of the alliances 14AA *Corynephorion canescentis* (**A**), 16AA *Junco-Molinion* (**B**), 16AB *Calthion palustris* (**C**), and 11AA *Ericion tetralicis* (**D**) (*left*), as well as absolute change in *P* as a result of the W+ scenario (2050) (*right*), assuming the whole area is managed as nature reserve with a short vegetation structure

The effect of a temperature rise is included in the computation of drought stress *TS*, oxygen stress *RS*, and mineralization rate *Pmin*, but the direct effects of temperature (i.e. structural damage due to freezing (e.g. Lenz et al. 2013)) are not accounted for. A possible solution might be the aforementioned international vegetation database and the use of a fourth explanatory axis with the indicator value for temperature according to Ellenberg (1992). Overheating due to high temperatures is strongly related to *TS*, and a more sophisticated treatment of temperature on *TS* may be possible in the near future by integrating of the optimization framework of Prentice et al. (2014) in our *TS* scheme.

At higher CO_2 levels plants transpire less water, which is considered in the simulation of actual evapotranspiration with WOFOST. Theoretically, elevated CO_2 might also influence the competition

Table 4 As Table 3, but now for alliances of woodlands

Area (ha)				% Transformation							
	C	W+	%	37AB	37AC	38AA	3639	40AA	42AA	43AA	43AB
37AB	530	540	2	**65**				1	31	1	2
37AC	30	28	−6		**91**			6	2		2
38AA	461	459	0			**99**					
3639	726	481	−34	1			**62**	21	2	14	
40AA	4,661	4,004	−14	1				**77**	20	1	
42AA	19,454	20,577	6						**99**		
43AA	1,122	923	−18	8			1	13	8	**68**	2
43AB	98	71	−28	12			2	19	31	5	**32**

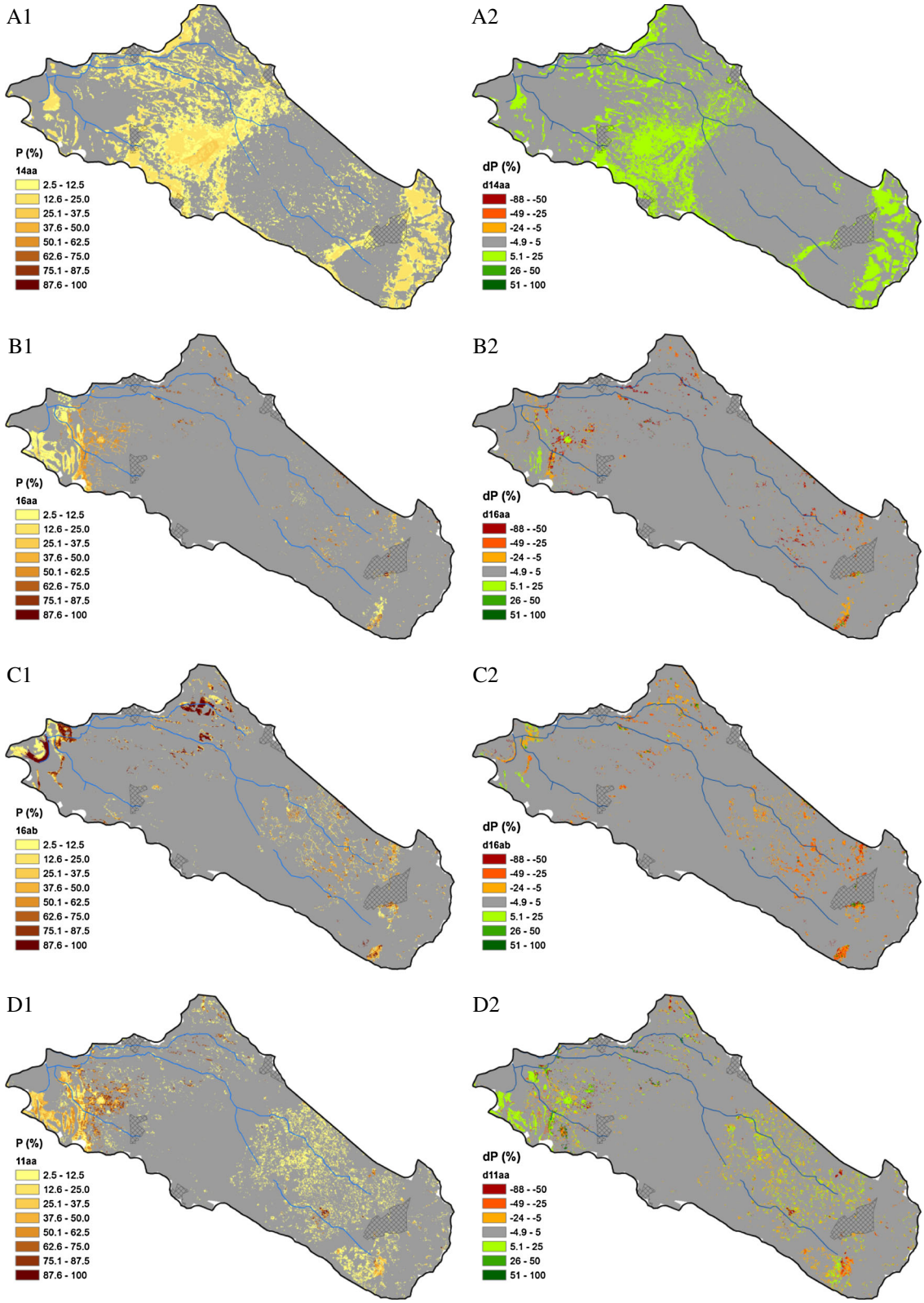

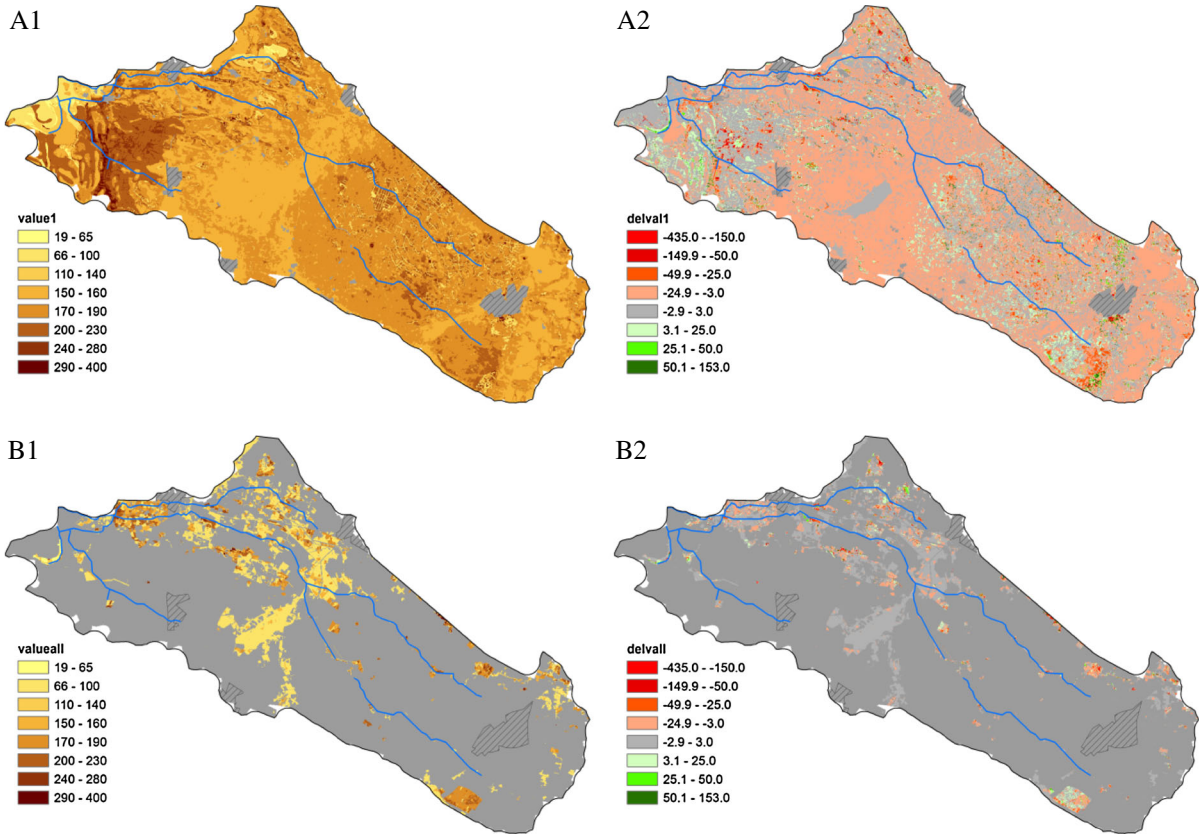

Fig. 8 Conservation value in the current climate (*left*) and change in value due to the W+ scenario (2050) (*right*). **a** Assuming a short vegetation structure, **b** with current vegetation structure and nature reserves only

between plant species, but since there is no proof that this will actually happen in natural ecosystems (Poorter and Navas 2003), neglecting this effect in PROBE seems justified.

Probably the biggest step forward for PROBE is a strongly improved simulation of nutrient availability. This requires more knowledge of crucial soil processes (such as mineralization, redox-processes, de-nitrification and precipitation; Fujita et al. (2013a; 2014), and accounting for the interaction with surrounding farmers (Kros et al., this issue), but maybe even more important is a reliable parameterization of the units of the utilized soil map (Van Ek et al. 2014).

Also a reliable prediction of the acidity of water in the root zone is crucial to enable better projections of occurrence probability of vegetation types. This is especially the case for groundwater-dependent ecosystems that are fed by upwelling groundwater, since such systems are very susceptible to changes in their hydrological regime (Cirkel et al. 2013). Therefore we have to take into account the buffering capacity of the soil, the occurrence and quality of upward seepage, and the shape and dynamics of rain water lenses floating on seepage water. Efforts to do so are being developed (Cirkel et al. 2010; De Louw 2013).

We have shown that on a relatively coarse resolution of 250 m, PROBE still produces highly plausible results ("Model plausibility" section), but in order to get results that are also meaningful in practice, we advise to use this model on a much finer spatial scale. In the practice of Dutch nature conservation, vegetation is commonly mapped on a 1:5,000 scale, which, corresponds to a resolution of 10 m. On the other hand, borders between vegetation units are usually very difficult to delineate and the standard soil map of the Netherlands (input to PROBE) has a 1:50,000 scale, which calls for a coarser resolution. A grid of 25 m, as used for the Baakse beek catchment, therefore seems an appropriate compromise.

Uncertainties in the input maps and in the modelled relationships eventually affect the outcomes of PROBE. In the near future, we will extend the model with a procedure to compute the accumulated effect of these uncertainties by simulating error propagation with the aid of Latin hypercube sampling (Helton and Davis 2003). Output errors can be judged at different scales, for instance at the scale of individual grid cells, and at landscape scale. Highly valued wetland vegetation, with vegetation types like 16AA *Junco-Molinion*, can be very susceptible to small changes in groundwater level, meaning that an *RMSE* of 0.22 m (Baakse beek catchment) will result in large prediction errors of such vegetation at the scale of individual grid cells. However, errors in simulated groundwater levels are auto-correlated, meaning that grid cells with too low or too high simulated levels are spatially clustered. This causes predicted vegetation patterns to shift downward or upward accordingly along the slope. In the case of the Baakse beek catchment, an *RMSE* of 0.22 m corresponds to a horizontal shift of about 250 m, or 10 grid cells. Such shifts may produce large errors for sensitive vegetation types at the grid cell level, but they may be acceptable for judging how scenarios affect the area of suitable habitats for vegetation types at landscape scale, for instance of a whole catchment, as was shown by Douma et al. (2012c).

Simulated effects of climate change

Our model shows that the warm and dry W+ scenario may seriously hamper the survival and development of wet and oligotrophic to mesotropic vegetation types, such as *Junco-Molinion* and *Calthion palustris* grasslands, while vegetation of dry and acidic soils seem to profit from this scenario.

According to PROBE, the current configuration of nature reserves is far from optimal with respect to conservation values: the highest potentials for the development of valuable vegetation types are mainly located in land that is currently in agricultural use. This situation is the result of an historical development where the elevated soils with a deep groundwater table were less profitable for agriculture and thus left as 'wasteland' for nature conservation. However, with the extension of the NEN, the maps of vegetation types and conservation values produced by PROBE may serve spatial planners to purchase those areas that are optimal for nature development. Such purchases are, however, hindered by limited purchasing power of nature organizations, and the desire of farmers to consolidate their property (Bakker et al. this issue).

Indicative simulations with PROBE revealed that the W+ scenario can be compensated by a rise in groundwater level of on average ca. 10 cm. This does not seem much, but it is a considerable step for wetland vegetation, and far from easy to realize in small reserves surrounded by well drained agricultural parcels on a highly permeable phreatic aquifer, as is the case in the Baakse beek catchment. Protection of wetland reserves will for instance require the creation of buffer zones and a ban on sprinkling in adjacent farmland. These measures will lead to (strong) local deviations in the general vegetation response, which can only be adequately forecasted by combining PROBE with a spatially distributed groundwater model. Such tailor-made solutions have been analysed with PROBE for the Tungelroyse beek catchment (Van der Knaap et al. this issue).

Our study demonstrated that the simulated effects of climate change are not univocal for each vegetation type, since areas of loss may partly be compensated with areas of gain. Shifts in vegetation patterns are associated with climate-induced changes in moisture, nutrients, and acidity. These are strongly influenced by edaphic and hydrological conditions, as is shown by the often contrasting PROBE outcomes, especially for the western and the more eastern part of the catchment. We believe these results could never have been foreseen on the basis of expert judgement and logic alone, which once more stress the importance of models to assess the ecological effects of climate change.

Conclusions

With PROBE we provide a robust eco-hydrological modelling framework, using process-based relationships between site factors and vegetation characteristics, and taking account of spatial relationships through hydrology. These features provide a clear step forward compared to current habitat distribution models, which are likely to be inadequate for climate projections. Due to the ability of PROBE to quickly generate output for millions of grid cells, it already has made the step from science to practice, as it has been applied in both regional and national scenario analysis.

The flexible modular structure of PROBE provides a valuable framework, which we can and will improve in the following years, driven by the continuing need to provide policymakers, nature managers, and spatial planners with adequate information about the feasibility of nature targets.

Acknowledgments This work was carried out within the joint research programme of the Dutch Water Utility sector (http://www.kwrwater.nl/BTO), and the project Climate Adaptation for Rural Areas (CARE), which was funded by the Knowledge for Climate Programme (http://knowledgeforclimate.climateresearchnetherlands.nl/climateadaptationforruralareas) as well as by the province of Gelderland and the water board Rijn en IJssel.

References

Baird AJ (1999) Modelling. In: Baird AJ, Wilby RL (eds) Ecohydrology. Plants and water in terrestrial and aquatic environment. Routlegde, London

Bakkenes M, Alkemade JRM, Ihle F, Leemans R, Latour JB (2002) Assessing effects of forecasted climate change on the diversity and distribution of European higher plants for 2050. Glob Change Biol 8(4):390–407

Bakker A, Bessembinder J (2007) Neerslagreeksen voor de KNMI'06 scenario's. H2O 22:45–47

Bartholomeus RP, Witte JPM (2013) Ecohydrological Stress - Groundwater To Stress Transfer. Theory and manual version 1.0. KWR Watercycle Research Institute, Nieuwegein

Bartholomeus RP, Witte JPM, Van Bodegom PM, Aerts R (2008) The need of data harmonization to derive robust empirical relationships between soil conditions and vegetation. J Veg Sci 19:799–808

Bartholomeus RP, Witte JPM, Van Bodegom PM, Van Dam JC, Aerts R (2011) Climate change threatens endangered plant species by stronger and interacting water-related stresses. J Geophys Res 116(G4):G04023

Bartholomeus RP, Witte JPM, Bodegom PM, Dam JC, Becker P, Aerts R (2012) Process-based proxy of oxygen stress surpasses indirect ones in predicting vegetation characteristics. Ecohydrology 5:746–758

Botkin DB, Saxe H, Araújo MB, Betts R, Bradshaw RHW, Cedhagen T, Chesson P, Dawson TP, Etterson JR, Faith DP, Ferrier S, Guisan A, Hansen A, Hilbert DW, Loehle C, Margules C, New M, Sobel MJ, Stockwell DRB (2007) Forecasting the effects of global warming on biodiversity. Bioscience 57(3):227–236

Buckley LB, Urban MC, Angilletta MJ, Crozier LG, Rissler LJ, Sears MW (2010) Can mechanism inform species' distribution models? Ecol Lett 13(8):1041–1054

Cirkel DG, Witte JPM, Van der Zee SEATM (2010) Estimating seepage intensities from groundwater level time series by inverse modelling: a sensitivity analysis on wet meadow scenarios. J Hydrol 385(1–4):132–142

Cirkel DG, Van Beek CGEM, Witte JPM, Van Der Zee SEATM (2013) Sulphate reduction and calcite precipitation in relation to internal eutrophication of groundwater fed alkaline fens. Biogeochemistry:1-19

Cirkel DG, Witte JPM, Nijp JN, van Bodegom PM, Zee SEATM (2014) The influence of spatiotemporal variability and adaptations to hypoxia on empirical relationships between soil acidity and vegetation. Ecohydrology 7:21–23

Dai A (2011) Drought under global warming: a review. Clim Change 2:45–65

De Haan M, Runhaar H, Cirkel G (2010) Waternood Kansrijkdommodule Pilotstudie in Noord-Nederland en toepassing voor vervaardiging waterkansenkaarten voor natuur. KWR, Nieuwegein, p 55

De Lange WJ, Prinsen GF, Hoogewoud JC, Veldhuizen AA, Verkaik J, Oude-Essink GHP, Van Walsum PEV, Delsman JR, Huinink JC, Massop HTL, Kroon T (2014) An operational, multi-scale, multi-model system for consensus-based, integrated water management and policy analysis: the Netherlands hydrological instrument. Environ Model Softw 59:98–108

De Louw PGB (2013) Saline seepage in deltaic areas—Preferential groundwater discharge through boils and interactions between thin rainwater lenses and upward saline seepage PhD. VU University Amsterdam, Amsterdam

Douma JC, Aerts R, Witte JPM, Bekker RM, Kunzmann D, Metselaar K, Van Bodegom PM (2012a) A combination of functionally different plant traits provides a means to quantitatively predict a broad range of species assemblages in NW Europe. Ecography 35:364–373

Douma JC, Bardin V, Bartholomeus RP, Bodegom PM (2012b) Quantifying the functional responses of vegetation to drought and oxygen stress in temperate ecosystems. Funct Ecol 26(6):1355–1365

Douma JC, Witte JPM, Aerts R, Bartholomeus RP, Ordoñez JC, Venterink HO, Wassen MJ, van Bodegom PM (2012c) Towards a functional basis for predicting vegetation patterns; incorporating plant traits in habitat distribution models. Ecography 35(4):294–305

Drake JA (1991) Community-assembly mechanics and the structure of an experimental species ensemble. Am Nat 137:1–26

Early R, Anderson B, Thomas CD (2008) Using habitat distribution models to evaluate large-scale landscape priorities for spatially dynamic species. J Appl Ecol 45(1):228–238

Easterling DR, Meehl GA, Parmesan C, Changnon SA, Karl TR, Mearns LO (2000) Climate extremes: observations, modeling, and impacts. Science 289(5487):2068–2074

Ellenberg H (1992) Zeigerwerte der Gefäßpflanzen (ohne *Rubus*). In: Ellenberg H., Weber H. E., Düll R., Wirth V., Werner W., Paulißen D. (eds), Zeigerwerte von Pflanzen in Mitteleuropa, Scripta Geobotanica, 18 edn

Fay PA, Kaufman DM, Nippert JB, Carlisle JD, Harper CW (2008) Changes in grassland ecosystem function due to extreme rainfall events: implications for responses to climate change. Glob Change Biol 14(7):1600–1608

Fujita Y, Van Bodegom PM, Runhaar J, Olde Venterink H, Witte JPM (2013a) Towards a proper integration of hydrology in predicting soil nitrogen mineralization rates along natural moisture gradients. Global Biogeochem Cycles 58:302–312

Fujita Y, Van Bodegom PM, Witte JPM (2013b) Relationships between nutrient-related plant traits and combinations of soil N and P Fertility. PLoS ONE 8(12):e83735

Fujita Y, Witte JPM, Van Bodegom PM (2014) Incorporating microbial ecology concepts into soil mineralization models to improve regional predictions of carbon and nitrogen fluxes. Soil Biol Biochem 28(3):223–238

Grime JP (2001) Plant strategies, vegetation processes and ecosystem properties. John Wiley and Sons, Chicester, UK

Guisan A, Thuiller W (2005) Predicting species distribution: offering more than simple habitat models. Ecol Lett 8(9):993–1009

Guisan A, Zimmermann NE (2000) Predictive habitat distribution models in ecology. Ecol Model 135:147–186

Harbaugh AW, Banta ER, Hill MC, McDonald MG (2000) MODFLOW 2000, The U.S. geological survey modular ground water model user guide to modularization concepts and the ground water flow process. Open-File Report 00-92. US Geological Survey, Reston, Virginia

Hazeu GW (2005) Landelijk Grondgebruiksbestand Nederland (LGN5); monitoring landgebruik van 1995–2004. GeoInfo 10(2):456–462

Helton JC, Davis FJ (2003) Latin hypercube sampling and the propagation of uncertainty in analyses of complex systems. Reliab Eng Sys Saf 81(1):23–69

Hertog AJ, Rijken M (1992) Geautomatiseerde bepaling van natuurbehoudswaarde in vegetatie-opnamen. Provincie Gelderland, Arnhem

Karl TR, Knight RW, Plummer N (1995) Trends in high-frequency climate variability in the twentieth century. Nature 377(6546):217–220

Karlsson IB, Sonnenborg TO, Jensen KH, Refsgaard JC (2014) Historical trends in precipitation and stream discharge at the Skjern River catchment Denmark. Hydrol. Earth Syst. Sci. 18(2):595–610

Keddy PA (1992) Assembly and response rules: two goals for predictive community ecology. J Veg Sci 3(2):157–164

Knapp AK, Beier C, Briske DD, Classen AT, Luo Y, Reichstein M, Smith MD, Smith SD, Bell JE, Fay PA, Heisler JL, Leavitt SW, Sherry R, Smith B, Weng E (2008) Consequences of more extreme precipitation regimes for terrestrial ecosystems. Bioscience 58(9):811–821

Kroes JG, Van Dam JC, Groenendijk P, Hendriks RFA, Jacobs CMJ (2008) SWAP version 3.4, Theory description and user manual. Wageningen University and Research Centre, Wageningen

Kros J, Reinds GJ, De Vries W, Latour JB, Bollen MJS (1995) Modelling of soil acidity and nitrogen availability in natural ecosystems in response to changes is acid deposition and hydrology. Report 95. SC-DLO, Wageningen

Laughlin DC, Joshi C, van Bodegom PM, Bastow ZA, Fulé PZ (2012) A predictive model of community assembly that incorporates intraspecific trait variation. Ecol Lett 15(11):1291–1299

Lenz A, Hoch G, Vitasse Y, Korner C (2013) European deciduous trees exhibit similar safety margins against damage by spring freeze events along elevational gradients. New Phytol 200:1166–1175

Levine JM, McEachern AK, Cowan C (2008) Rainfall effects on rare annual plants. J Ecol 96(4):795–806

McGill BJ, Enquist BJ, Weiher E, Westeboy M (2006) Rebuilding community ecology from functional traits. Trends Ecol Evol 21(4):178–185

Ordoñez JC, Van Bodegom PM, Witte JPM, Wright IJ, Reich PB, Aerts R (2009) A global study of relationships between leaf traits, climate and soil measures of nutrient fertility. Glob Ecol Biogeogr 18(2):137–149

Parton WJ, Scurlock JMO, Ojima D, Gilmanov TG, Scholes RJ, Schimel DS, Kirchner T, Menaut JC, Seastedt T, Garcia Moya E, Kamnalrut A, Kinyamario JI (1993) Observations and modeling of biomass and soil organic matter dynamics for the grassland biome worldwide. Global Biogeochem Cycles 7:785–809

Pearson RG, Dawson TP (2003) Predicting the impacts of climate change on the distribution of species: are bioclimate envelope models useful? Global Ecol Biogeogr. 12:361–371

Poorter H, Navas M-L (2003) Plant growth and competition at elevated CO2: on winners, losers and functional groups. New Phytol 157(2):175–198

Porporato A, Daly E, Rodriguez-Iturbe I (2004) Soil water balance and ecosystem response to climate change. Am Nat 164(5):625–632

Prentice IC, Dong N, Gleason SM, Maire V, Wright IJ (2014) Balancing the costs of carbon gain and water transport: testing a new theoretical framework for plant functional ecology. Ecol Lett 17(1):82–91

Pulles JW (1985) Beleidsanalyse voor de waterhuishouding in Nederland/PAWN. Hoofdirectie van de Waterstaat

Schaminée JHJ, Stortelder AHF, Westhoff V (1995a) De Vegetatie van Nederland. Inleiding tot de plantensociologie: grondslagen, methoden en toepassingen. Opulus press, Uppsala/Leiden

Schaminée JHJ, Weeda EJ, Westhoff V (1995b) De vegetatie van Nederland. Wateren, moerassen, natte heiden. Opulus Press, Uppsala

Schaminée JHJ, Stortelder W, Weeda EJ (1996) De vegetatie van Nederland. Graslanden, zomen, droge heiden. Opulus Press, Uppsala

Schaminée JHJ, Weeda EJ, Westhoff V (1998) De vegetatie van Nederland. Opulus Press, Uppsala, SE, Leiden, NL

Solomon S, Qin D, Manning M, Alley RB, Berntsen T, Bindoff NL, Chen Z, Chidthaisong A, Gregory JM, Hegerl GC, Heimann M, Hewitson B, Hoskins BJ, Joos F, Jouzel J, Kattsov V, Lohmann U, Matsuno T, Molina M, Nicholls N, Overpeck J, Raga G, Ramaswamy V, Ren J, Rusticucci M, Somerville R, Stocker TF, Whetton P, Wood RA, Wratt D (2007) Technical Summary. In: Solomon S, Qin D, Manning M et al (eds) Climate Change 2007: The physical science basis. Cambridge University Press, Cambridge, United Kingdom and New York, NY, USA, Contribution of working group I to the fourth assessment report of the intergovernmental panel on climate change

Stortelder AHF, Schaminée JHJ, Hommel PWFM (1999) De vegetatie van Nederland. Opulus Press, Uppsala, SE, Leiden, NL

Ter Maat J, Haasnoot M, Van der Vat M, Hunink J, Prinsen G, Visser M, Boderie P, Van Ek R, Maarse M, Van der Sligte R, Verheij H, Wesselius C (2014) Effecten van maatregelen voor de zoetwatervoorziening in Nederland in de 21e

eeuw, Deltaprogramma - Deelprogramma Zoetwater - fase 4. 1209141-001. Deltares, Delft

Thomas CD, Cameron A, Green RE, Bakkenes M, Beaumont LJ, Collingham YC, Erasmus BFN, Fereira de Siqueira M, Grainger A, Hannah L, Hughes L, Huntley B, van Jaarsveld AS, Midgley GF, Miles L, Ortega-Huerta MA, Peterson AT, Phillips OL, Williams SE (2004) Extincition risk from climate change. Nature 427:145–148

Tilman D (1985) The Resource-Ratio Hypothesis of Plant Succession. Am Nat 125:827–852

Trenberth KE, Dai A, van der Schrier G, Jones PD, Barichivich J, Briffa KR, Sheffield J (2014) Global warming and changes in drought. Nat Clim Change 4(1):17–22

Van Bodegom PM, Douma JC, Witte JPM, Ordoñez JC, Bartholomeus RP, Aerts R (2012) Going beyond limitations of plant functional types when predicting global ecosystem–atmosphere fluxes: exploring the merits of traits-based approaches. Glob Ecol Biogeogr 21(6):625–636

Van Dam JC, Groenendijk P, Hendriks RFA, Kroes JG (2008) Advances of modeling water flow in variably saturated soils with SWAP. Vadose Zone J 7(2):640–653

Van den Hurk B, Klein Tankink A, Lenderink G, Van Ulden A, Van Oldenborgh GJ, Katsman C, Van den Brink H, Keller F, Bessembinder J, Burgers G, Komen G, Hazeleger W, Drijfhout S (2006) KNMI Climate change scenarios 2006 for the Netherlands. KNMI, De Bilt, NL

Van der Maarel E, Sykes MT (1993) Small-scale plant-species turnover in a limestone grassland—the carousel model and some comments on the niche concept. J Veg Sci 4:179–188

Van der Meijden R, Odé B, Groen CLG, Witte JPM, Bal D (2000) Bedreigde en kwetsbare vaatplanten in Nederland Basisrapport met voorstel voor de Rode Lijst. Gorteria 26(4):85–208

Van der Sande C, Soudarissanane S, Khoshelham K (2010) Assessment of relative accuracy of AHN-2 laser scanning data using planar features. Sensors 10:8198–8214

Van Ek R, Janssen G, Kuijper M, Veldhuizen AA, Wamelink GWW, Mol J, Groot A, Schipper P, Kroes J, Supit I, Simmelink E, Van Geer F, Janssen P, Van der Sluijs J, Bessembinder J (2012) NMDC-Innovatieproject van Kritische zone tot Kritische Onzekerheden: case studie Baakse beek. NMDC rapport 1205952

Van Ek R, Witte JPM, Mol-Dijkstra JP, De Vries W, Wamelink GWW, Hunink J, Van der Linden W, Runhaar J, Bonten L, Bartholomeus R, Mulder HM, Fujita Y (2014) Ontwikkeling van een gemeenschappelijke effect module voor terrestrische natuur. Amersfoort, STOWA, p 150

Van Oene H, Berendse F, De Kovel CGF (1999) Model analysis of the effects of historic CO_2 levels and nitrogen inputs on vegetation succession. Ecol Appl 9(3):920–935

van Walsum PEV, Groenendijk P (2008) Quasi Steady-State Simulation of the Unsaturated Zone in Groundwater Modeling of Lowland Regions. Vadose Zone J 7(2):769–781

van Walsum PEV, Supit I (2012) Influence of ecohydrologic feedbacks from simulated crop growth on integrated regional hydrologic simulations under climate scenarios. Hydrol Earth Syst Sci 16(6):1577–1593

Weltzin JF, Loik ME, Schwinning S, Williams DG, Fay PA, Haddad BM, Harte J, Huxman TE, Knapp AK, Lin G, Pockman WT, Shaw MR, Small EE, Smith MD, Smith SD, Tissue DT, Zak JC (2003) Assessing the response of terrestrial ecosystems to potential changes in precipitation. Bioscience 53(10):941–952

Witte JPM (1998) National water management and the value of nature. Landbouwuniversiteit, Wageningen

Witte JPM, Meuleman JAM, Van der Schaaf S, Raterman B (2004) Eco-Hydrol Biodivers. In: Feddes RA, De Rooij GH, Van Dam JC (eds) Unsaturated zone modelling: Progress, challenges and applications. Wageningen University and Research Centre, Wageningen, pp 301–329

Witte JPM, Wójcik RB, Torfs PJJF, De Haan MWH, Hennekens S (2007) Bayesian classification of vegetation types with Gaussian mixture density fitting to indicator values. J Veg Sci 18:605–612

Witte JPM, Runhaar J, Van Ek R (2008) Ecohydrological modelling for managing scarce water resources in a groundwater-dominated temperate system. In: Harper D, Zalewski MEJ, Pacini N (eds) Ecohydrology: Processes, Models and Case Studies. CABI Publishing, Oxfordshire, pp 88–111

Witte JPM, Pastoors R, Van der Hoek DJ, Bartholomeus RP, Van Loon A, Van Bodegom PM (2011a) Is het Nationaal Hydrologische Instrumentarium gereed voor het voorspellen van natuureffecten? Stromingen 17(2):15–26

Witte JPM, Strasser T, Slings R (2011b) Kwantitatieve vegetatiewaardering beperkt bruikbaar Landschap 28(2):56-66

Witte JPM, Runhaar J, van Ek R, van der Hoek DCJ, Bartholomeus RP, Batelaan O, van Bodegom PM, Wassen MJ, van der Zee SEATM (2012) An ecohydrological sketch of climate change impacts on water and natural ecosystems for the Netherlands: bridging the gap between science and society. Hydrol Earth Syst Sci 16(11):3945–3957

Wösten JHM, Pachepsky YA, Rawls WJ (2001) Pedotransfer functions: bridging the gap between available basic soil data and missing soil hydraulic characteristics. J Hydrol 251:123–150

Van der Knaap YAM, De Graaf M, Van Ek R, Witte JPM, Bierkens MFP, Van Bodegom PM (this issue) Potential impacts of groundwater conservation measures on catchment-wide vegetation patterns in a future climate. Landscape Ecol